

THE TEMPERATURE WAVE METHOD
OF MEASURING THERMAL DIFFUSIVITY AND
THERMAL CONTACT CONDUCTANCE

by 687

MIHAEL TOMSIC

Dipl. Ing., University of Ljubljana, 1964

A MASTER'S THESIS

submitted in partial fulfillment of the

requirements for the degree

MASTER OF SCIENCE

Department of Nuclear Engineering

KANSAS STATE UNIVERSITY
Manhattan, Kansas

1969

Approved by


Major Professor

LD
2668
74
1969
T65

TABLE OF CONTENTS

1. INTRODUCTION	1
2. THEORY	5
3. EXPERIMENT DESIGN.	31
4. DESCRIPTION OF APPARATUS	37
5. EXPERIMENTAL PROCEDURE	52
6. DATA ANALYSIS.	57
7. EXPERIMENTAL RESULTS	64
8. DISCUSSION OF RESULTS AND EXPERIMENT	76
9. SCOPE FOR FURTHER WORK	81
10. ACKNOWLEDGEMENTS	82
11. LITERATURE CITED	83
12. APPENDICES.	
APPENDIX A: Transient Response of an Elemental Heat Channel	86
APPENDIX B: Correlation Technique	93
APPENDIX C: Analysis of Correlator Response	101
APPENDIX D: Analysis of Tape Recorder Response and Recording and Playback Circuits	112
APPENDIX E: Regression Analysis	116
APPENDIX F: Correlator Output Analysis Computer Program	125

LIST OF TABLES

I.	Evaluation of the transient solution	9
II.	Thermal diffusivity measurement results.	65
III.	Thermal contact conductance measurements, pair A11-A12 . .	66
IV.	Thermal contact conductance measurements, pair A14-A15 . .	67
V.	Thermal contact conductance measurements, pair A13-A14 . .	69
VI.	Thermal contact conductance measurement, pair A14-II . . .	71
VII.	Summary of thermal contact conductance results	74

LIST OF FIGURES

1. Amplitude and phase of the temperature wave in a slab. Thickness of the slab = $1 L_{1/e}$	12
2. Amplitude and phase of the temperature wave in a slab. Thickness of the slab = $3 L_{1/e}$	13
3. Amplitude and phase of the temperature wave in a slab. Thickness of the slab = $5 L_{1/e}$	14
4. Reflected wave amplitude at interface.	21
5. Reflected wave phase	22
6. Transmitted wave amplitude at interface.	23
7. Transmitted wave phase at interface.	24
8. Phase difference at interface.	26
9. Phase lag profile before interface $\Gamma = .316$	27
10. Phase lag profile before interface $\Gamma = 1$	28
11. Phase lag profile before interface $\Gamma = 1.258$	29
12. Phase lag profile before interface $\Gamma = 3.162$	30
13. Temperature distribution in a cylindrical rod with constant circumferential surface temperature at one end.	34
14. Contact conductance specimen; dimensions	39
15. Contact conductance specimen	40
16. Mechanical and thermal equipment	42
17. Cross section of the experimental vessel	43
18. Experimental vessel internals.	44
19. Load cell.	46
20. Experimental equipment in the recording position	49

21. Experimental equipment in the record analyzing position	50
22. Temperatures in the specimens and the guard sleeve.	54
23. Temperature records	55
24. Correlator background response function	61
25. Contact thermal conductance measurement results	75
26. Thermocouple interdependence.	77
27. Two models of elemental heat channel.	87
28. Correlator amplitude response, square wave input.	103
29. Correlator amplitude response, sine wave input.	104
30. Correlator amplitude response, randomized sine inputs	107
31. Correlator amplitude response, sinusoidal inputs, products of voltage amplitudes 1	108
32. Filtering and amplifying circuits	113
33. Parameter confidence region for two linear parameters	124
34. Correlation function, run no. 7, A1 5- I 1, 550 lb.	166

NOMENCLATURE

A	Amplitude of oscillations
A_r	Amplitude of the reflected wave
A_t	Amplitude of the transmitted wave
a	Coefficient
b	Linear dimension
b, b_i	Parameter vector, element
$b_o, b_{i,o}$	Parameter vector, element, giving least sum of squares
$b_{mj}, b_{i,mj}$	Parameter vector, element, at support plane confidence limit for parameter b_j
C	Constant
C_f	Feedback capacitance
c_p	Specific heat
d	Linear dimension
e	Vector of errors
$F_{cb}(x_i)$	Correlator background function
f	Frequency
f_b	Break frequency
f_N	Nyquist frequency
$f(t)$	Record in time
$g(t)$	Record in time
$H(w)$	Frequency response function
h	Heat transfer coefficient
k	Integer, number of parameters
k	Thermal conductivity

L	Length, thickness
$L_{1/e}$	Temperature wave attenuation length
l	Length
n	Integer, number of data points
n(t)	Noise record
P	Matrix of derivatives of predicted values
q"	Heat flow per unit area
R	Thermal resistance
R_i, R_f	Input and feedback electric resistance
SS	Sum of deviations squared
s	Laplace transform variable
s(t)	Signal component of record in time
s_e	Standard deviation estimate
T	Temperature
T_o	Steady temperature level
t	Time
t_i	Integration time
t_o	Period of oscillations
U_i, U_o	Voltage, input and output
V	Temperature
X_i	Independent variable vector
y	Vector of observations
$y^{(x_i)}, y_i$	Observation corresponding to X_i
\hat{y}, \hat{y}_i	Predicted values vector and element corresponding to X_i

$\hat{y}_o, \hat{y}_{i,o}$	Predicted values vector giving least sum of errors squared, element corresponding to x_i
$\hat{y}[b]$	Predicted values vector corresponding to parameter vector b
x	Distance
Z	Matrix of component function values
$Z_j(x_i)$	Component function value corresponding to x_i

Greek Symbols

α	Thermal diffusivity
Γ	Ratio of thermal properties
γ	Heat transfer parameter
δ	Phase angle
δ_r, δ_t	Reflected and transmitted wave phase change at interface
λ	Reciprocal of attenuation length
ξ	Distance
ρ	Density
σ	Standard deviation
τ	Delay time
τ_m	Maximal delay time
$\phi_{f_g}(\tau)$	Correlation function
ϕ	Phase angle
ω	Angular velocity
ω_b	Break angular velocity

1. INTRODUCTION

Angstroem (3, 4) reported first measurements of thermal diffusivity of metals by the temperature wave method more than 100 years ago. Since that time numerous investigators have examined the method as the measuring equipment improved (21, 30, 29). Generally, the accuracy of the results obtained was comparable to stationary measurements, yet the method never achieved widespread use since it is more time consuming, both in acquisition and interpretation of data. The method has an advantage for the measurement of the thermal diffusivity (dimensions: length²/time) since only distance and time measurements are necessary, compared to the conductivity measurements where heat flow also has to be determined.

In the temperature wave method the measurements are made when periodic temperature variations are achieved in the specimen. Related to this method are the transient methods, where the temperature development is followed after a pulse or step input is applied to the specimen. A transient method was developed recently by several investigators (11, 13, 26) for measurements of the thermal diffusivity of small samples. The temperature history of the back side of a thin sample is followed after a pulse of intensive radiation is delivered to the front side from a laser beam. The method is fast and applicable to a wide range of materials and temperature levels and has been successfully used in practical measurements (22, 25).

The present investigation was in part stimulated by the intensive investigation of neutron diffusion waves (31), which are governed in the diffusion approximation by the same equations. Some similarities

exist although the differences are probably greater than the similarities. One of the interesting similarities is that of the concept of reflection and transmission of diffusion waves. Since temperature waves (or heat waves) fall in this category, it is thought that the contact resistance for the heat flow across an interface might be better understood with the application of this analytical technique. As no literature has been uncovered which reports on the use of this technique for this purpose, it may be of great value. The success of this investigation may have great practical application for the measurement of the thermal contact resistance between the cladding and the fuel in a nuclear fuel element. The idea is to determine the thermal properties of the assembly from the response of the cladding temperature to variations (oscillations) of the fuel power level. BURDG et al. (9) performed some experiments, but concluded that the sensitivity of the method is not satisfactory, in part due to the unrefined data analysis.

The uncertainty of the contact resistance in nuclear fuel elements for a while spurred the research in this field. Since nuclear fuel elements are currently designed by experience, good predictions are still lacking for the contact thermal resistance. Presently the most interest for this problem is centered in the area of space technology.

The additional resistance to the heat flow at the interface of two solids arises primarily from the reduced heat flow cross section area, as the real surfaces contact only on a fraction of the apparent contact area. This is due to the waviness and roughness of the surfaces. The heat flow is split at the interface and constricted to individual points

of real contact. The problem of predicting the contact resistance is usually subdivided into three steps: determination of the constriction resistance for an elemental channel (region of the solids associated with a single contact point), determination of the number of contact points, their dimensions and distribution, and third, superposition of the elemental channel solutions. Early investigators, e.g. Holm (13), assumed rather idealized conditions of uniformly spaced contact points. Later much attention was given to the determination of the number and distribution of the real contacts (10, 32). Here important influences are pressure, roughness, waviness, indentation hardness and the elastic properties of the solids in contact. Most investigators that were attempting to correlate the experiments with the predictions did so for nominally flat surfaces, the specimens were prepared by roughening surfaces that were previously polished to optical flatness. In machined joints the waviness is however often more important than the roughness. The third task, superposition of the solutions for the elemental channels of various sizes and nonuniform distribution has also not yet been solved satisfactorily. Recently some progress has been made in this area (24, 32).

An interesting anomaly in the contact resistance was noted, to the elucidation of which the temperature wave method may prove valuable. It was noticed that in an aluminum-steel pair the resistance is higher for the heat flow from steel to aluminum than in the reverse direction (6, 28). The difference amounted to approximately 20% in air and 100% in vacuum being approximately the same in absolute value, in the measure-

ments reported by Rogers (28). Postulated causes for this effect were attributed to the influence of local strains (32) and to different electric potentials of the two metals that impede the movement of electrons in one direction (28). None of the predicting theories includes a satisfactory explanation for this directional effect. With the temperature wave method, a new mode of heat flow is available. Periodic heat flow is applied and, more important, the temperature differences can be quite small compared to the steady state measurements.

Very few references exist in the literature concerning the temperature wave method of measuring the thermal resistance of contacts. Green (16) investigated the thermal impedance of the surface layers but his work is only partially relevant to this investigation. Alzofon (2) theoretically investigated the optical properties of temperature waves, but with the intention of constructing the steady state solutions. Heasley (17) and others (12, 18) treated the transient contact resistance for the evaluation of the heat transfer between bodies at different temperatures brought into contact. The problem in this later case is symmetric while when a temperature wave approaches a discontinuity the situation in the two solids is not identical.

Based on the reported work in the areas briefly outlined above the purpose of this investigation was set at designing and building the equipment for the temperature wave measurements and establishing the method of analyzing the data. Both results can be used in the further investigation of the contact thermal resistance and the application of the temperature wave method in other research.

2. THEORY

In this investigation the temperature waves were generated in a metallic rod or in an assembly of two contacting rods by alternating the heat input at one end and keeping the other end at a constant temperature. The rods were of substantial diameter and well insulated. In the case of two contacting specimens the interface was perpendicular to the axis of the specimens. Thus the heat conduction problems are of a one dimensional transient nature. The analytical solutions of these problems are investigated in this section.

For the case of two contacting solids a constant heat transfer coefficient is considered to be applicable. It may be questionable whether some variable heat transfer coefficient would be more appropriate because the heat transfer is periodic. Also it may be doubtful that the heat transfer coefficient so measured corresponds to the stationary measured quantity. In Appendix A the transient response of an elemental heat channel is investigated and it is shown that, by considering the dimensions of the real contacting points and their spacing in the contacts of flat metallic surfaces, the time scale on which the transient effects are important is of the order of .1 sec. The periods considered for the experiments are of the order of 100 seconds and thus the transient effects certainly can be neglected.

Whether the heat transfer coefficient measured by the periodic heat flow method is identical to the one obtained by a stationary method cannot be resolved at this time. A possible reason for a systematic difference could be a directional heat flow effect. For

steel-aluminum contacts, differences of up to 100% have been observed between measurements with different directions of heat flow (16, 17). As the exact mechanism of this effect is not known, a similar discrepancy for the periodic heat flow case cannot be ruled out but should be investigated experimentally.

2.1 Temperature Waves in a Slab

2.1.1 Stationary Boundary at Constant Temperature

The one dimensional heat conduction problem is solved for a slab with periodic temperature on one boundary and constant temperature on the other boundary. The governing equation is

$$\alpha \frac{\partial^2 T(x,t)}{\partial x^2} = \frac{\partial T(x,t)}{\partial t} \quad (1)$$

where $\alpha = \frac{k}{\rho c_p}$

The initial condition is

$$T(x,0) = 0 \quad (2)$$

and the boundary conditions are

$$\begin{aligned} T(L,t) &= A \sin \omega t & t > 0 \\ T(0,t) &= 0 & t > 0 \end{aligned} \quad (3)$$

To obtain the solution of this problem the Laplace transform technique

is used. Transforming the variable t into the Laplace variable s the governing equation is

$$\alpha \frac{d^2 \bar{T}(x,s)}{dx^2} = s\bar{T}(x,s) - T(x,0) \quad (4)$$

applying the initial conditions this reduces to

$$\frac{d^2 \bar{T}(x,s)}{dx^2} = \frac{s}{\alpha} \bar{T}(x,s) \quad (4a)$$

This equation has the general solution

$$\bar{T}(x,s) = C_1(s) e^{\sqrt{\frac{s}{\alpha}} x} + C_2(s) e^{-\sqrt{\frac{s}{\alpha}} x} \quad (5)$$

The transformed boundary conditions are

$$\bar{T}(0,s) = 0$$

$$\bar{T}(L,s) = \frac{A\omega}{\omega^2 + s^2} \quad (6)$$

From these boundary conditions the constants C_1 and C_2 are evaluated:

$$C_2 = -C_1$$

$$C_1 = \frac{A\omega}{\sinh\left(\sqrt{\frac{s}{\alpha}} L\right) (\omega^2 + s^2)} \quad (7)$$

$$\bar{T}(x, s) = \frac{A\omega}{\omega^2 + s^2} \frac{\sinh \sqrt{\frac{s}{\alpha}} x}{\sinh \sqrt{\frac{s}{\alpha}} L} \quad (8)$$

The inverse transform is found by the theorem of residues, as the only singularities are poles. Furthermore all poles are simple. The first part of the denominator has two zeroes, $s = \pm i\omega$. It can be shown that the only zeros of the function $\sinh \sqrt{\frac{s}{\alpha}} L$ are at

$$\sqrt{\frac{s}{\alpha}} L = in \pi$$

and thus

$$s = -\frac{2n^2\pi^2}{L^2} \alpha \quad n = 1, 2, \dots \quad (9)$$

Omitting the algebraic steps in the evaluation of the residues, the final result is

$$\text{Residue at } (i\omega) + \text{Residue at } (-i\omega) = \frac{2A}{\cosh 2\lambda L - \cos 2\lambda L} [\sin \omega t$$

$$(\sinh \lambda x \cos \lambda x \sinh \lambda L \cosh \lambda L + \cosh \lambda x \sin \lambda x \cosh \lambda L \sin \lambda L)$$

$$+ \cos \omega t (-\sinh \lambda x \cos \lambda x \cosh \lambda L \sin \lambda L + \cosh \lambda x \sin \lambda x$$

$$\sinh \lambda L \cos \lambda L)]$$

$$\text{where } \lambda = \sqrt{\frac{\omega}{2\alpha}} \quad (10)$$

The residue at any pole, $s_n = -\frac{n\pi}{L^2} \alpha$, is

Residue at $(-\frac{n\pi\alpha}{L^2}) =$

$$\frac{2A\omega(-1)^{n+1}}{(\omega^2 L^2 + \alpha^2 \frac{n^4 \pi^4}{L^2})} n\pi\alpha \sin \frac{n\pi x}{L} e^{-\frac{\alpha n^2 \pi^2}{L^2} t} \quad (11)$$

These terms decay with time and represent the transient part of the solution, while the terms corresponding to the poles $\pm i\omega$ represent the asymptotic part of the solution. The transient solution is not particularly interesting as the measurements are performed after steady state is achieved. The magnitude of the transient part is briefly evaluated as follows.

Introducing $t_0 = \frac{2\pi}{\omega}$ (period of oscillation) and $L_{1/e} = 1/\lambda = \sqrt{\frac{2\alpha}{\omega}}$ (attenuation distance) the time necessary for the slowest decaying term to be reduced by a certain factor can be evaluated. In Table I the number of periods for a 100 fold reduction of the slowest decaying term in slabs of different thicknesses are presented.

Table I

Evaluation of the transient solution.

Dimensionless thickness of the slab, $L/L_{1/e}$	Reduction of the first transient term per period	No. of periods for a 100 fold reduction
4	.135	2.2
6	.422	5.2
8	.618	9.5
10	.734	14.5

2.1.2 Asymptotic Solution for a Thick Slab.

Two useful approximations can be derived from the asymptotic solution Eq. (10) for thick slabs ($L/L_1/e$ large). For $\lambda L \gg 1$ the approximation

$$\cosh \lambda L \approx \sinh \lambda L \approx \frac{1}{2} e^{\lambda L}$$

can be used and $\cos 2\lambda L$, which is always less than unity can be neglected in the denominator of Eq. (10). Substituting the exponential expressions for the hyperbolic functions and implementing the addition theorems for the harmonic functions the result

$${}_1T(x,t) = \frac{A}{\lambda L} [e^{\lambda x} \sin(\omega t - \lambda(L-x)) - e^{-\lambda x} \sin(\omega t - \lambda(x+L))] \quad (12)$$

is obtained.

This expression shall be called the "one reflection approximation".

If furthermore x is large, i.e. only the regions far from the stationary boundary are observed, the result is

$${}_0T(x,t) = A e^{-\lambda(L-x)} \sin(\omega t - \lambda(L-x)) \quad (13)$$

This expression shall be called the "no reflection approximation".

The one reflection approximation, Eq. (12), can be interpreted as the sum of two waves, one approaching the boundary with the constant temperature and the other wave leaving this boundary with reversed sign.

Each wave has the form

$$C e^{-\lambda \xi} \sin(\omega t - \lambda \xi) \quad (14)$$

where ξ is the linear dimension measured in the direction of the wave travel.

The amplitudes and the phase lags were calculated from the three expressions, the exact asymptotic solution, Eq. (10), the no- and one-reflection approximations, Eqs. (12) and (13); for slabs of various thicknesses. The results are presented in Figures 1 to 3. From the numerical results the following can be concluded: For slabs thicker than $3 L_{1/e}$ the no-reflection approximation is adequate, except closer than $1.5 L_{1/e}$ from the stationary boundary where the one reflection approximation is to be used. For slabs thinner than $1.5 L_{1/e}$ the exact solution is to be used instead of the reflection approximations.

2.1.3. Stationary Boundary Insulated

The governing equation, initial condition and the periodic boundary condition are same as before, Eqs. (1), (2) and (3), but on the stationary boundary the following condition is applied:

$$\frac{\partial T}{\partial x}(0, t) = 0 \quad (15)$$

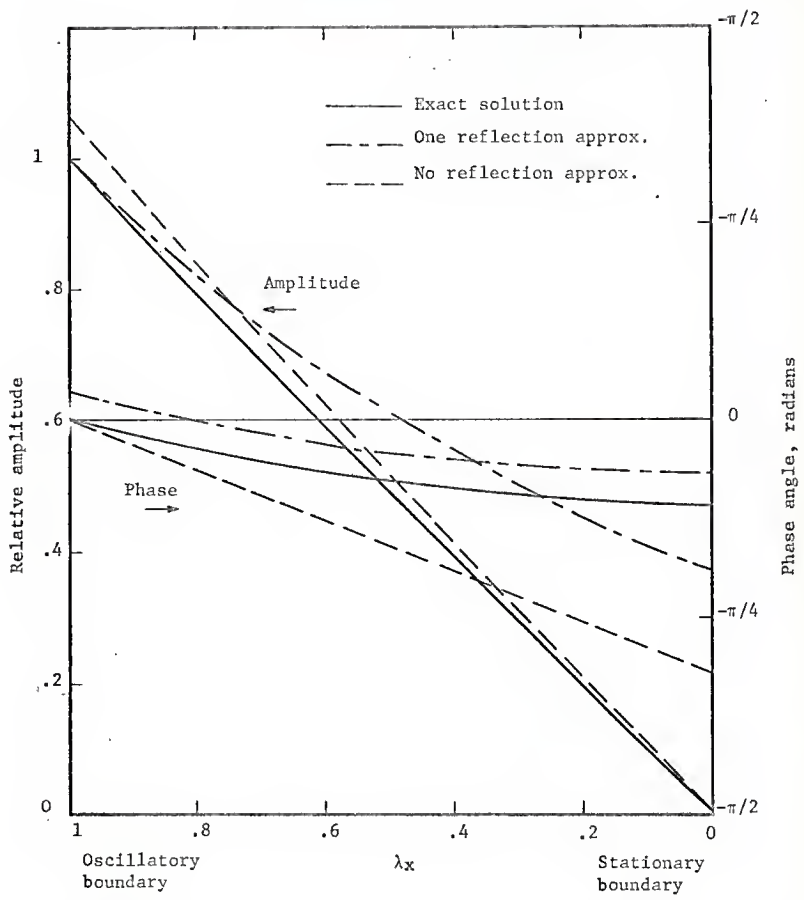


Figure 1. Amplitude and phase of the temperature wave, thickness of the slab = $1 L_1/e$.

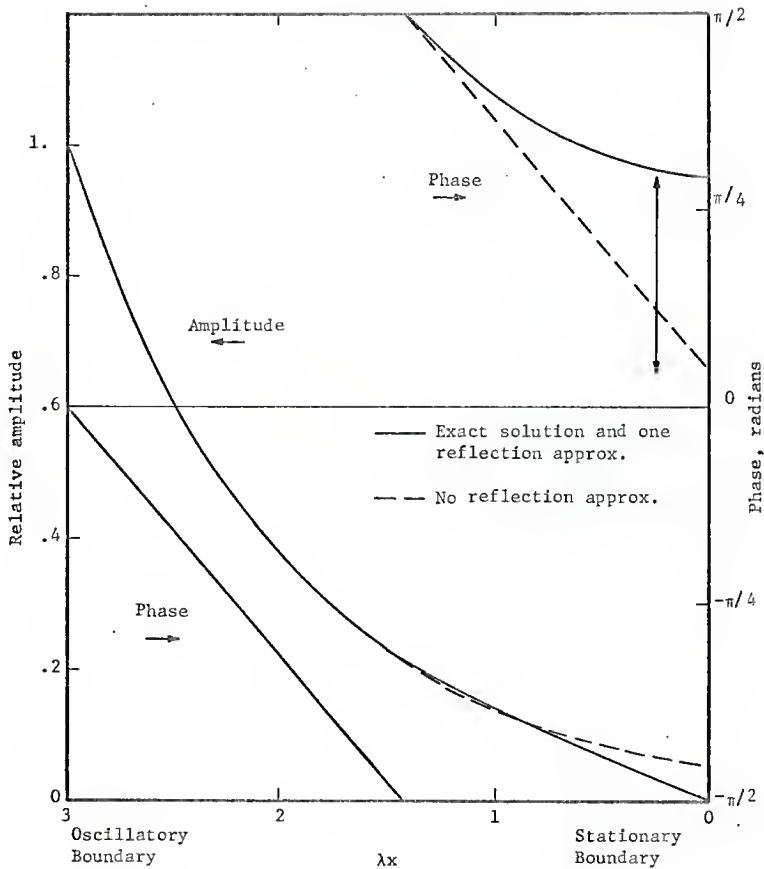


Figure 2. Amplitude and phase of the temperature wave, thickness of the slab = $3L_{1/e}$.

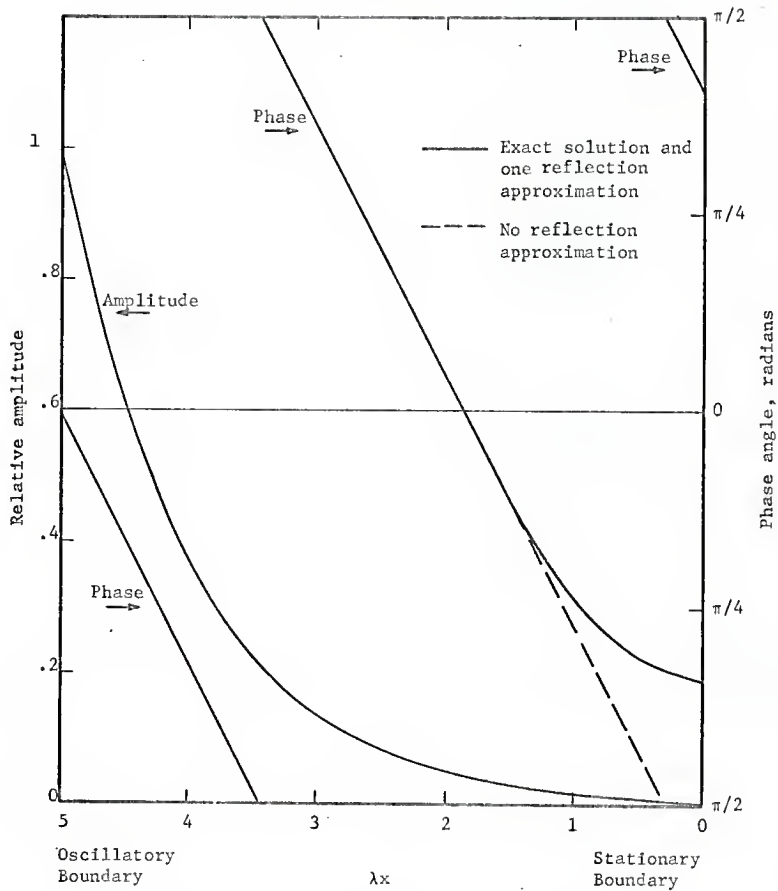


Figure 3. Amplitude and phase of the temperature wave, thickness of the slab = $5 L_{1/e}$

Due to this boundary condition the relation of the constants in the Laplace transformed solution is

$$C_1(s) = C_2(s) \quad (16)$$

Further the solution is obtained in a similar way as before, and the result is

$$\bar{T}(x,s) = \frac{A}{\omega^2 + s^2} \frac{\cosh \sqrt{\frac{s}{\alpha}} x}{\cosh \sqrt{\frac{s}{\alpha}} L} \quad (17)$$

The inverse transform can again be obtained by evaluation of the residues. The first part of the transform has two simple poles, $s_{1,2} = \pm i\omega$ and it can be shown that the function $\cosh \sqrt{\frac{s}{\alpha}} L$ has zeroes at

$$s_n = -\frac{(2n-1)^2 \pi^2}{2L^2} \alpha \quad (18)$$

i.e. when

$$\sqrt{\frac{s}{\alpha}} L = i \left(\frac{2n-1}{2} \right) \pi \quad n = 1, 2, \dots,$$

These poles are on the negative real axis and thus the contribution of their residuals is of transient nature. The residues at the two poles on the imaginary axis form the asymptotic solution;

Residue at $(i\omega)$ + Residue at $(-i\omega)$ =

$$= \frac{A}{(\cosh 2\lambda L + \cos 2\lambda L)} [\cos \omega t (-\cosh \lambda x \cos \lambda x \sinh \lambda L \sin \lambda L +$$

$$+ \sinh \lambda x \sin \lambda x \cosh \lambda L \cos \lambda L) + \sin \omega t (\cosh \lambda x \cos \lambda x \cosh \lambda L \cos \lambda L +$$

$$+ \sinh \lambda x \sin \lambda x \sinh \lambda L \sin \lambda L)] \quad (19)$$

For thick slabs using the same assumptions as in section 2.1.2, the result becomes

$$T(x,t) = Ae^{-\lambda L} [e^{\lambda x} \sin(\omega t - \lambda(L-x)) + e^{-\lambda x} \sin(\omega t - \lambda(L+x))] \quad (20)$$

This result can be interpreted as consisting of two parts, a first term representing a wave approaching the insulated boundary at $x = 0$ and a second term representing a wave leaving this boundary. At the boundary the two waves are in phase and reinforce each other, while in the case of the constant boundary temperature they were of opposite phase.

2.2 Temperature Wave at a Discontinuity

The behavior of a plane temperature wave at a contact of two solids, the contacting surface being perpendicular to the direction of the wave travel, shall be investigated. The heat transfer characteristics of the discontinuity is assumed to be

$$q'' = h\Delta T \quad (21)$$

where q'' is the heat flow per unit area, h is the heat transfer coefficient and ΔT is the temperature drop across the discontinuity. The coordinate x is placed parallel to the direction of the approaching temperature wave (perpendicular to the discontinuity) and the origin is placed at the discontinuity. In analogy with the case of the insulated boundary or the stationary boundary the solution is expected to consist of a reflected wave with some phase change but with the same period and a transmitted wave, also with some phase change. The forms assumed are, the amplitudes being normalized so that the approaching wave has amplitude 1 at discontinuity:

Approaching wave

$$e^{-\lambda_1 x} \cos(\omega t - \lambda_1 x) \quad (22)$$

Reflected wave

$$A_r e^{\lambda_1 x} \cos(\omega t + \delta_r + \lambda_1 x) \quad (23)$$

Transmitted wave

$$A_t e^{-\lambda_2 x} \cos(\omega t + \delta_t - \lambda_2 x) \quad (24)$$

Taking the amplitude of the approaching wave as unity at $x = 0$, the time dependent temperatures in solids 1 and 2 are

$$T_1(x, t) = e^{-\lambda_1 x} \cos(\omega t - \lambda_1 x) + A_r e^{\lambda_1 x} \cos(\omega t + \delta_r + \lambda_1 x) \quad x \leq 0 \quad (25)$$

$$T_2(x, t) = A_t e^{-\lambda_2 x} \cos(\omega t + \delta_t - \lambda_2 x) \quad x \geq 0 \quad (26)$$

Substituting these expressions into the equations of heat balance at the discontinuity

$$-k_1 \frac{\partial T_1}{\partial x}(0, t) = q''(0, t) = h(T_1(0, t) - T_2(0, t)) \quad (27)$$

$$-k_2 \frac{\partial T_2}{\partial x}(0, t) = q''(0, t) = h(T_1(0, t) - T_2(0, t)) \quad (28)$$

yields

$$\begin{aligned} -k_1 \lambda_1 [A_r (\cos(\omega t + \delta_r) - \sin(\omega t + \delta_r)) - (\cos \omega t - \sin \omega t)] = \\ = h[\cos \omega t + A_r \cos(\omega t + \delta_r) - A_t \cos(\omega t + \delta_t)] \end{aligned} \quad (29)$$

and

$$\begin{aligned} k_2 \lambda_2 A_t [\cos(\omega t + \delta_t) - \sin(\omega t + \delta_t)] = \\ = h[\cos \omega t + A_r \cos(\omega t + \delta_r) - A_t \cos(\omega t + \delta_t)] \end{aligned} \quad (30)$$

The material constants and the heat transfer coefficient can be grouped in dimensionless quantities

$$\gamma_1 = h/k_1 \lambda_1 \quad \gamma_2 = h/k_2 \lambda_2 \quad (31)$$

This quantity relates the heat transfer distance k/h , i.e. the thickness of the solid causing the same temperature drop as the discontinuity, to the $1/e$ length of the temperature waves, $L_{1/e} = 1/\lambda = \frac{\sqrt{2\alpha}}{\omega}$.

After using the summation theorems for the trigonometric functions and observing that the identity has to be conserved at all times, four equations are obtained from Eq. (29) and (30)

$$\begin{aligned}
 -(1+\gamma_1) A_r \cos \delta_r + A_r \sin \delta_r + \gamma_1 A_t \cos \delta_t &= -(1-\gamma_1) \\
 A_r \cos \delta_r + (1-\gamma_1) A_r \sin \delta_r - \gamma_1 A_t \sin \delta_t &= 1 \\
 -\gamma_2 A_r \cos \delta_r + (1+\gamma_2) A_t \cos \delta_t - A_t \sin \delta_t &= 2 \\
 \gamma_2 A_r \sin \delta_r + A_t \cos \delta_t + (1+\gamma_2) A_t \sin \delta_t &= 0
 \end{aligned} \tag{32}$$

From this system of linear equations for $A_r \cos \delta_r$, $A_r \sin \delta_r$, $A_t \cos \delta_t$ and $A_t \sin \delta_t$ these quantities can be calculated for any values γ_1 and γ_2 and from them the amplitude and phase of the temperature oscillation at any point in both solids can be obtained.

The asymptotic solution for γ_1 and γ_2 approaching infinity cannot be obtained from the system Eq. (32), as the problem formulation Eqs. (27), (28) is not correct in this case. The following conditions have to be used at the interface

$$T_1(0, t) = T_2(0, t) \tag{33}$$

$$k_1 \frac{\partial T_1}{\partial x} (0, t) = k_2 \frac{\partial T_2}{\partial x} (0, t) \quad (34)$$

Introducing the assumed wave forms, Eqs. (22), (23), (24), performing the algebraic manipulations and solving the resulting linear system of equations the following is obtained

$$\begin{aligned} A_t \cos \delta_t &= \frac{2\Gamma}{1+\Gamma} & A_t \sin \delta_t &= 0 \\ A_r \cos \delta_r &= \frac{\Gamma-1}{\Gamma+1} & A_r \sin \delta_r &= 0 \end{aligned} \quad (35)$$

where Γ is defined as

$$\Gamma = \frac{k_1 \lambda_1}{k_2 \lambda_2} = \sqrt{\frac{k_1 c_p \rho_1}{k_2 c_p \rho_2}} = \frac{\gamma_2}{\gamma_1} \quad (36)$$

The quantities A_r , δ_r , A_t , δ_t as functions of γ_1 are plotted for various ratios γ_2/γ_1 in Figures 4 to 7. The asymptotic values are also indicated. The value of the ratio γ_2/γ_1 , i.e. Γ , for metallic pairs ranges between 4 and 1/4. Of all metals the best conductor-capacitor is copper, with the $k\rho c_p$ value of $1,390 \text{ J}^2/\text{m}^4 \text{ c}^2 \text{ sec}$, while poor conductors and capacitors like stainless steel have values around 80 for this parameter.

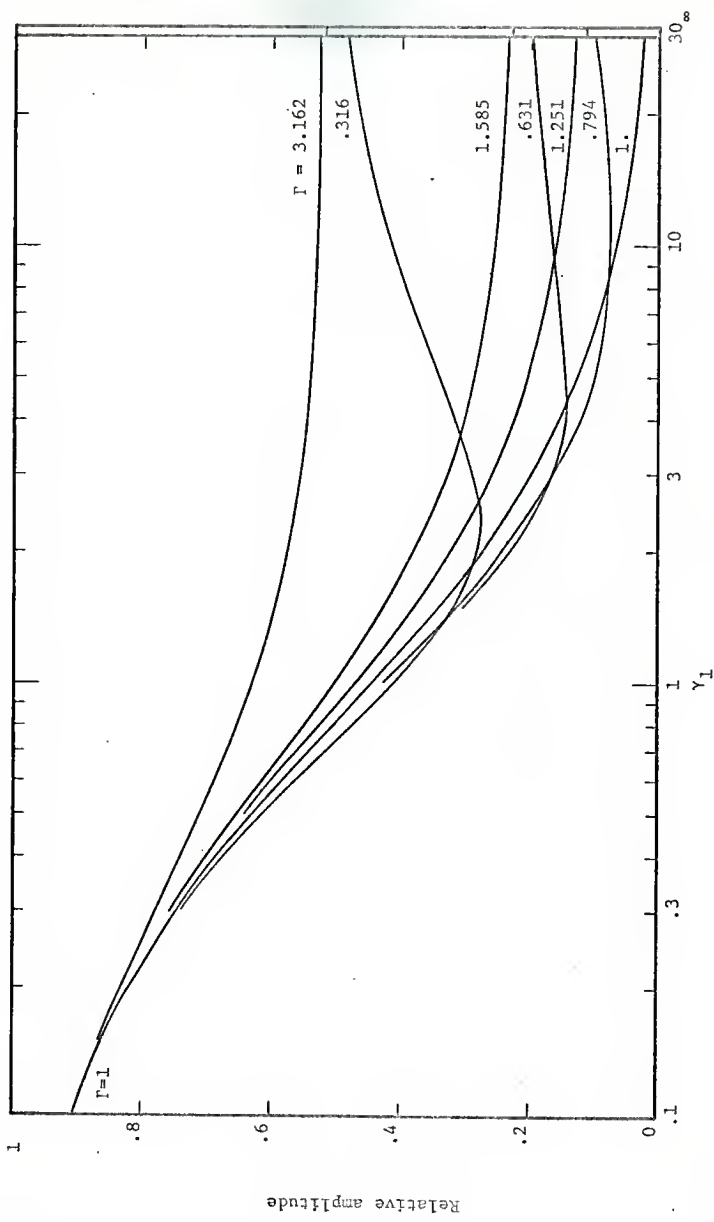


Figure 4. Reflected wave amplitude at interface.

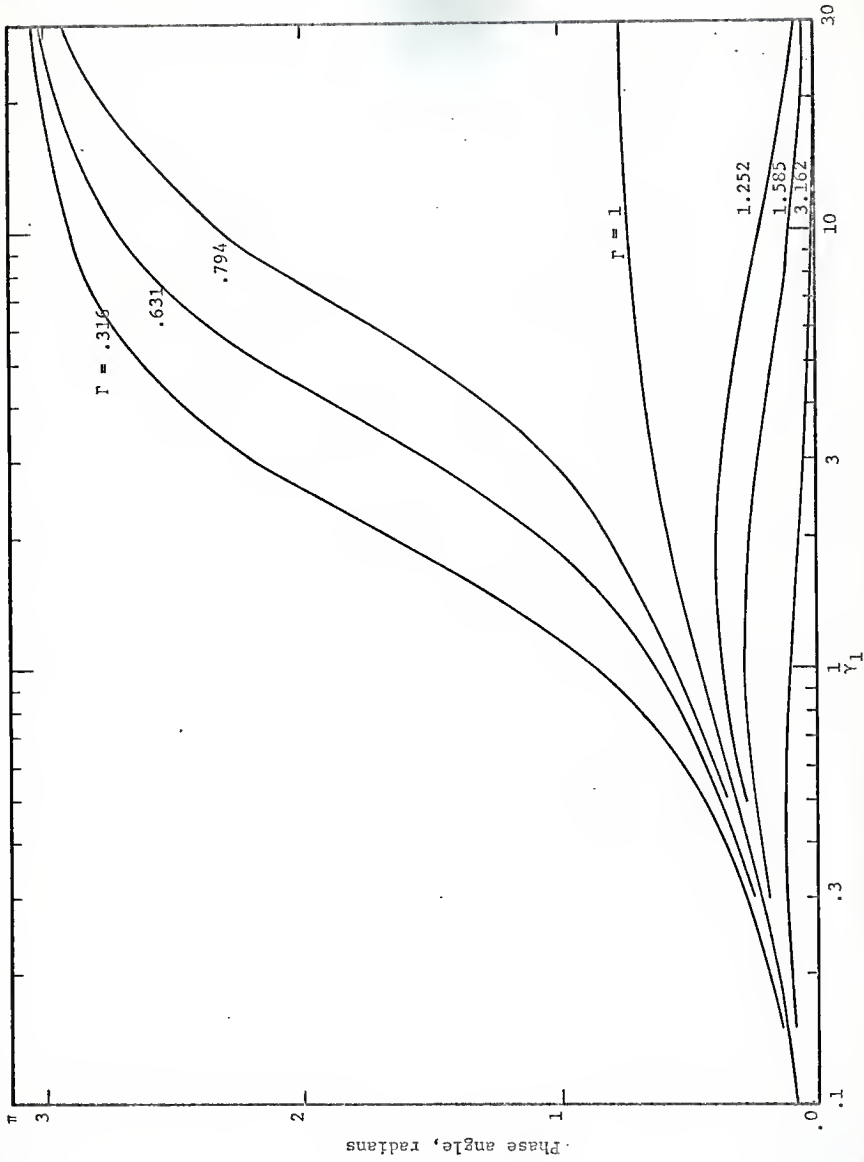


Figure 5. Reflected wave phase at interface.

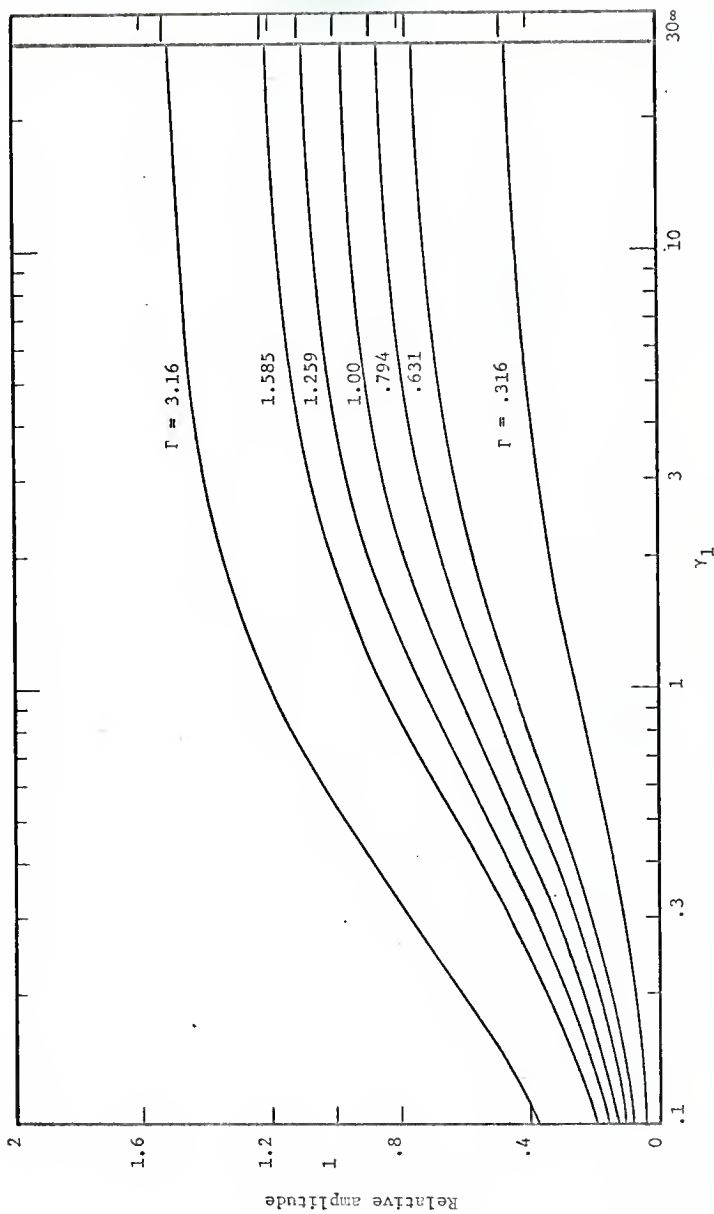


Figure 6. Transmitted wave amplitude at interface.

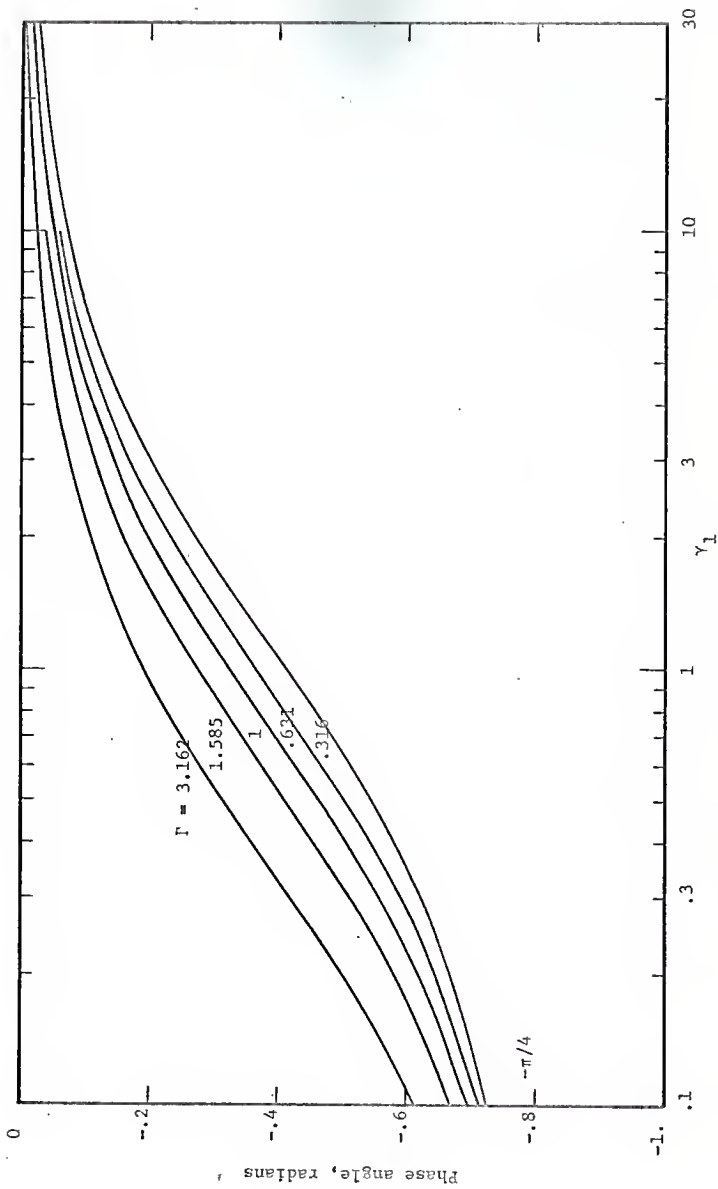


Figure 7. Transmitted wave phase angle at interface.

The graphs of the phase angles and the reflected and transmitted fractions reveal some interesting properties (Figures 5 and 7). The reflected wave always precedes the incoming wave (positive angle δ_r) and the angle asymptotically approaches three values, 0, $\pi/4$ and π , depending on the γ_2/γ_1 ratio. For Γ less than one, i.e. when the second material is a better conductor-capacitor, the reflected wave has opposite phase to that of the incoming wave. The same relation was obtained in the case of the stationary boundary temperature case, only now the amplitude is less than that of the incoming wave and depends on the Γ value. For Γ larger than one the phase approaches zero for large γ_1 and the situation is similar to the insulated boundary case. Note also that for Γ larger than one the transmitted wave amplitude rises above unity, i.e. is larger than that of the approaching wave. This does not violate the boundary conditions at the interface as the reflected wave is in phase with the incoming wave and the sum (vectorial) is always larger than the amplitude of the transmitted wave.

For the ideal contact ($\gamma \rightarrow \infty$, $h \rightarrow \infty$) only two values of the reflected wave phase angle are possible, 0 and π . The curve for $\Gamma = 1$ approaches $\pi/4$, but at infinity the amplitude is zero.

In Fig. 8 the phase difference between the sum of the approaching and the reflected wave and the transmitted wave at the interface is plotted.

In Fig. 9 to Fig. 12 the phase lag profiles in the incoming solid are presented. Note that here the phase lag is plotted, which is defined with the opposite sign as the phase difference.

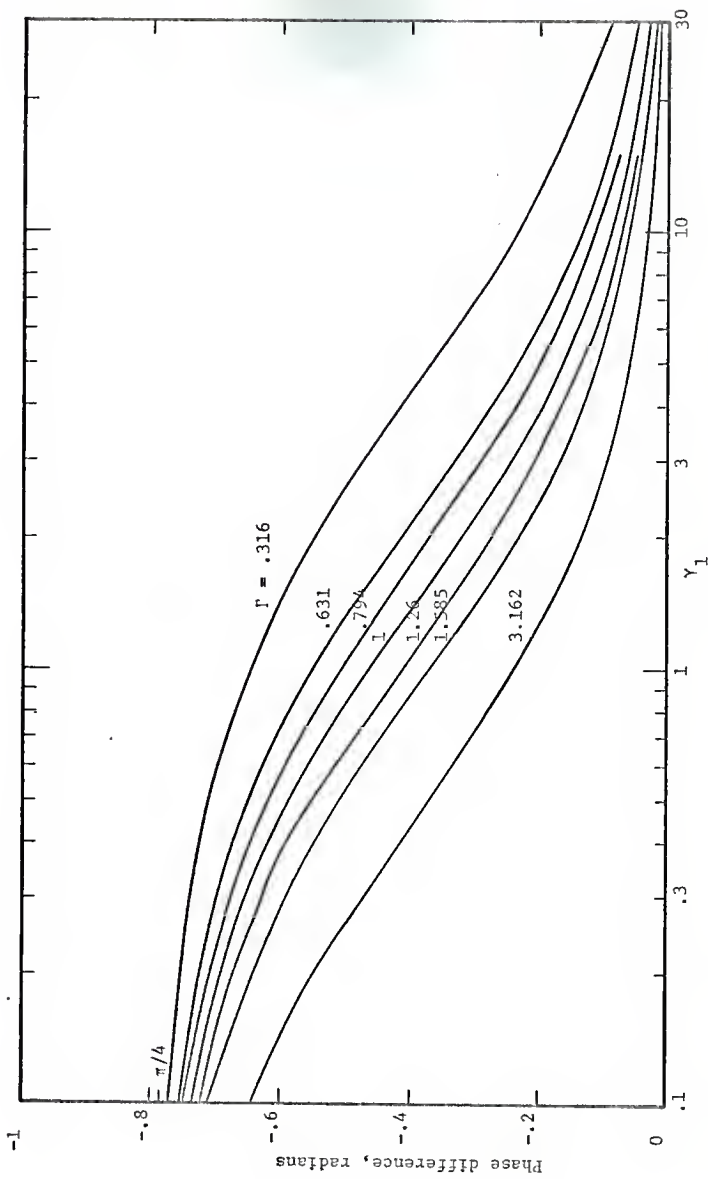
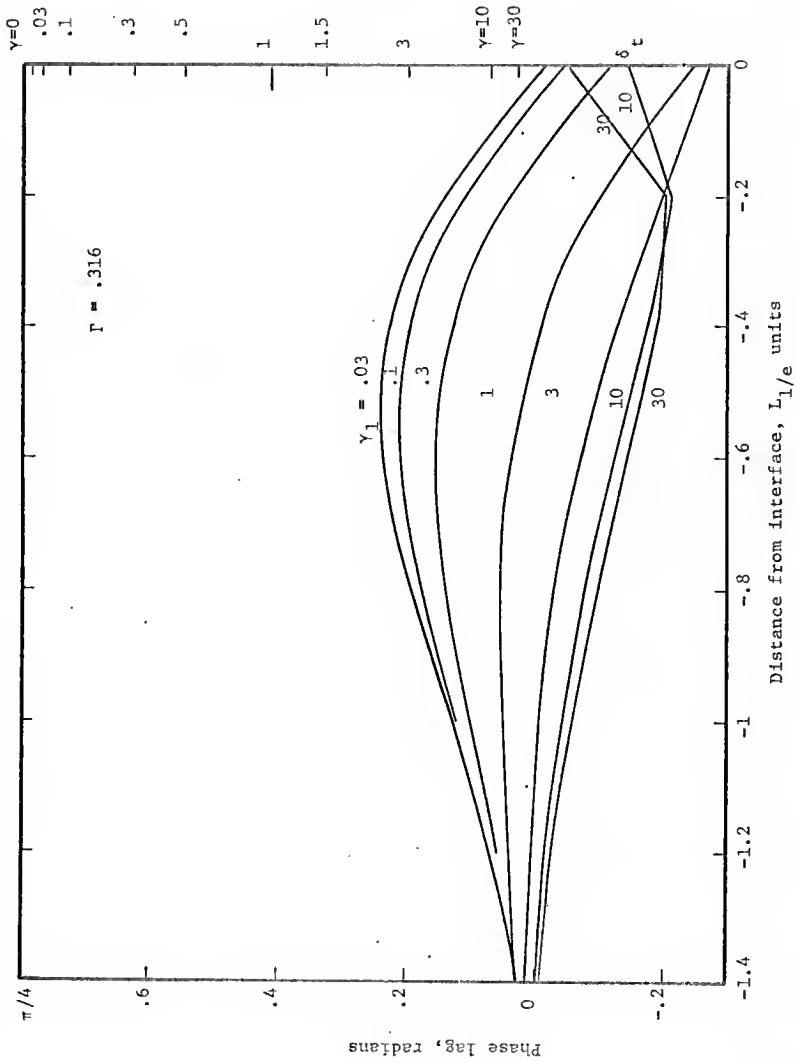


Figure 8. Phase difference at interface

Figure 9. Phase lag profile before interface, $\Gamma = .316$.

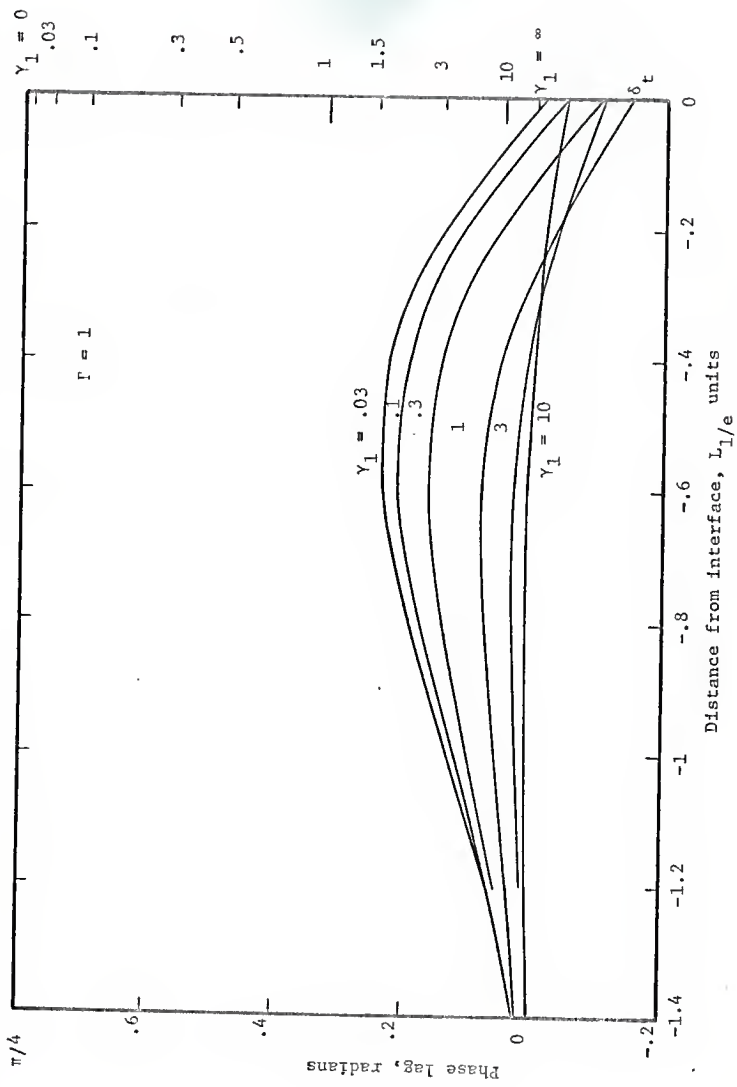


Figure 10. Phase lag profile before interface, $\gamma = 1$

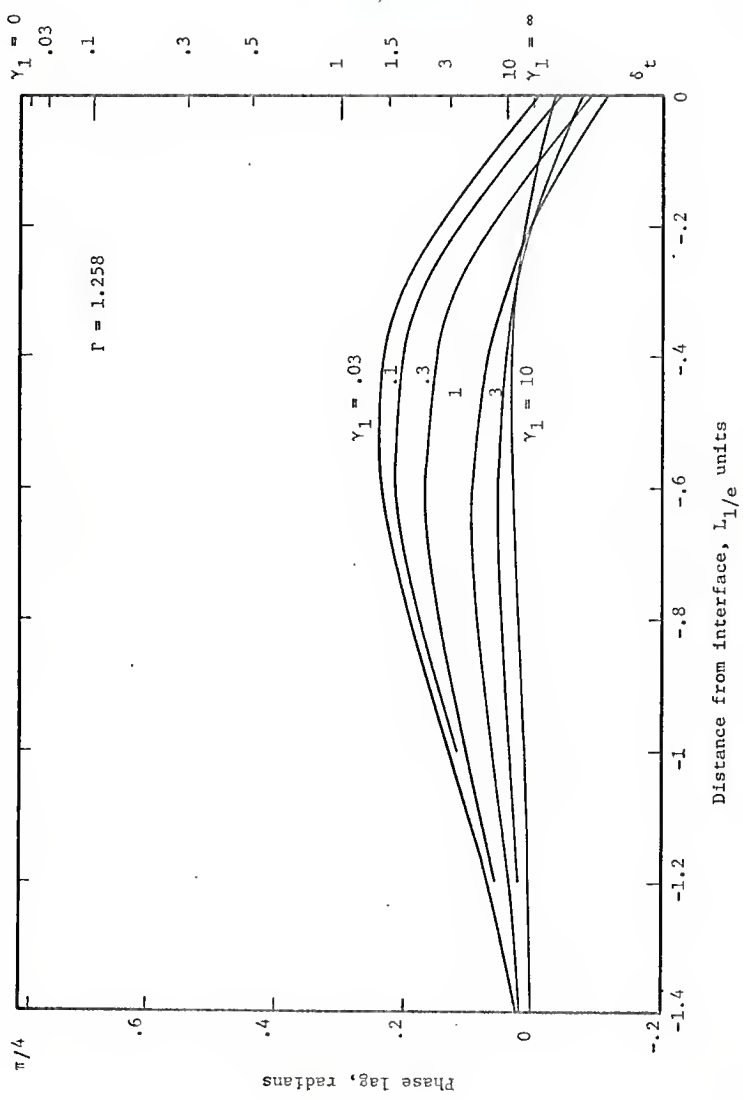


Figure 11. Phase lag profile before interface, $\Gamma = 1.258$

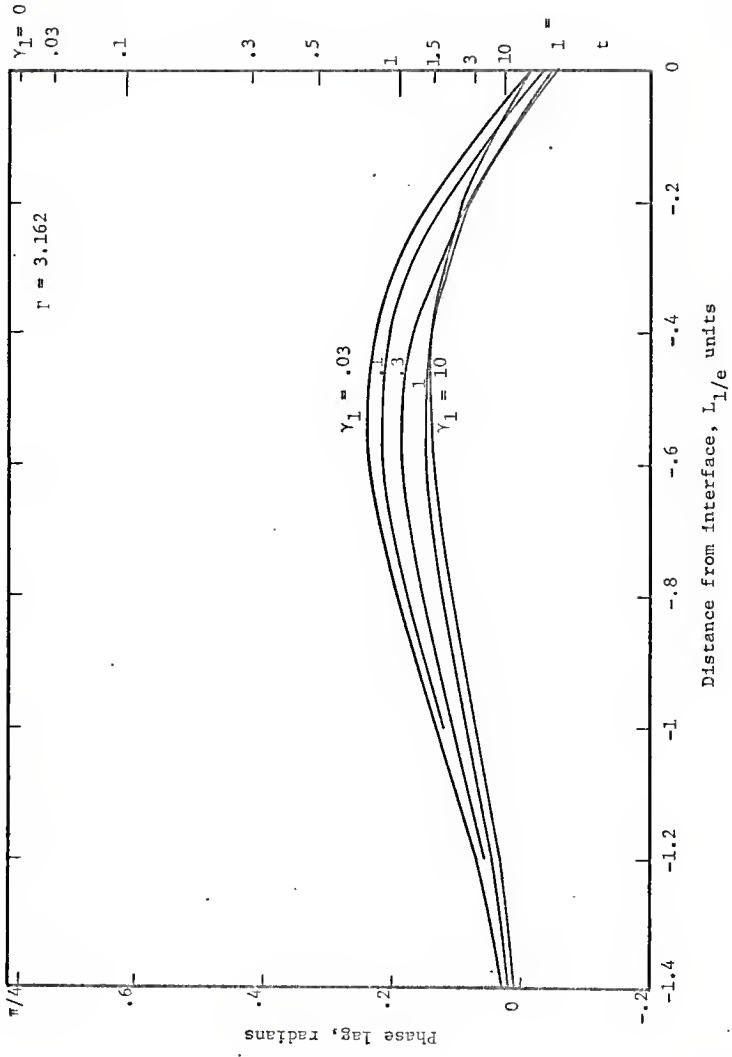


Figure 12. Phase lag profile before interface, $\Gamma = 3.162$

3. EXPERIMENT DESIGN

The purpose of the experimental work was to review the temperature wave method of thermal diffusivity measurements and to investigate the feasibility of contact resistance measurements by this method. Thus there were two groups of preceding experiments to be considered, the temperature wave measurements and the contact conductance measurements. To accomplish the combined task the present experiment differs in some respects from both groups of prototypes.

Angstroem (3) and most later investigators of the temperature wave method (21, 29, 30) did not attempt to restrict the surface heat losses from the specimens, which were in some cases in the form of wires. They rather accounted for these losses in the analysis. In this case the temperature oscillations have to be measured at least at three points. For the contact resistance measurement the specimens have to be of substantial cross section and the heat losses would make the temperature field two dimensional due to the radial flow. To avoid any such further complication, as the contact between the two specimens already introduces some, it was considered preferable in the present experiment to eliminate these surface heat losses if possible.

In the contact resistance experiments, two specimens are usually sandwiched between calibrated heat flow metering sections, possibly other layers of different materials, with the heater and cooler at opposite sides. In such arrangements the temperature waves would be greatly attenuated at each interface. For this reason the specimens

should be in direct contact with the heater and the cooler. The surface heat losses were eliminated in the contact resistance and conductivity measurements by placing a guard sleeve around the specimen with the same temperature gradient as in the specimen. Due to the temperature oscillation, only the mean temperature can be matched in this way. To avoid the heat losses due to the deviations from this mean, insulation is required.

The basic differences of the present design from the two groups of prototype experiments are that the specimens are of substantial diameter and are insulated and in good contact with the heater and cooler. The length of the specimens was chosen primarily with regard to the precision of the thermocouple positioning and the thermocouple dimensions. The temperatures were measured on the axis of the specimens and the thermocouples placed in holes drilled into the specimens. The position of the thermocouple in the hole is not well determined, so the diameter of the hole must be considered as the uncertainty interval for the thermocouple location. With the hole diameters used, .03" or .05", and the thermocouple separation distance of 2", the uncertainty is 3% or 5%, respectively, and it was considered that a shorter distance should not be used. The length of the contact resistance specimens was 7 1/2" and the length of the thermal diffusivity measurement specimens was 15". The periods of oscillation to be used were determined from the distance between the temperature measuring points, so that the attenuation would not be excessive. If the amplitude of the oscillation at the first thermocouple is of the order of a few degrees (higher amplitude would be undesirable),

and the estimated limit of detection is of the order of $.01^{\circ}\text{C}$, it was determined that the distance between the extreme positions should not exceed 5 attenuation lengths, i.e. the attenuation length should not be shorter than $1/5$ of the longest distance.

In the first design, the heater, which generates the temperature oscillations of one end of the specimen, was equipped with a copper plate at the bottom which was placed in contact with the end of the specimen rod. Such arrangement produced very small oscillations of temperature in the specimen due to relatively large thermal capacity of the heater and poor contact with the specimen. The design was subsequently changed in favor of a band heater tightened around the end of the specimen. In this case doubts arise concerning the uniformity of the temperature across the specimen bar. A numerical analysis of the temperature profile was performed and in Fig. 13, the lines of equal temperature are plotted for a rod with constant temperature on part of its circumference and uniform heat flow at a distance from the end. It is evident that the heat flow becomes completely one dimensional less than one diameter from the limits of the uniform temperature of the perimeter. It is assumed that the same is valid for the periodic heat flow and a conservative margin of two rod diameters from the heater was used for the positioning of the first thermocouple. The rod diameter of one inch was chosen arbitrarily.

This arrangement produced temperature oscillations of sufficient amplitude, but a high temperature gradient was needed to deliver the heat to the cooler at the other end of the specimen. Thus a potentially

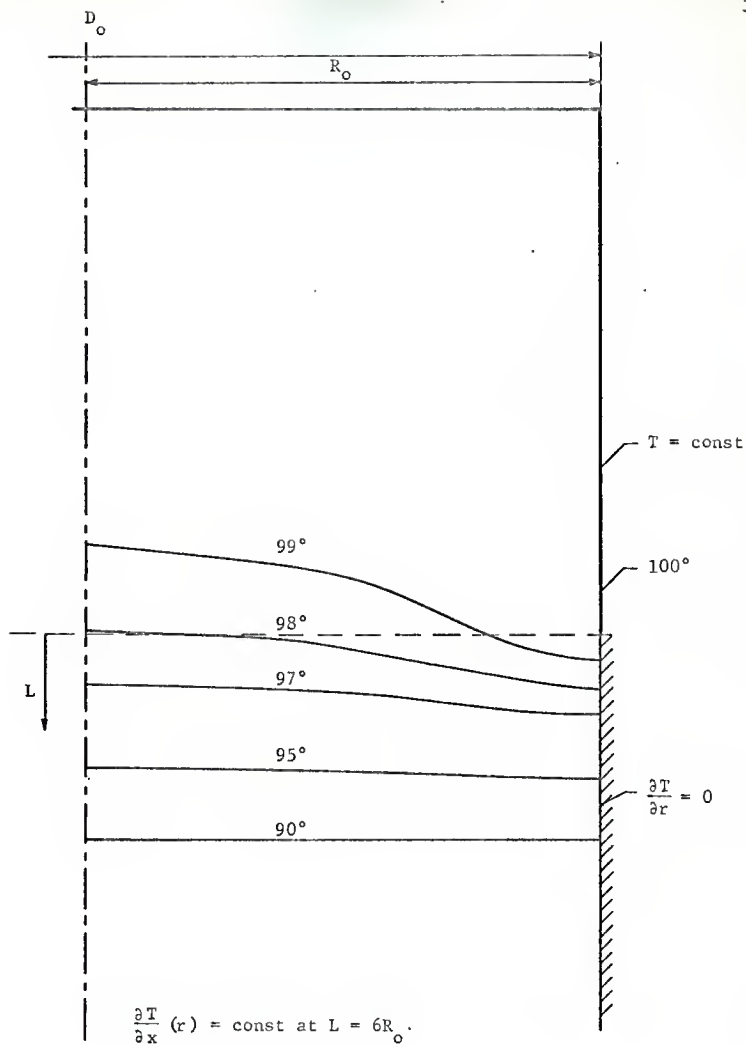


Figure 13. Temperature distribution in a cylindrical rod with constant circumferential surface temperature at one end.

important advantage of the temperature wave method, that it does not intrinsically require large temperature gradients, was lost. Subsequently a cooler was installed at this end, and the flow of coolant was oscillated at the same frequency as the heater. However, the solenoid valve used caused unacceptable disturbances in the thermocouple voltage output due to magnetic induction, so the valve was removed and the coolant flow was maintained constant. Contrary to the expectations, the temperature oscillation amplitude did not decrease significantly when the cooler was operated continuously, and the constant temperature level decreased. This small effect of coolant flow can be attributed to poor heat transfer from the specimen to the coolant as the coolant velocity was quite low.

The theory of the temperature waves was developed for sinusoidal temperature variation on the boundary. To approximate this condition a mechanism was constructed to vary the voltage on the heater harmonically. It was soon perceived that this is not necessary, as any higher harmonic components are very weakly excited in the specimen and die out rapidly along its length. A cam operated on-off control of the heater was installed. With this arrangement, the first higher harmonic was detected only in the first thermocouple output and had a barely significant amplitude.

The largest body of thermal contact conductance data available is for contacts in vacuum. The specimen and heater housing in this investigation was designed for vacuum, but due to undetected faults the required vacuum was not achieved.

Due to the inherent attenuation characteristics of the temperature waves it was anticipated that the signal to noise ratio from the more distant thermocouples would require a refined data analysis technique, considering the accuracy required. The correlation technique offers a possibility of analyzing noisy signals. An outline of the technique is given in Appendix B.

The data acquisition and analysis equipment is centered around the correlation computer. The thermocouple outputs were first recorded on a magnetic tape recorder and analyzed later. A few initial measurements were performed by recording the temperature oscillations on a strip chart recorder and analyzing the records manually, but this proved highly unpractical. One problem of the temperature measurements was associated with the elimination of the electronic noise that was picked up by the thermocouple leads. The noise was mostly of high frequency and was eliminated by passing the signal through a low-pass filter before recording. Later it was found that in the tape recorder itself some high frequency noise is generated and another low-pass filter was used between the tape recorder and the correlator. The analysis of these circuits is given in Appendix D.

The description of the present equipment is given in the following section and an evaluation in section 8.

4. EXPERIMENTAL APPARATUS

The experimental equipment consists of the mechanical and thermal system and of the data acquisition system. The individual parts of the equipment are described below from the specimens to the correlation computer.

4.1 Specimens

For the two types of measurements, the thermal diffusivity measurements and for the contact conductance measurements, two types of specimens were used. The contact resistance specimens were used in pairs, the total length of the pair being the same as a single diffusivity specimen. The choice of the dimensions of the specimens is discussed in section 3.

4.1.1 Thermal Diffusivity Specimens

Solid rods of the material under consideration, 1 inch in diameter and 15 inches long, were used for the thermal diffusivity measurements. Five holes were drilled in each specimen, 2 1/2 inches apart, the first hole being 3 inches from the end that was to be subjected to periodic temperature conditions. The holes were .05 inch diameter and 1/2 inch deep, i.e. they reached the center of the rod. Holes were drilled in both ends of the specimen with a #5 countersink drill to a depth of 1/2 inch, as required for the cooler centering. Thirty gage copper constantan thermocouple wire was used for the thermocouples. The junctions were formed by mercury pool immersion welding and cemented in the holes with Sauereisen cement. Before the installation of the

thermocouples the distance between the thermocouple holes was measured precisely.

4.1.2 Thermal Contact Resistance Specimens

The thermal contact resistance specimens were 1 inch O.D. rods, 7 1/2 inches long (Fig. 14). Three holes were drilled along the rod 2 inches apart, the distance of the closest point from the contacting surface being 1/2 inch. All holes were .031 inch diameter and 1/2 inch deep, the bottom, located at the center of the rod. In one end of the specimen a hole was drilled with a #5 countersink drill, as required for the cooler positioning. The other end was ground to the best possible flatness obtainable on a horizontal grinding machine. After machining, the contacting surface was carefully protected. The roughness was measured on a Micrometrical Manufacturing Co. Profilometer (Model 741, IE 838) and the hardness of the material was tested on a side surface using the Rockwell ball method.

Junctions on a 36 gage copper constantan thermocouple wire were made by the mercury immersion technique and the thermocouples were cemented in respective holes with Sauereisen cement. The electric resistance between the two wires and between the wires and the specimen was measured in order to check the wire junction and the junction contact with the specimen. A photograph of the specimen is presented in Fig. 15.

4.2 Mechanical and Thermal Equipment

The experimental vessel and all adjoining mechanical and thermal equipment are mounted for flexibility of arrangement on a Unistrut

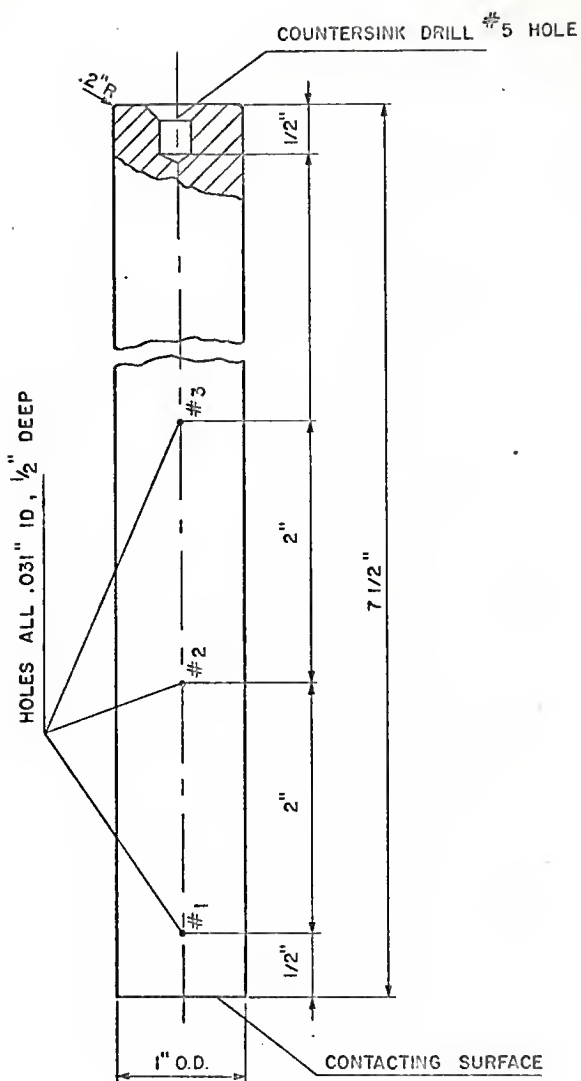


Figure 14. Contact conductance specimen; dimensions

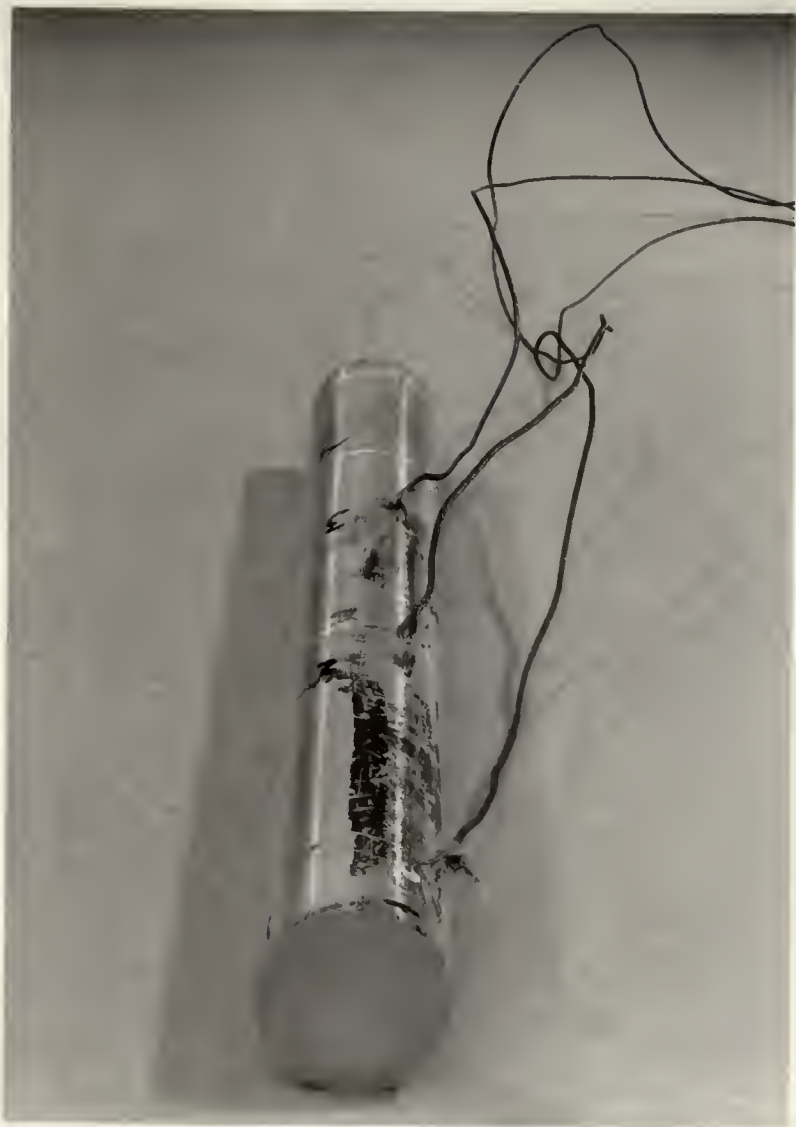


Figure 15. Contact conductance specimen.

frame with roller casters. The principal parts of the mechanical and thermal equipment are the experimental vessel with the internals, the loading mechanism and the heating and cooling control. The arrangement of the mechanical components is shown in the photograph in Fig. 16.

4.2.1 Experimental Vessel and Internals

The cross section drawing of the experimental vessel is presented in Fig. 17 and a photograph of internals in Fig. 18.

The specimen or specimen pair is inserted in the lower cooler, which is supported flexibly on a steel sphere. The steel column supporting the lower cooler is equipped with an auxiliary heater to prevent condensation on the cold surfaces of the lower section of the experimental vessel.

The upper part of the specimen (or specimen pair) is equipped with a band heater, rated at 100 W at 110 V, produced by Ogden Manufacturing Company. This heater was controlled by a cam operated microswitch and produced temperature oscillations in the specimen. A force was applied to the top cooler by the loading ram, which is equipped with strain gages and is considered a part of the loading mechanism.

Both the top and the bottom cooler tube connections are in the bottom plate. The tubes coming out of the bottom plate are copper with Tygon plastic connections for greater flexibility. The coolers are provided with O-ring seals to make them water tight.

The heat losses from the specimens are prevented by insulation of the specimens and by the guard sleeve, which was maintained at the same temperature as the specimens during the measurements. The temper-

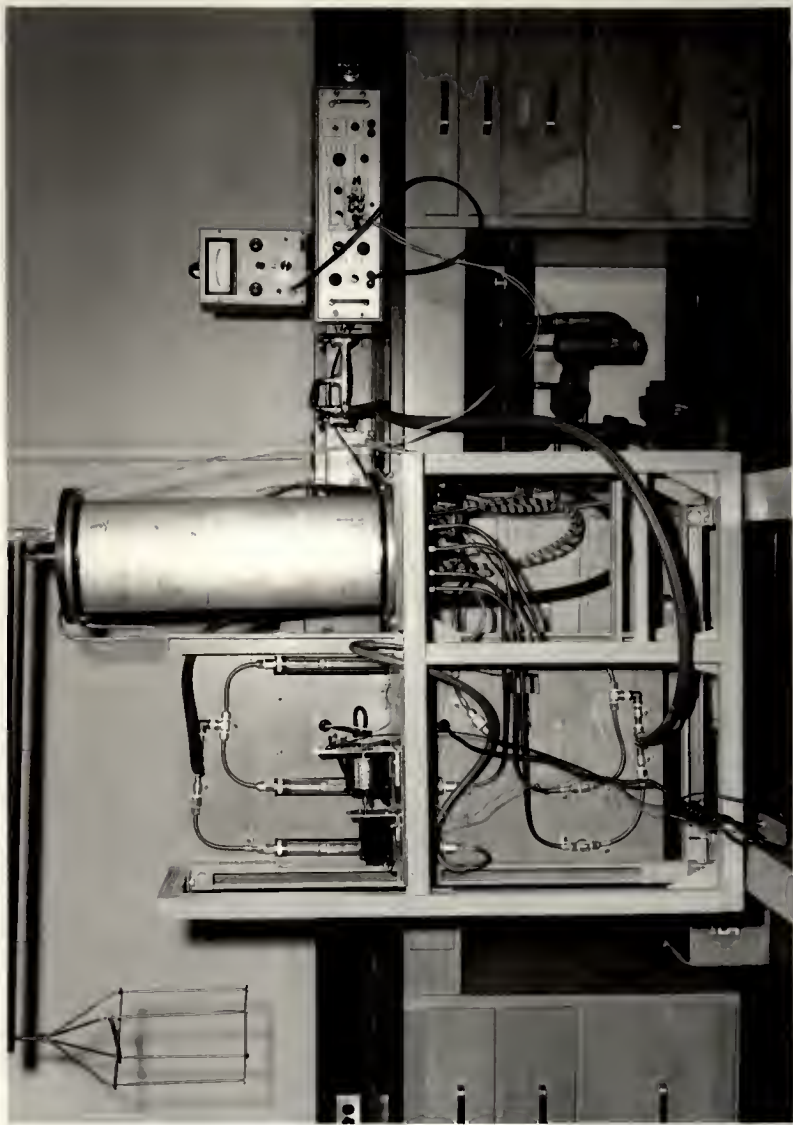


Figure 16. Mechanical and thermal equipment.

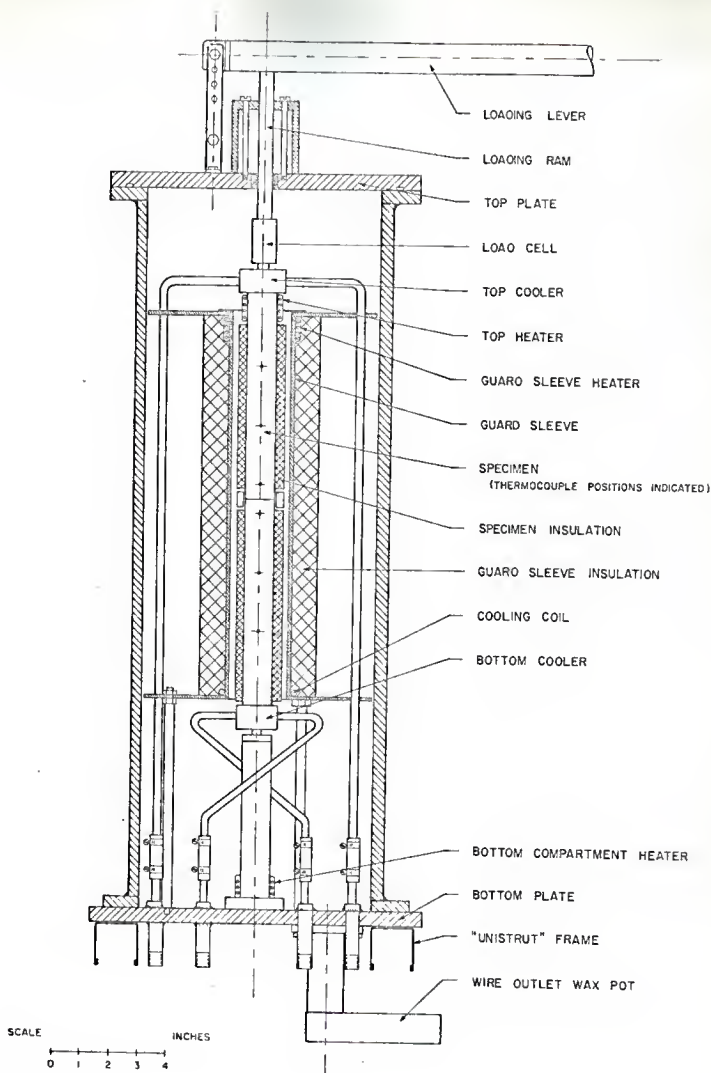


Figure 17. Experimental vessel cross section

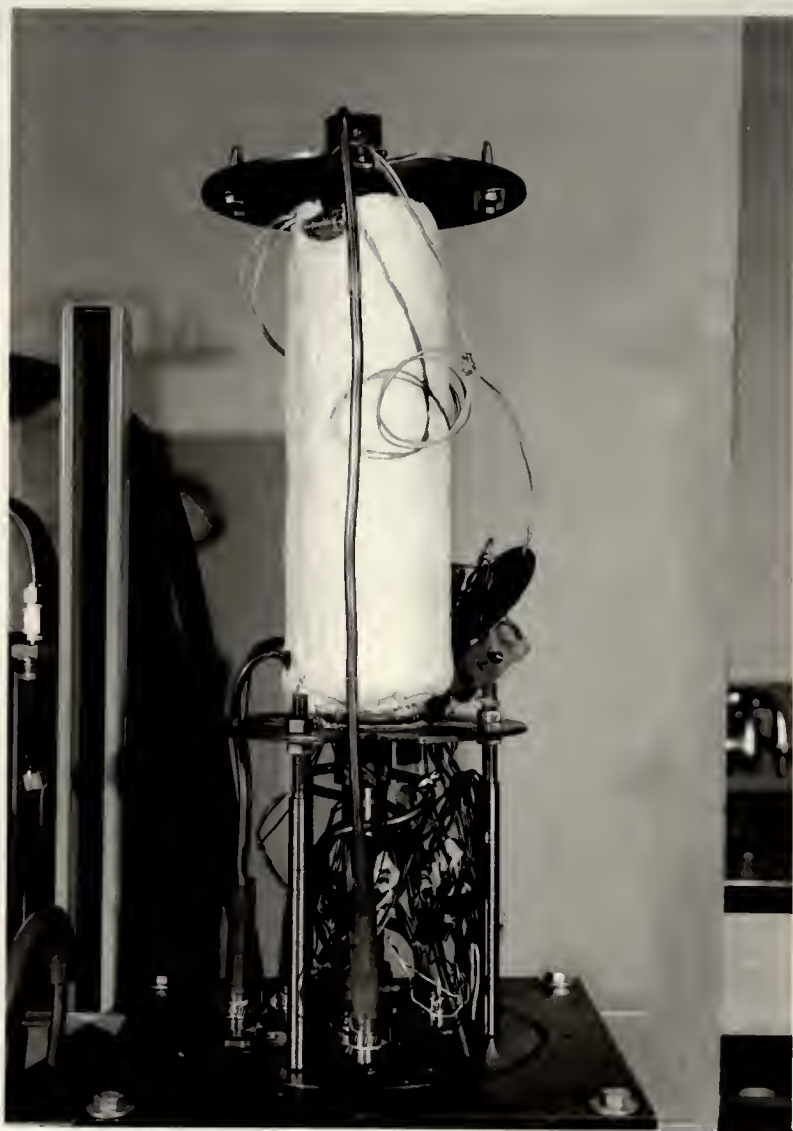


Figure 18. Experimental vessel internals.

ature gradient was controlled by a heater at the top end of the guard sleeve and by a cooling coil at the bottom end. Six thermocouples were installed in the sleeve and additional insulation was placed on the outside. The specimen insulation is a glass fiber material and the guard sleeve insulation a refractory felt.

The cylindrical part of the vessel, made of aluminum, was bolted to the bottom and top plates. All connecting surfaces are provided with O-ring grooves, but O-rings were not in place during experiments as no experiment with reduced pressure was performed. The power and thermocouple wires are conducted from the vessel through a wax filled pot to provide a gas tight seal. The loading mechanism consists of the loading lever with the weight basket and the load ram with guides. The lower part of the loading ram serves as a load cell. At that position a hole is drilled in the center of the ram to allow larger strain. Two strain gages were placed on the opposite sides of the load cell section. The strain gages were connected to an universal amplifier with a strain gage input box (Brush Electronic, Universal Amplifier, Model BL-520). A precision voltmeter provided the output reading (Keithley Electrometer 600 A, NE 906). The load cell was calibrated against a load ring certified by the National Bureau of Standards. A photograph of the load cell portion of the loading ram is presented in Fig. 19.

4.2.2 Heating and Cooling Control

The heating and cooling control devices are located on the control



Figure 19. Load cell.

panel. Two autotransformers for continuous power setting of the heaters are provided, one for the specimen heater and the other for the guard sleeve heater. Both were connected to unregulated 110 V mains. A microswitch, operated by a cam drive is installed in the top heater transformer power line. The cam is driven by a 10 rpm synchronous motor through a reduction gear. The reduction gear consists of a gear pair and a multiratio gearbox (Precision Instrument Co., Dial-A-Ratio Gearbox). The gear pair ratios used were 1.3: 1, 1: 1 and 1: 1.3 and the available gearbox reduction ratios were 2.5, 5, 10, 25, 50 and 100. Fifteen different periods could be obtained from .192 to 13 minutes with a 30% maximum step between two ratios.

Cold tapwater was used as the coolant. The water flow to the three coolers, the top and bottom specimen coolers and the guard sleeve cooler, the top and bottom specimen coolers and the guard sleeve cooler, was monitored on three flow meters and regulated by manual valves. A solenoid valve was provided for the intermittent operation of the top specimen cooler but was not used in the experiments.

4.3 Data Acquisition Equipment

The specimen thermocouple voltage outputs were amplified and recorded on a magnetic tape recorder. Later the records were analyzed with the aid of a correlation computer. The correlation computer output represents the raw data that was further analyzed by the digital computer. For steady temperature measurements a potentiometer was used (Leeds and Northrup, Portable Potentiometer).

4.3.1 Recording Equipment

The recording equipment arrangement is shown in Fig. 20.

The thermocouple reference point was provided by a thermos vessel filled with an ice-water slurry. The thermocouple voltage output was fed to the amplifying and filtering circuits, composed of the components of an analog computer (Electronic Associates Co. PACE TR-10, NE 916). The schematic diagram and analysis of these circuits are given in Appendix D.

The number of thermocouple outputs that could be recorded was limited to four by the available number of tape recorder channels. A maximum of seven channels can be installed on the recorder used (TMC Magnetic Tape Recording System, Model 700, NE 1346) but only four plug-in circuits were available. The tape recorder can be operated at four different tape speeds, 1 7/8, 3 3/4, 15 and 30 inches per second.

4.3.2 Analyzing Equipment

The tape recorder and the analog computer were used in the record analysis in conjunction with a hybrid correlation computer (TMC Correlation Computer, Model 257, NE 1363 with TMC Computer of Average Transients, CAT 400C, NE 1364). A photograph of the arrangement is presented in Fig. 21.

The thermocouple outputs were analyzed in sets of two on the correlation computer at a higher tape speed than that used during recording. Briefly, the functioning of the hybrid, analog-digital, correlation computer is as follows. One of the inputs, which have to be in the range ± 3 V,

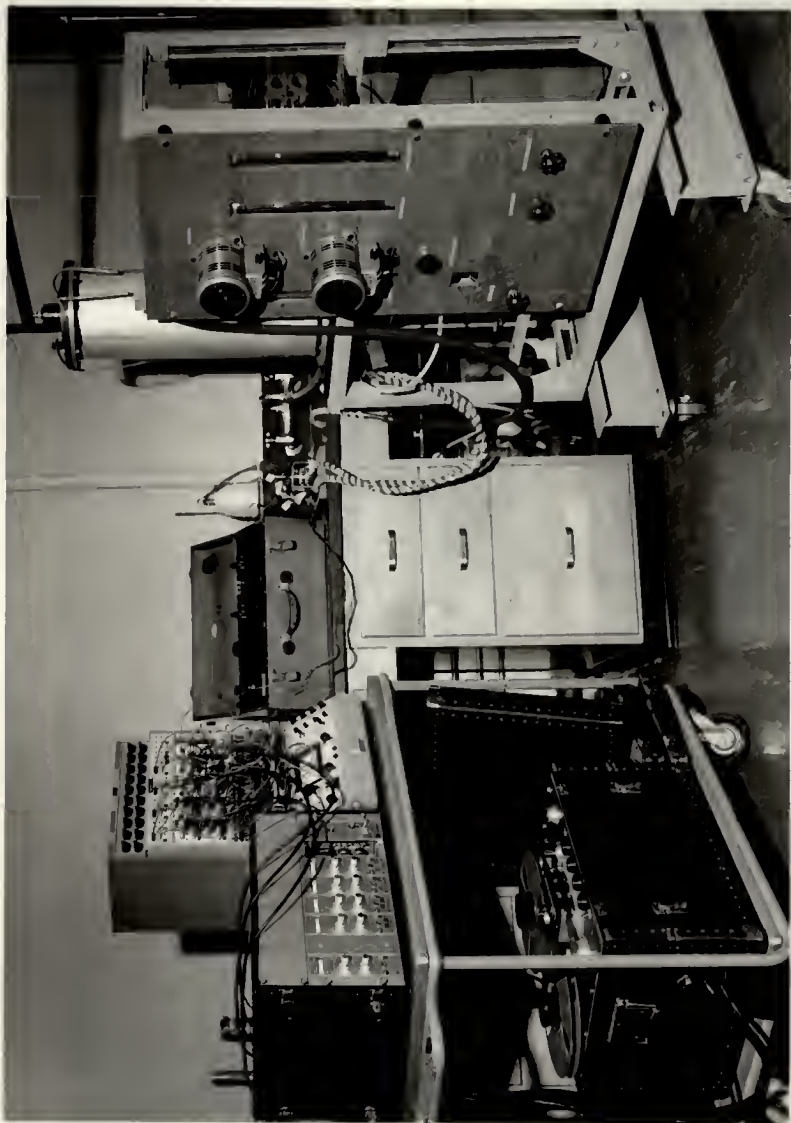


Figure 20. Experimental equipment in the recording position.



Figure 21. Experimental equipment in the record analyzing position.

is digitized and the value stored in a 256 location ferritic core memory, where up to 255 values of the same input at past times spaced by the delay increment time are kept. During each delay increment time the whole memory of the past values of the first input is scanned and each value is multiplied by the instantaneous value of the other input. The products thus obtained are accumulated in the memory of the Correlator of Average Transients (CAT). In the first location of the CAT memory the products of the simultaneous values of the two inputs are accumulated, in the second location the products of the values spaced by one delay increment, and so on. The precision of the digitalization of the inputs is claimed by the manufacturer to be one part in 512 of the 3 V maximal input. A discussion of the correlator response is given in Appendix C, and an outline of the correlation technique in Appendix B.

Three output devices are available for the correlation computer: punched paper tape, analog output and teletype output. A Tally Co. paper tape punch was normally used and a plot of the correlation function was produced on an X-Y plotter, mainly for identification purposes.

5. EXPERIMENTAL PROCEDURE

The experimental procedure for the two measurements, the thermal diffusivity measurement and the contact resistance measurement, was identical except for the specimen manipulations.

A special device was used for the alignment of the thermal contact resistance specimens. Two polyethylene half rings, $3/4$ inch wide were placed around the contacting sections of the two specimens. The ring was tightened by a steel band with a sliding latch. When the locking piece was in place the two specimens were tightly connected and could be manipulated as a unit.

To install the specimens the loading lever, the top plate, and the cylindrical part of the experiment vessel were removed, as well as the top cooler. The specimen rod was pressed into the bottom cooler and the top heater and cooler were installed. The specimen thermocouple wires were soldered to permanent extension leads in the bottom compartment of the vessel. The cylinder and the top plate were assembled with the loading ram resting on the top cooler. When the loading lever was replaced and the specimens were secured in position by force, the sliding latch was released by pulling a wire. The parts of the aligning ring thereafter were not in contact with the specimens. The desired load was applied and the heaters, coolers and the microswitch cam drive were set into operation.

The temperatures of both the guard sleeve and the specimen(s) were measured with the potentiometer. The guard sleeve heater and cooler

were adjusted so that the guard sleeve temperature matched the mean specimen temperature at the same vertical position as closely as possible. For specimens of different conductivity, the slope could not be matched completely, but the differences were kept small (Fig. 22). When there was no more temperature drift, the specimen thermocouples were connected to the amplifying and filtering circuits. The bias voltages were adjusted and appropriate amplification chosen. The amplification varied from 10^3 for the thermocouple closest to the oscillation source to 10^5 for the distant thermocouples. When very high amplifications were used it was difficult to retain the amplified signal within the 1 volt input range required by the tape recorder, as a deviation of $.1^\circ\text{C}$ would drive the signal beyond that limit. Most of the time amplifications of up to 2×10^4 were used.

Next the recorder was started, using a recording speed of $1 \frac{7}{8}$ inches per second.

Records of 2 to $2 \frac{1}{2}$ hours duration were usually taken, which represents 80 to 100 periods of the 2.5 minute period waves (the longest period used). The recording was mostly done at night or on weekends when the disturbances in the water and power supply were small. During busy switching hours the amplified thermocouple output would regularly drift out of range due to the change of line voltage and/or change of water temperature and pressure. In Fig. 23 typical temperature records obtained are shown.

The thermocouple number 1 record contains higher harmonic components.

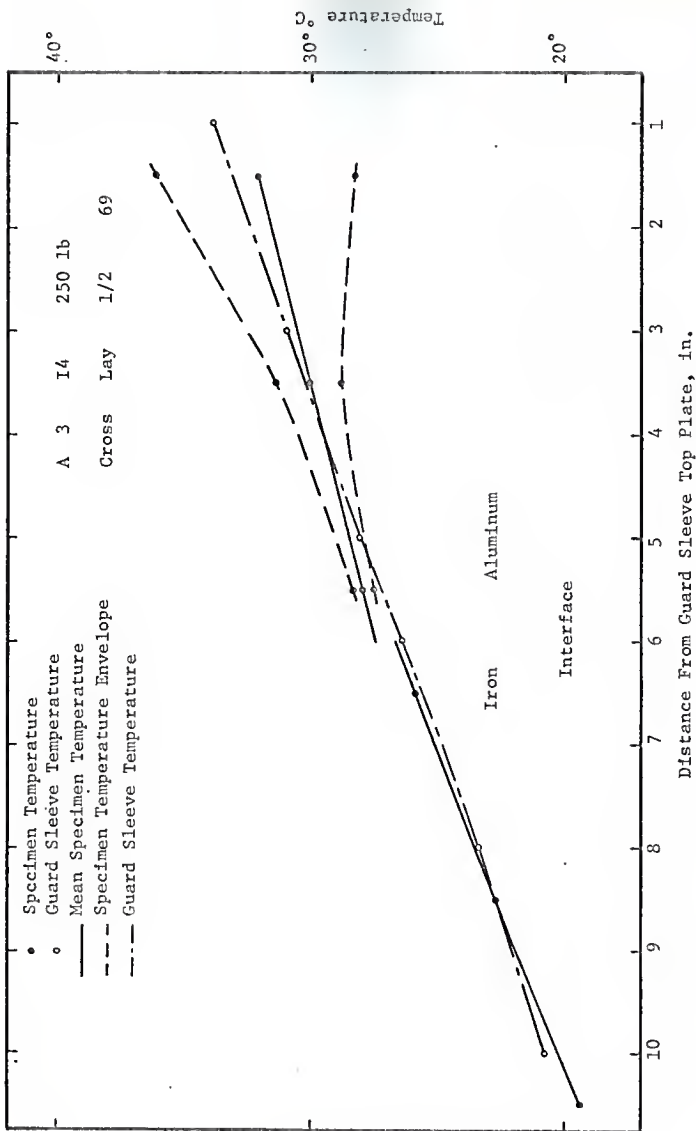
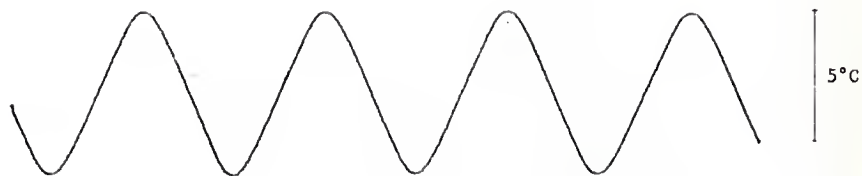
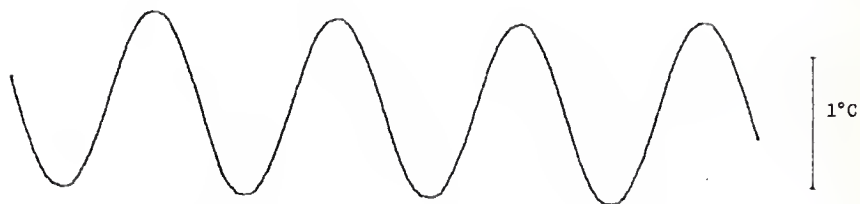


Figure 22. Temperature in the specimens and the guard sleeve.

Aluminum 15" specimen



Thermocouple #1



Thermocouple #2



Thermocouple #3

1 min

Figure 23. Temperature records.

The ratio of the next higher harmonic to the fundamental mode is estimated at $1/.172$ from the autocorrelation function. No significant higher harmonic was found in the thermocouple number 2 record. There is a significant noise component in the output of the thermocouple number 4 record. Note the different amplifications.

The magnetic tape was later played back at 16 times the recording speed (i.e. at 30 inches per second) and the individual records or pairs of records were analyzed on the correlation computer. The autocorrelations, which should provide the amplitude information, were later omitted as it was found that the amplitude response of the correlator is quite unreliable. The correlation function was subsequently punched on the paper tape and an analog output was obtained (an example is presented in Fig. 34). The paper tape was converted to magnetic tape and subsequently to punched cards. These cards in turn served as the input for the correlation function analysis code described in Appendix F.

6. DATA ANALYSIS

6.1 Analysis of Temperature Records

The purpose of the data collecting system in the temperature wave experiment is to obtain the information on the temperatures at various positions along the specimen either continuously in time or at certain time intervals. In this investigation the temperatures, represented by the thermocouple voltage outputs, were recorded continuously on a magnetic tape recorder. From such simultaneous records of thermocouple outputs the information on the phase difference and the amplitude ratio between them is to be obtained. Various methods can be employed for this purpose. At present a relatively convenient method of analyzing voltage records containing noise components (and therefore requiring averaging over long periods of time) is available which utilizes correlation computers with analog input. Previously, the correlation technique, the theory of which is briefly outlined in Appendix B, was possible only for digitized data.

The cross correlation function is defined as the average product of two records with the delay time between them as the argument

$$\phi_{fg}(\tau) = \lim_{t_i \rightarrow \infty} \frac{1}{2t_i} \int_{-t_i}^{t_i} f(t)g(t+\tau)dt \quad (37)$$

where $f(t)$ and $g(t)$ are the two records and τ the delay time for the record $g(t)$. A record can also be correlated with itself, in which case the above function is termed the autocorrelation function.

In Appendix B the important relationship between the Fourier

transform of the correlation function and the original record transforms are derived,

$$F\{\phi_{ff}(\tau)\} = \lim_{t_1 \rightarrow \infty} \frac{\sqrt{2\pi}}{2t_1} |F\{f(t)\}|^2 \quad (38)$$

$$F\{\phi_{fg}(\tau)\} = \lim_{t_1 \rightarrow \infty} \frac{\sqrt{2\pi}}{2t_1} F\{f(t)\}^* F\{g(t)\} \quad (39)$$

where the symbol F denotes the Fourier transform and the asterisk the complex conjugate value. Thus from the correlation functions (auto- and cross-) the amplitude and phase relationship of the frequency components of the records are available.

The correlation of the records with one prominent frequency, as are obtained in the temperature wave measurements, is a special case of the general correlation and the pertaining relations can be derived directly, as is shown in Appendix B, Eq. (B 13) to Eq. (B 17). The lag between the harmonic functions is in this case retained as the lag of the cosine.

For finite and discrete correlation functions certain limitations have to be considered. The Fourier transform is not applicable but is reduced to the Fourier series representation. The fact that the frequencies in the Fourier series are spaced by $1/T$, where T is the length of the correlation function, reflects the uncertainty with which the frequency can be determined. The discrete nature of the correlation function makes it impossible to distinguish between the basic frequency

and its aliases, $2kf_N - f$, $2kf_N + f$, where k is any integer and f_N is the Nyquist frequency, $f_N = 1/2\Delta\tau$. ($\Delta\tau$ is the distance between the points). This effect can be predicted from the development of the Fourier series on a set of discrete points, but the development is not presented here since, for the correlations performed, the Nyquist frequency was in the range where the filtering circuits eliminated any significant component from the records.

The information that the record and consequently the correlation function contains a discrete prominent frequency, led to a different frequency analysis approach than the Fourier series expansion. A linear combination of a polynomial and one or more harmonic terms were fitted to the correlation function in the least sum of squares sense. The polynomial part was introduced to represent the decaying exponential component in the case of the autocorrelation function of a noisy record. This model was found to be correct as the residuals were random in the great majority of cases. The frequency so determined should still be considered uncertain in the interval $\Delta f = 1/T$ where T is the length of the correlation function, in the sense that should another harmonic be present within the interval it would not be possible to determine them simultaneously. In this case the one harmonic model would prove incorrect (many harmonics would have to be introduced), and the coefficients of the two harmonics would be highly correlated.

An anomaly was discovered in the response of individual channels of the correlation computer and an additional function was introduced as a component of the linear combination to be fitted to the correlation

function. The response of the correlator is discussed in Appendix C and a plot of the correlator background function is presented in Fig. 24. The inclusion of this background function reduced the number of cases in which the residuals were not random and a further refinement might completely eliminate the occurrence of such cases. In this regard, it is expected that the individual channel response is also nonlinear as is the case with the overall amplitude response (cf. Appendix C). Although the peaks of the background function were always found at the same location their relative amplitude may not be the same for different inputs.

The least squares fit of the analytic form to the correlation function provided the amplitude and phase of the prominent harmonic in the correlation function. The thermal diffusivity and the thermal contact resistance were calculated from the phase angle information, as described in the following section. The amplitude information was not used as it was considered too unreliable in view of the findings on the correlator response (Appendix C).

The theory of the regression analysis (least square fitting) is given in Appendix E and the computer program that performs the task is described in Appendix F.

6.2 Thermal Diffusivity Determination

The thermal diffusivity specimens were of sufficient length, compared with the attenuation distance for the periods used, that the no-reflection approximation for the behavior of the temperature wave could be used (Eq. (13)). For the thermal diffusivity calculation the following expression is used

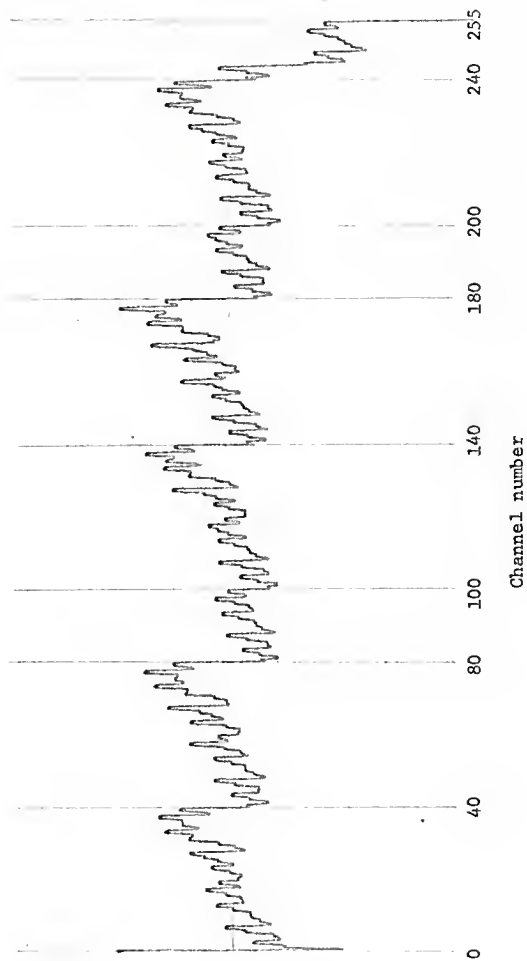


Figure 24. Correlator background response function.

$$\alpha = \frac{\dot{\omega}}{2} \left(\frac{\Delta l}{\Delta \phi} \right)^2 = \frac{\pi}{t_0} \left(\frac{\Delta l}{\Delta \phi} \right)^2 \quad (40)$$

where Δl is the distance between the thermocouples and $\Delta \phi$ is the phase lag between the thermocouple outputs.

6.3 Contact Conductance Determination

The results derived in section 2.2 were used for the determination of the contact conductance parameter from the phase lag information. The assumption of a discontinuity in an infinite medium is valid as the distance from the boundaries was several times greater than the attenuation length.

The contact conductance h cannot be determined solely from the phase or amplitude ratio and the distances between the measuring points, which is evident also from its dimensionality. Only the dimensionless parameter $\gamma = h/k\lambda$ can be obtained, and the knowledge of the thermal conductivity and thermal diffusivity (contained in λ together with the period of oscillations) is needed. Furthermore for the determination of γ the knowledge of the material properties ratio Γ (Eq. (36)) is necessary. This latter quantity can be obtained from the ratio of the thermal conductivities and the ratio of thermal diffusivities.

From the results of the present experiments the value of γ was obtained and the thermal contact conductance was calculated using the values for conductivity from the literature. The ratio of the conductivities of the two materials was estimated from the temperature gradient ratio in the two specimens (since the same amount of heat flows through

both).

The thermal contact conductance parameter was determined from the phase difference between the two thermocouples closest to the discontinuity, which is most sensitive to this parameter. As no explicit expression is available the parameter was determined by iteration in a computer code. The input data were the thermal diffusivities of the two materials, the ratio of the conductivities, the distances of the thermocouples from the discontinuity and the phase difference. For each value of γ the reflected and transmitted wave amplitude and phase at the discontinuity were calculated (system of equations Eqs. (32)) and from these the phase difference at the two thermocouple positions. The procedure was iterated until a satisfactory convergence was reached (the difference of the two consecutive estimates less than 1%).

7. EXPERIMENTAL RESULTS

7.1 Thermal Diffusivity Measurements

The thermal diffusivity of an aluminum alloy, 2024-T4, and Armcro iron was measured using the temperature wave method described herein. The data on these materials and the experimental results are given in Table II. Values for the thermal diffusivity computed from data obtained from the literature are included for comparison. The experimental values agree very well with the literature data.

7.2 Thermal Contact Conductance Measurements

The thermal contact conductance of aluminum-aluminum and aluminum-iron contacts was measured. The measurements were performed at different applied pressures. Four specimen pairs were used and 12 complete data recordings and evaluations were performed.

In the calculations of the contact conductance parameter the values of the thermal diffusivity measured as a part of this investigation were used, the values being $.485 \text{ cm}^2/\text{sec}$ for aluminum and $.208 \text{ cm}^2/\text{sec}$ for iron. The ratio of the thermal conductivities of the two materials was estimated from the temperature gradients in the two specimens (cf. Fig. 22), but as the experiment was not designed for this purpose the data from the literature were used. From the literature (1, 5) the ratio is 1.65 while the mean of the graphical estimates was 1.69.

The information on the specimen pairs used and the results of the correlation runs are summarized in Tables III to VI. The thermocouple position 1 is closest to the oscillating heater, the thermocouple 3 last

Table II

Thermal diffusivity measurement results

Specimen material: Aluminum 2024-T4. Oscillation period: 1.92 min.

Thermocouple positions	Thermocouple distance (cm)	Phase difference (radians)	$L_{1/e}$ (cm)
1 - 2	6.33	1.5107	4.20
1 - 3	12.8	3.0095	4.26
1 - 4	19.0	4.5528	4.17
Average $L_{1/e}$			= 4.21

Thermal diffusivity measured $.485 \text{ cm}^2/\text{sec}$

Thermal diffusivity from literature data* $.465 \text{ cm}^2/\text{sec}$

Specimen material: Armco Iron. Oscillation period: 3.25 min.

Thermocouple positions	Thermocouple distance (cm)	Phase difference (radians)	$L_{1/e}$ (cm)
1 - 2	6.40	1.809	3.55
1 - 3	12.80	3.454	3.71
1 - 4	19.2	5.403	3.56
Average** $L_{1/e}$			= 3.55

Thermal diffusivity measured $.203 \text{ cm}^2/\text{sec}$

Thermal diffusivity from literature data* $.208 \text{ cm}^2/\text{sec}$

*Aluminum (1, 5): density = 2.73 g/cm^3 , specific heat = $.23 \text{ cal/g}^\circ\text{C}$
thermal conductivity = $.29 \text{ cal/cm sec}^\circ\text{C}$

Armco Iron: density = 7.86 g/cm^3 , specific heat at 30°C $.108 \text{ cal/g}$
thermal conductivity at 30°C = $.176 \text{ cal/cm sec}^\circ\text{C}$.

**Thermocouple at position number 3 was found defective so the data for this point were excluded from evaluation.

Table III

Thermal contact conductance measurements, pair A11-A12

	Specimen 1	Specimen 2
Identification code	A1 1	A1 2
Material	2024-T4	2024-T4
Hardness, H_{R_b} (1/16", 100 kp)	77	77
Test surface roughness, μ in rms	15	10
Thermocouple no. 3 (in specimen 1), distance from interface	1.27 cm	
Thermocouple no. 4 (in specimen 2), distance from interface		1.27 cm

Load 250 lb (pressure 320 psi), parallel lay

Date of recording 12/7/1968, Period of oscillation 1.92 min.

Correlation, thermocouple no.	Phase difference, radians
1 - 2	1.2057
1 - 2	1.2018
1 - 3	2.3294
1 - 4	3.0780
2 - 4	1.8510
3 - 4	.6410

Average phase difference 1 - 3 2.3318 1 - 4 3.0345

3 - 4 .6718

Load 580 lb (pressure 790 psi), parallel lay

Date of recording 12/8/1968, Period of oscillation 1.92 min.

Correlation, thermocouple no.	Phase difference, radians
1 - 2	1.1990
1 - 3	2.3326
1 - 3	2.3524
1 - 4	2.9354
2 - 4	1.8503
3 - 4	0.7150

Average phase difference 1 - 3 2.3425 1 - 4 2.9955

3 - 4 0.6531

Table IV

Thermal contact conductance measurements, pair A14-A15

	Specimen 1	Specimen 2
Identification code	A1 4	A1 5
Material	2024-T4	2024-T4
Hardness, $HR_b(1/16", 100 \text{ kp})$	78	77
Test surface roughness, $\mu\text{in rms}$	30	25
Thermocouple no. 3 (in specimen 1), distance from interface	1.27 cm	
Thermocouple no. 4 (in specimen 2), distance from interface	1.32 cm	

Load 300 lb (pressure 380 psi), parallel lay

Date of recording 12/9/1968, Period of oscillation 1.92 min.

Correlation, thermocouple no. Phase difference, radians

1 - 2	1.1743
1 - 3	2.2673
1 - 3	2.2579
1 - 4	3.1099
1 - 4	2.9811
1 - 4	3.0640
3 - 4	0.8344

Average phase difference 1 - 3 2.2734 1 - 4 3.0655

3 - 4 .7913

Load 630 lb (pressure 850 psi), parallel lay

Date of recording 12/8/1968, Period of oscillation 1.92 min.

Correlation, thermocouple no. Phase difference, radians

1 - 2	1.1796
1 - 3	2.2518
1 - 3	2.1731
1 - 4	2.9892
1 - 4	3.0143
3 - 4	0.7712

Average phase difference 1 - 3 2.2124 1 - 4 2.9973

3 - 4 .7849

Table IV. continued

Load 1750 lb (pressure 2250 psi), parallel lay
 Date of recording 12/10/1968, Period of oscillation 1.92 min

Correlation, thermocouple no.	Phase difference, radians			
1 - 2		1.3596		
1 - 3		2.2045		
1 - 4		2.8784		
1 - 4		2.9026		
3 - 4		0.6703		
Average phase difference	1 - 3	2.2045	1 - 4	2.8853
	3 - 4	<u>.6808</u>		

Table V

Thermal contact conductance measurements, pair A13-T4

	Specimen 1	Specimen 2
Identification code	A1 3	I 4
Material	2024-T4	Armco-Iron
Hardness, H_{R_b} (1/16", 100 kp)	76	76
Test surface roughness, $\mu\text{in rms}$	50	35
Thermocouple no. 3 (in specimen 1), distance from interface	1.27 cm	
Thermocouple no. 4 (in specimen 2), distance from interface	1.29 cm	

Load 250 lb (pressure 320 psi), cross lay

Date of recording 1/2/1969, Period of oscillation 2.5 min.

Correlation, thermocouple no.	Phase difference, radians			
1 - 2	1.0685			
1 - 3	2.1000			
1 - 4	2.8505			
1 - 4	2.7847			
2 - 3	1.0664			
2 - 4	1.8270			
3 - 4	0.8180			
Average phase difference	1 - 3	2.1174	1 - 4	2.8875
	3 - 4	<u>0.7701</u>		

Load 550 lb (pressure 750 psi),

Date of recording 1/2/1969, Period of oscillation 2.5 min.

Correlation, thermocouple no.	Phase difference, radians			
1 - 2	1.0529			
1 - 3	2.0550			
1 - 4	2.7492			
2 - 3	1.0163			
2 - 4	1.7032			
3 - 4	0.6782			
Average phase difference	1 - 3	2.0616	1 - 4	2.7480
	3 - 4	<u>.6864</u>		

Table V. continued

Load 900 lb (pressure 1170 psi), cross lay
 Date of recording 1/2/1969, Period of oscillation 2.5 min

Correlation, thermocouple no.	Phase difference, radians			
1 - 2		1.0719		
1 - 3		2.0912		
1 - 4		2.7787		
2 - 3		1.0413		
2 - 4		1.7324		
3 - 4		0.6757		
Average phase difference	1 - 3	2.1022	1 - 4	2.7867
	<u>3 - 4</u>	<u>.6844</u>		

Table VI

Thermal contact conductance measurements, pair Al4-I1

	Specimen 1	Specimen 2
Identification code	Al 4	I 1
Material	2024-T4	Armco Iron
Hardness, HR _B (1/16", 100 kp)	78	72
Test surface roughness, μ in rms	15	10
Thermocouple no. 3 (in specimen 1), distance from interface	1.27 cm	
Thermocouple no. 4 (in specimen 2), distance from interface	1.315 cm	

Load 250 lb (pressure 320 psi), cross lay

Date of recording 1/4/1969, Period of oscillation 2.5 min.

Correlation, thermocouple no.	Phase difference, radians	
1 - 2	1.0573	
1 - 3	2.0649	
1 - 4	2.7313	
2 - 3	1.0097	
2 - 4	1.6963	
3 - 4	0.6773	

Average phase difference	1 - 3	2.0665	1 - 4	2.7425
	<u>3 - 4</u>		<u>0.6761</u>	

Load 550 lb (pressure 700 psi), cross lay

Date of recording 1/5/1969, Period of oscillation 2.5 min.

Correlation, thermocouple no.	Phase difference, radians	
1 - 2	1.0912	
1 - 3	2.0706	
1 - 4	2.7343	
2 - 3	1.0124	
2 - 4	1.6706	
3 - 4	0.6736	

Average phase difference	1 - 3	2.0866	1 - 4	2.7520
	<u>3 - 4</u>		<u>0.6654</u>	

Table VI. continued

Load 900 lb (pressure 1140 psi), cross lay
 Date of recording 1/4/1969, Period of oscillation 2.5 min.

Correlation, thermocouple no.	Phase difference, radians			
1 - 2	1.0611			
1 - 3	2.0599			
1 - 4	2.7214			
2 - 3	1.0134			
2 - 4	1.6594			
3 - 4	0.6629			
Average phase difference	1 - 3	2.0671	1 - 4	2.7270
	3 - 4	<u>0.6598</u>		

Load 1200 lb (pressure 1510 psi),
 Date of recording 1/4/1969, Period of oscillation 2.5 min.

Correlation, thermocouple no.	Phase difference, radians			
1 - 2	1.0290			
1 - 3	2.0132			
1 - 4	2.7300			
2 - 3	0.9735			
3 - 4	0.6974			
Average phase difference	1 - 3	2.0079	1 - 4	2.7176
	3 - 4	<u>0.7098</u>		

in specimen 1 before the interface and thermocouple 4 is in specimen 2.

The resulting thermal contact conductance values are presented in Table VII and in Fig. 25. In Fig. 25 the experimental values and theoretical prediction as given in reference (15) are plotted for the aluminum 2024-T4 - Armco iron contact. The data and the theoretical curve are for a rms roughness of 150μ in, which is much higher than that of the specimens used in this work.

The phase difference between the two thermocouples closest to the interface, used in the calculation of the thermal conductance parameter, is the average value for this phase difference as indicated by the difference of phase between correlations 1-3 and 1-4; 2-3 and 2-4 and the direct correlation 3-4. The correlations with the thermocouples 1 and 2 give a more reliable estimate than the direct correlation of the two thermocouples close to the interface (3 - 4) alone, as the records 1 and 2 have much smaller relative noise and provide good reference records.

Table VII

Summary of thermal contact conductance results

Specimen pair	Applied pressure (psi)	Conductance parameter	Thermal contact conductance	
			($\text{Btu/hr-ft}^2 \text{ } ^\circ\text{F}$)	($\text{cal/cm}^2 \text{ sec } ^\circ\text{C}$)
A1 1-A1 2	320	6.8	6.4	.47
" "	740	9.5	8.8	.65
A1 4-A1 5	380	2.3	2.16	.159
" "	810	2.4	2.24	.165
" "	2250	7.6	7.1	.525
A1 4-I 1	320	10.0	8.15	.60
" "	710	12.8	10.5	.77
" "	1150	14.9	12.1	.89
" "	1540	5.9	4.7	.355
A1 3-I 4	320	3.2	2.8	.206
" "	710	10.7	8.7	.64
" "	1150	11.3	9.2	.68

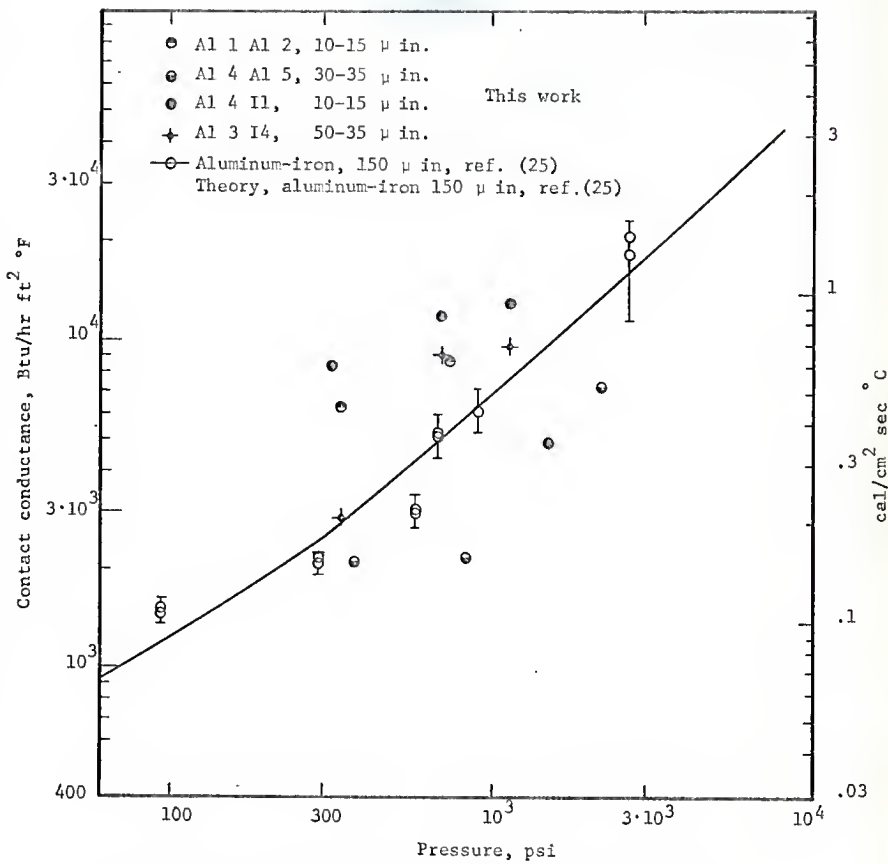


Figure 25. Contact thermal conductance experiment results.

8. DISCUSSION OF RESULTS AND EXPERIMENT

The experiments performed demonstrated the feasibility of determining the thermal contact conductance by the temperature wave method, the determination of the thermal diffusivity having been accomplished before. In the following the interpretation of results is given and some shortcomings of the present work are discussed.

The thermal diffusivity measurement results agree very well with the published data for the materials examined. The choice of the aluminum alloy in the tempered condition was not the most appropriate for this purpose as its properties are given only as approximate while for the alloy in the annealed condition more exact data are available. The difference in results is within 5% and the agreement can be considered as very good. The measured value of the thermal diffusivity was used in the further analysis as it is considered more applicable for the particular material than the general value from the literature.

A minor deficiency of the experimental procedure may be illustrated with the data obtained in the thermal diffusivity measurement of aluminum. Due to the necessary connection of one wire of each thermocouple to the analog computer ground, additional loops were created between the thermocouples as they were mostly in good electrical contact with the specimen (loop ABC in Fig. 26c). In these loops current flowed due to the temperature difference between the two thermocouple positions, where the thermocouple copper-specimen material was created. The minute current caused a voltage drop in each leg (AB and AC), which was added or subtracted

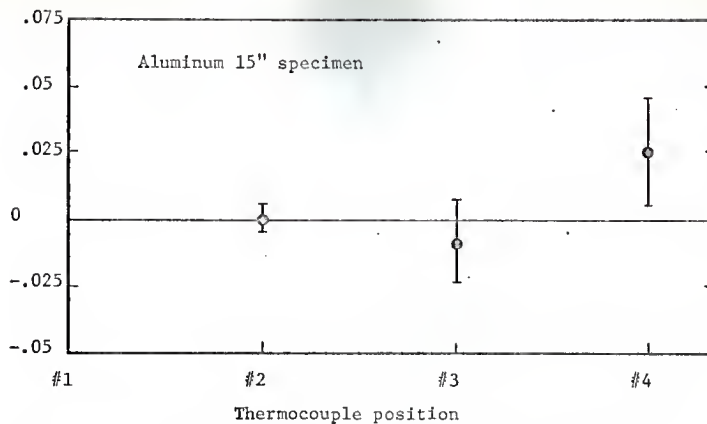


Figure 26.a. Deviations of phase angle from linearity

Figure 26.b. Phase angle and relative amplitude of thermocouple outputs

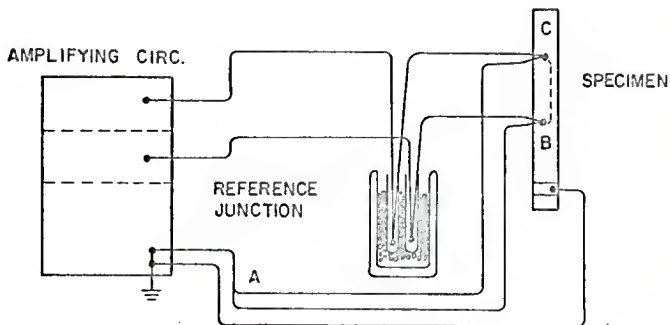
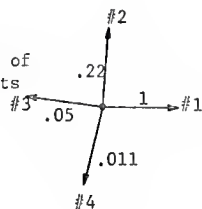


Figure 26.c. Thermocouple wire connections.

Figure 26. Thermocouple interdependence.

from the voltage generated by the respective thermocouples. This was true as well for the steady part as for the oscillatory part of the temperature. Among the oscillatory voltages the dominant was the output of the thermocouple with the highest temperature amplitude and it influenced the others, though this effect was small. The phase relation of the thermocouples in the aluminum thermal diffusivity specimen as well as the effect on the phase deviation from the mean phase slope can be seen from Fig. 26 a and b. The effect is in this case hardly significant, but was noticed in other results also. The uncertainty intervals are the confidence limits for the phase determination from the correlation function (cf. Appendix E). Though small this effect should be avoided by securing insulation of the thermocouples from the specimen. The magnitude of the deviations was still smaller for the thermal contact conductance measurements as the ratios of amplitude were more modest.

The thermal contact conductance parameter measurements rely on the ability to determine the deviations from linearity of the phase relations and are thus less accurate than the diffusivity measurements. In Fig. 25 the measured contact conductances are plotted together with the measurements reported in reference (15), which were the only measurements found in the literature for the material pair used and with air as the interstitial medium. It should be noted that the contacting surfaces for which the contact conductances are reported in reference (15) were much rougher than the ones used here, the rms deviation being 150 $\mu\text{in.}$ compared to 10 to 50 $\mu\text{in.}$ used in this investigation. For surfaces of

different roughness the difference of the contact conductance may amount to up to one order of magnitude, as reported in reference (24).

A deficiency of the thermal contact conductance measurement program was that no detailed information on the contacting surface waviness was available. The surfaces were machined very carefully and no waviness could be detected by measurements with a dial indicator at several points on the surface. No satisfactory assurance is though given that the surfaces were indeed flat. This fact does not imply that the results for the thermal contact conductance are inaccurate but only that the comparison with other experimental results is hindered.

A few experimental points evidently fall beyond the random error of the measurements. These are the points for Al 3 - I 4, 320 psi and Al 4 - I 1, 1540 psi. The documents of the experiments were reviewed and it was found that the erroneous points were obtained from records with considerable drift while in the other records the drift was negligible. It should be noted that the expressions of the correlation theory (Appendix B) are derived for stationary records and any drift of important slope will cause disturbance in the phase relationships obtained. Care should be therefore taken that the steady condition is indeed obtained and maintained. The records should be inspected for drift and the experiment repeated to avoid the rather uncomfortable posterior rejection of erroneous points on the basis that they do not agree with other results. One of the erroneous points (Al 3 - I 4, 320 psi) was obtained in an experiment where the matching of the specimen and guard

sleeve temperatures was poor (difference of 2 to 3°C) and the record also contained some unstationarity, the latter probably being the main source of error.

The experimental points show the expected trend of higher conductance for smoother surfaces and higher pressure. Also lower slope in the conductance - pressure diagram can be expected for smoother surfaces, as the measurements indicate.

The thermal contact conductance of all-aluminum pairs also falls in the range of aluminum-iron results, as the hardness, roughness and the method of machining the surfaces was close. The choice of the parallel lay position is somewhat inappropriate as in this case the contacting points are distributed in a quite different pattern than in the cross-lay position.

Evaluating the results of the thermal contact conductance measurements it can be stated that satisfactory accuracy can be achieved with this method if sufficient care is taken to maintain stationary conditions. The ultimate and not very remote limitation to accuracy may be in the present experimental equipment, particularly in the method of analyzing the records with the correlation computer. The adequacy of the method for the thermal contact conductance measurements is further supported by the fact that the reproducibility of the phenomenon itself is on the order of 20 to 30% error, as estimated from various compilations of data (10, 15).

9. SCOPE FOR FURTHER WORK

The method of thermal contact conductance measurement can be considered established and the investigation of the phenomenon itself should be pursued. The method of temperature waves may be particularly valuable in providing new insight in the directional effect in contact conductance. In this respect a modification of the experimental apparatus should be considered, which would allow steady state and temperature wave measurements, with heat flow in either direction, obtainable without displacing the specimens.

The present temperature record analysis system was found inadequate for determining the amplitude relations of the records. A different kind of data acquisition system might be considered, or the present one improved. The sampling interval of the temperatures is several seconds (in the present equipment 2.5 seconds) and the records are not excessive in length, so that the digitizing of the thermocouple voltage output may be appropriate and all further analysis performed in the digital form. A precision analog-digital converter would be needed (digital voltmeter) and a digital, computer readable, storage (magnetic tape).

Such arrangement could provide for more measuring points in the specimens and monitoring of the temperatures outside the specimen. An additional advantage of such system would be that the sampling could be synchronized with the oscillation generating devices (heater and cooler) and so an ideal reference record for correlation would be provided. Such equipment could also be used for other experiments with temperature waves.

10. ACKNOWLEDGEMENTS

The author wishes to express his gratitude to Dr. M. J. Robinson, under whose direction this study was conducted, for his advice, help and encouragement. Special thanks are to Dr. R. Kladnik whose ideas prompted this study. Sincere appreciation is also extended to Dr. W. R. Kimmel for his personal interest in the progress of this study. Various parts of the equipment were manufactured with much appreciated help from Mr. C. Nelson, Prof. F. J. McCormick and mostly Mr. G. W. Abshire. Recognition should be given to the Department of Nuclear Engineering for the use of facilities and the National Science Foundation for the financial support of the research. The authors residence at the Kansas State University was made possible through the U.S.-Yougoslav exchange program, administered in the United States by the Institute of International Education.

11. LITERATURE CITED

1. Alcoa Aluminum Handbook. Aluminum Company of America, Pittsburgh, 1967.
2. Alzofon, F. E.
Retardation and Diffraction Aspects of the Conduction of Heat in Solids. Am. J. Phys. 30, 285 (1962).
3. Angstroem, A. J.
New Method of Determining the Thermal Conductibility of Bodies. Phil. Mag. 25, 130 (1863).
4. Angstroem, A. J.
On the Conducting Power of Copper and Iron for Heat at Different Temperatures. Phil. Mag. 26, 161 (1863).
5. ASM Metals Handbook. American Society of Metalurgists, 1948.
6. Barzelay, M. E. et al.
Effect of Pressure on Thermal Conductance of Contact Joints. NACA TN-3295 (1955).
7. Bendat, J. S.
Principles and Applications of Random Noise Theory. J. Wiley and Sons, New York, 1958.
8. Blackman, R. B., Tuckey, J. W.
The Measurement of Power Spectra. Dover, New York, 1958.
9. Burdg, C. E. et al.
Development and Testing of a Temperature Transient Method for Performing In-Pile Thermal Conductance Testing. CEND-3336-260 (1966).
10. Carfagno, S. P.
Review of Literature on Thermal Contact Conductance in a Vacuum. N 68-16898 (1967).
11. Cowan, R. D.
Pulse Method of Measuring Thermal Diffusivity at High Temperatures. J. Appl. Phys. 34, 926 (1963).
12. Davies, W.
Thermal Transients in Graphite-Copper Contacts. Brit. J. Appl. Phys., 10, 516 (1959).

13. Deem, H. W., Wood, W. D.
Flash Thermal Diffusivity Measurements Using a Laser.
Rev. Sci. Instr., 33, 1107 (1962).
14. Draper, N. R., Smith, H.
Applied Regression Analysis. J. Wiley and Sons, New York, 1966.
15. Fenech, H., Rohsenow, W. M.
Prediction of Thermal Conductance of Metallic Surfaces in Contact.
Trans. ASME, J. Heat Transfer, 85, 15 (1963).
16. Green, D. R.
Thermal Surface Impedance for Plane Heat Waves in Layered
Materials. J. Appl. Phys. 37, 3095 (1966).
17. Heasley, J. H.
Transient Heat Flow between Contacting Solids.
Int. J. Heat and Mass Transfer. 8, 147 (1965).
18. Holm, R.
Calculation of the Temperature Development in a Contact Heated
in the Contact Surface, and Applications to the Problem of the
Temperature-Rise in a Sliding Contact. J. Appl. Phys. 19,
361 (1948).
19. Holm, R.
Electrical Contacts Handbook. Springer, Berlin 1958.
20. Keeping, E. S.
Introduction to Statistical Inference.
D. Van Nostrand, Princeton 1962.
21. King, R. W.
A Method of Measuring Heat Conductivities. Phys. Rev. 6, 41
(1915).
22. Lagedrost, J. F. et al.
Thermal Conductivity of PuO_2 as Determined from Thermal Diffusivity
Measurements. Nucl. Applic. 4, 54 (1968).
23. Marquard, D. W.
Least-squares Estimation of Nonlinear Parameters. NLIN: Share
Distribution Program No. 3094 (1964), NLIN-2: ibid. (1965).
24. Mikic, B. B., Rohsenow, W. M.
Thermal Contact Resistance. DSR-74542-41 (1966).
25. Nakata, M. M. et al.
Thermophysical Properties of SNAP Fuel Materials. NAA-SR-1159.

26. Parker, W. R. et al.
Flash Method of Determining Thermal Diffusivity, Heat Capacity and Thermal Conductivity. J. Appl. Phys. 32, 1679 (1961).
27. Rapier, A. C. et al.
The Thermal Conductance of Uranium Dioxide/Stainless Steel Interfaces. Int. J. Heat and Mass Transfer 6, 397 (1963).
28. Rogers, G. F. C.
Heat Transfer at the Interface of Dissimilar Metals.
Int. J. Heat and Mass Transfer 2, 150 (1961).
29. Sidles, P. H., Danielson, G. C.
Thermal Diffusivity of Metals at High Temperatures.
J. Appl. Phys. 25, 58 (1954).
30. Starr, C.
An Improved Method for Determination of Thermal Diffusivities.
Rev. Sci. Instr. 8, 61 (1937).
31. Uhrig, R. F., ed.
Neutron Noise, Waves and Pulse Propagation.
AEC Symposium Series 9. USAEC Division of Technical Information Extension, Oak Ridge, Tenn. (1967).
32. Yovanovich, M. M., Rohsenow, W. M.
Influence of Surface Roughness and Waviness upon Thermal Contact Resistance. Dep. Mech. Engg., MIT, Rep. no. 76361-48 (1967).

APPENDIX A: Transient Response of Elemental Heat Channel

In the investigation of the phase change and the amplitude of the reflected and transmitted waves at the interface of two solids a constant heat transfer coefficient is assumed and no heat capacity is assigned to the resistance. The resistance is due to the constriction of the heat flow area and the flow lines are displaced to a certain distance from the actual contact, so some thermal capacity may be associated with it.

In order to obtain the step input response of an elemental channel with constriction resistance the shape of the heat flow channel is approximated by the shape shown in Fig. 27, as suggested by Heasley (17). In this approximation the area of the conical part increases with the square of the distance from the apex of the cone. It is not implied that the geometrical shape of the actual elemental channel is similar to the one presented but only that the heat is assumed to flow through a path that can be represented in this way. The transient response of this elemental channel shall be compared to that of a uniform channel (rod) with the step rise of temperature applied to one end through a constant heat transfer coefficient (Fig. 27).

For the constant cross section channel the problem is formulated as follows.

The governing equation is

$$\frac{\partial^2 T(x,t)}{\partial x^2} = \frac{1}{\alpha} \frac{\partial T(x,t)}{\partial t} \quad (A-1)$$

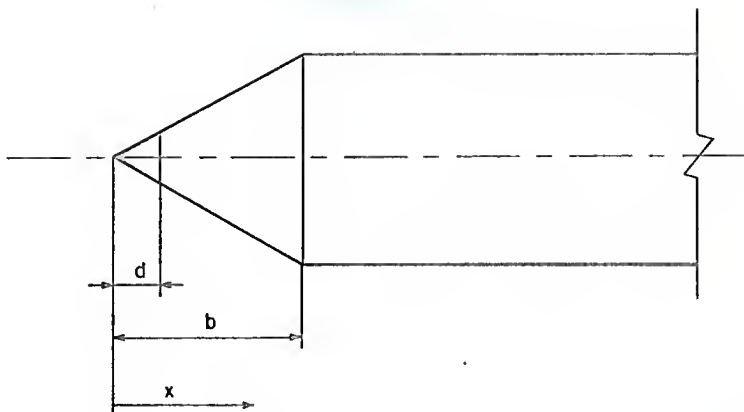


Figure 27.a. Constricted heat channel model

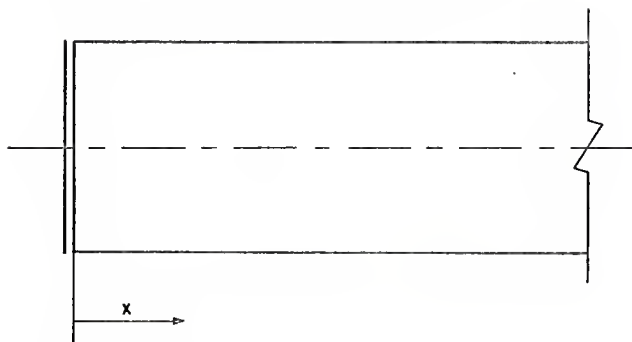


Figure 27.b. Constant cross section heat channel model with input resistance.

Figure 27. Two models of elemental heat channel.

where $\alpha = \frac{k}{C\rho}$ is the thermal diffusivity.

The boundary condition applied at $x = 0$ is

$$-k \frac{\partial T(x,t)}{\partial x} = h(T_0 - T(x,t)) \quad x = 0, t > 0 \quad (\text{A-2})$$

where T_0 is the temperature level applied at $t = 0$, and h is the heat transfer coefficient at the surface.

The initial condition is

$$T(x,0) = 0$$

and the other boundary condition

$$\lim_{x \rightarrow \infty} T(x,t) = 0$$

Applying the Laplace transform to the governing equation we have

$$\frac{\partial^2 \bar{T}(x,s)}{\partial x^2} = \frac{s}{\alpha} \bar{T}(x,s) \quad (\text{A-3})$$

which has the general solution

$$\bar{T}(x,s) = C_1 e^{\sqrt{\frac{s}{\alpha}} x} + C_2 e^{-\sqrt{\frac{s}{\alpha}} x} \quad (\text{A-4})$$

Since the temperature should be bounded for large x , $C_1 = 0$, and application of the boundary condition at $x = 0$ yields

$$k\sqrt{\frac{s}{\alpha}} C_2 e^{-\sqrt{\frac{s}{\alpha}} x} = h(T_0/s - C_2 e^{-\sqrt{\frac{s}{\alpha}} x}) \quad (\text{A-5})$$

The transformed solution is thus found to be

$$\bar{T}(x, s) = \frac{hT_0}{s(k\sqrt{\frac{s}{\alpha}} + h)} e^{-\sqrt{\frac{s}{\alpha}} x} \quad (\text{A-6})$$

The inverse transform of this expression can be readily obtained, however this is not true for the next case and thus only a comparison of the transformed solutions shall be made.

For the approximate constricted elemental channel (Fig. 27) it shall be assumed that the heat flow lines in the conical part are straight and diverge from the common origin on the axis of the heat channel at $x = 0$. With this assumption we have a one dimensional transient problem in the conical region also. The two governing equations are

$$\frac{\partial^2 V(x, t)}{\partial x^2} + \frac{2}{x} \frac{\partial V(x, t)}{\partial x} = \frac{1}{\alpha} \frac{\partial V(x, t)}{\partial t} \quad d < x < b \quad (\text{A-7})$$

$$\frac{\partial^2 T(x, t)}{\partial x^2} = \frac{1}{\alpha} \frac{\partial T(x, t)}{\partial t} \quad x > b \quad (\text{A-8})$$

where V is the temperature in the conical region.

The boundary and the initial conditions are

$$\begin{aligned}
 T(x,0) = V(x,0) &= 0 & x > d \\
 V(d,t) &= T_0 & t > 0 \\
 V(b,t) &= T(b,t) & t \geq 0 \\
 \frac{\partial V}{\partial x}(b,t) &= \frac{\partial T}{\partial x}(b,t) & t \geq 0 \\
 \lim_{x \rightarrow \infty} T(x,t) &= 0 & t \geq 0
 \end{aligned} \tag{A-9}$$

The Laplace transformed equations are

$$\frac{1}{x} \frac{d^2(x\bar{V}(x,s))}{dx^2} - \frac{s}{\alpha} \bar{V}(x,s) = 0 \quad d < x < b \tag{A-10}$$

$$\frac{d^2\bar{T}(x,s)}{dx^2} - \frac{s}{\alpha} \bar{T}(x,s) = 0 \quad b < x \tag{A-11}$$

The solution of Eq. (A-7) satisfying the conditions (A-9) is

$$\bar{V}(x,s) = \frac{T_0 d}{sx} \cosh\left(\frac{\sqrt{s}}{\alpha}(x-d)\right) + \frac{C_1}{x} \sinh\left(\frac{\sqrt{s}}{\alpha}(x-d)\right) \tag{A-12}$$

and the solution of Eq. (A-8) satisfying the conditions Eq. (A-9) is

$$\bar{T}(x,s) = C_2 e^{-\frac{\sqrt{s}}{\alpha}(x-b)} \tag{A-13}$$

Using the boundary conditions at $x = b$ to evaluate the constants C_1 and C_2 we obtain for the temperature in the uniform part of the rod (temperature in the conical part being of lesser interest)

$$\bar{T}(x, s) = \frac{T_o e^{-\sqrt{\frac{s}{\alpha}}(x-b)} \quad \text{---}}{sb \left[\sinh\left(\sqrt{\frac{s}{\alpha}}(b-d)\right) + \cosh\left(\sqrt{\frac{s}{\alpha}}(b-d)\right) - \frac{1}{\sqrt{\frac{s}{\alpha}}} \sinh\left(\sqrt{\frac{s}{\alpha}}(b-d)\right) \right]} \quad (\text{A-14})$$

To compare this result with the one obtained previously we should calculate the resistance of the constriction to a steady heat flow. Under the same assumptions as stated before for the heat flow lines the resistance due to constriction is

$$R = \frac{b(b-d)}{kd} = 1/h \quad (\text{A-15})$$

If we expand the hyperbolic functions in Eq. (A-14) into series and retain only the linear terms we obtain

$$\bar{T}(x, s) = \frac{T \frac{d}{ob(b-d)} e^{-\sqrt{\frac{s}{\alpha}}(x-b)} \quad \text{---}}{s \left(\sqrt{\frac{s}{\alpha}} + \frac{d}{b(b-d)} \right)} \quad (\text{A-16})$$

This expression is identical to Eq. (A-6) if the stationary constriction resistance is substituted for the heat transfer resistance $1/h$.

In order that the truncation of the series be acceptable the ratio of the lowest order term neglected to the terms retained should be

much less than one. We have the condition

$$\sqrt{\frac{s}{\alpha}} (b-d) \ll 2$$

$$s < \frac{2}{(b-d)^2} \quad (\text{A-17})$$

Thus the time constant of the transient effect is of the order

$$t_{\text{trans.}} \approx \frac{(b-d)^2}{2} \quad (\text{A-18})$$

A rough estimate of typical values for metallic contacts follows.

Using the ratio of apparent to real area of contact $b^2/d^2 = 100$, $k = .2 \text{ cal/cm sec } ^\circ\text{C}$ and $h = .2 \text{ cal/cm}^2 \text{ sec } ^\circ\text{C}$, the expression for the steady state resistance of the channel model with contraction Eq. (A-15) yields

$$b - d = \frac{k d}{h b} = .1 \text{ cm}$$

Assuming for α a typical value for metals, $.5 \text{ cm}^2/\text{sec}$, we have

$$t_{\text{trans.}} = \text{Order } (.1 \text{ sec})$$

Since in the present investigations periods of oscillation have been employed that are 3 orders of magnitude longer than this time it is concluded that the measured contact conductance is identical to the stationary conductance as far as the transient effects are concerned.

APPENDIX B: Correlation Technique.

In the analysis of records containing random noise components, the cross- and autocorrelation techniques have proven useful. With the development of convenient hybrid correlation computers, the correlation analysis of a much wider class of records has become possible, including high frequencies of the communication technology, whereas before only digitized records could be analyzed.

B.1 Correlation Function Definition and Properties

Although actually discrete analysis is performed on records of finite length, it is convenient to derive the theorems of the correlation technique for continuous records and infinite length.

The auto- and crosscorrelation functions are defined as

$$\phi_{ff}(\tau) = \lim_{t_i \rightarrow \infty} \frac{1}{2t_i} \int_{-t_i}^{t_i} f(t)f(t+\tau)dt \quad (\text{B-1})$$

and

$$\phi_{fg}(\tau) = \lim_{t_i \rightarrow \infty} \frac{1}{2t_i} \int_{-t_i}^{t_i} f(t)g(t+\tau)dt \quad (\text{B-2})$$

The functions $f(t)$ and $g(t)$ are the records under consideration and τ , the argument of the correlation functions, is the delay time. The autocorrelation function is a measure of the similarity of a record and its time delayed version, while the crosscorrelation function

relates a given record to a time delayed version of another record. The advantage of this procedure is to average the relationship between the records over the length of the records and thus eliminate any random fluctuations in either of them.

The relationship of the Fourier transform of the correlation functions to the Fourier transform of the functions is of considerable interest. The Fourier transform of the record is

$$\bar{F}\{f(t)\} = \bar{F}(\omega) = \frac{1}{\sqrt{2\pi}} \int_{-\infty}^{\infty} f(t)e^{i\omega t} dt \quad (\text{B-3})$$

The Fourier transform is a complex function of the frequency and let it be noted here that

$$\bar{f}(-\omega) = \bar{f}(\omega)^* \quad (\text{B-4})$$

where the asterisk denotes the complex conjugate.

Let the Fourier transform representation in Eq. (B-1) be substituted for the function $f(t+\tau)$. Reversing the order of integration and noting that

$$\lim_{t_1 \rightarrow \infty} \frac{1}{2t_1} \int_{-t_1}^{t_1} f(t)e^{-i\omega t} dt = \lim_{t_1 \rightarrow \infty} \frac{\sqrt{2\pi}}{2t_1} \bar{F}(-\omega) \quad (\text{B-5})$$

the following result is obtained

$$\phi_{ff}(\tau) = \lim_{t_i \rightarrow \infty} \frac{1}{2t_i} \int_{-\infty}^{\infty} \bar{f}(\omega) \bar{f}(-\omega) e^{-i\omega\tau} d\omega \quad (\text{B-6})$$

and taking the Fourier transform on both sides

$$F\{\phi_{ff}(\tau)\} = \lim_{t_i \rightarrow \infty} \frac{\sqrt{2\pi}}{2t_i} |\bar{f}(\omega)|^2 \quad (\text{B-7})$$

A similar result is obtained for the cross correlation function, following the same steps

$$\lim_{t \rightarrow \infty} \frac{\sqrt{2\pi}}{2t_i} \bar{f}(-\omega) \bar{g}(\omega) = \frac{1}{\sqrt{2\pi}} \int_{-\infty}^{\infty} \phi_{fg}(\tau) e^{i\omega\tau} d\tau \quad (\text{B-8})$$

From these expressions the possibility of evaluating the frequency response of a system is obvious. The frequency response function is defined as

$$H(\omega) = \frac{\bar{g}(\omega)}{\bar{f}(\omega)} \quad (\text{B-9})$$

where $\bar{g}(\omega)$ and $\bar{f}(\omega)$ are the Fourier transforms of the output and input, respectively. Substituting into Eq. (B-9) according to Eqs. (B-7) and (B-8) the following important result is obtained

$$|H(\omega)|^2 = \frac{|\bar{g}(\omega)|^2}{|\bar{f}(\omega)|^2} = \frac{F\{\phi_{gg}(\tau)\}}{F\{\phi_{ff}(\tau)\}} \quad (\text{B-10})$$

$$H(\omega) = \frac{\bar{g}(\omega)}{\bar{f}(\omega)} = \frac{F\{\phi_{fg}(\tau)\}}{F\{\phi_{ff}(\tau)\}} \quad (\text{B-11})$$

From the autocorrelation functions, only information on the amplitude of the frequency response function is available, but from the cross- and autocorrelation functions the complete (complex) frequency response function can be obtained.

A case of particular interest to this investigation is the cross-correlation of a harmonic function and a delayed function with the same period.

$$\begin{aligned} \text{Let } f(t) &= A \sin \omega t \\ g(t) &= B \sin(\omega t - \delta) \end{aligned} \quad (\text{B-12})$$

then

$$\phi_{fg}(\tau) = \frac{AB}{2t_i} \int_{-t_i}^{t_i} \sin \omega t \sin(\omega(t+\tau) - \delta) dt \quad (\text{B-13})$$

Here the crosscorrelation of a limited record is considered, of the length $2t_i + \tau_{\max}$. Use of addition theorems for the harmonic function leads to

$$\begin{aligned} \phi_{fg}(\tau) &= \frac{AB}{2t_i} \int_{-t_i}^{t_i} [\sin^2 \omega t (\cos \omega \tau \cos \delta + \sin \omega \tau \sin \delta) + \\ &\quad + \sin \omega t \cos \omega t (\sin \omega \tau \cos \delta - \cos \omega \tau \sin \delta)] dt \end{aligned} \quad (\text{B-14})$$

Note that

$$\int_{-t_i}^{t_i} \sin^2 \omega t dt = t_i - \frac{1}{2\omega} \sin 2\omega t_i$$

$$\int_{-t_i}^{t_i} \sin \omega t \cos \omega t \, dt = 0 \quad (\text{B-15})$$

and the result is

$$\phi_{fg}(\tau) = \left(\frac{1}{2} - \frac{\sin 2\omega t_i}{4\omega t_i} \right) AB \cos(\omega t - \delta) \quad (\text{B-16})$$

Thus the delaying angle δ is preserved in the crosscorrelation function as the lag of the cosine.

For the autocorrelation function it can be similarly shown that

$$\phi_{ff}(\tau) = \left(\frac{1}{2} - \frac{\sin 2\omega t_i}{4\omega T} \right) A^2 \cos \omega t \quad (\text{B-17})$$

for $f(t) = A \sin(\omega t + \delta)$

From the crosscorrelation and the autocorrelation functions both the phase lag and the amplitude ratio can be determined, as shown before for a more general case.

It should be noted that the square of the original amplitude appears in the autocorrelation function. If the original record contains several harmonic functions the ratios of their amplitudes in the autocorrelation function is the square of the amplitude ratio in the record. Thus a square wave with the period $\frac{2\pi}{\omega}$, in Fourier series representation

$$f(t) = A(\cos \omega t - \frac{1}{3} \cos 3\omega t + \frac{1}{5} \cos 5\omega t - \dots) \quad (\text{B-18})$$

has a sawtooth autocorrelation function, the Fourier representation of which is

$$\phi_{ff}(\tau) = \frac{A^2}{2} \left(\cos\omega\tau + \frac{1}{3^2} \cos 3\omega\tau + \frac{1}{5^2} \cos 5\omega\tau + \dots \right) \quad (\text{B-19})$$

Thus the harmonic with the highest amplitude is emphasized in the autocorrelation function.

The advantage of the use of the correlation function instead of the direct investigation of the records (by frequency analysis) is that the noise components are greatly reduced by the averaging process of the correlation function computation, which requires much simpler operation than the frequency analysis. This is illustrated in the following analysis.

Assume a record containing a signal and a noise component

$$f(t) = s(t) + n(t)$$

the noise component being characterized by zero expectation of the mean and certain total power (variance). The autocorrelation function in this case is

$$\phi_{ff}(\tau) = \lim_{t_1 \rightarrow \infty} \frac{1}{2t_1} \int_{-t_1}^{t_1} (s(t) + n(t))(s(t+\tau) + n(t+\tau)) dt \quad (\text{B-20})$$

which reduces to the four terms

$$\phi_{ff}(\tau) = \phi_{ss}(\tau) + \phi_{sn}(\tau) + \phi_{ns}(\tau) + \phi_{nn}(\tau) \quad (\text{B-21})$$

If the noise is not correlated with the signal, the middle two terms approach zero and only the signal and the noise autocorrelation functions remain. For white noise and infinite integration time the noise autocorrelation function is a δ -function in τ . For limited lengths of the record and for limited bandwidth the autocorrelation function of the noise is a decaying exponential. In the case of crosscorrelation of a noisy record with a reference record that does not contain noise there are only two terms

$$\phi_{fg}(\tau) = \phi_{sg}(\tau) + \phi_{ng}(\tau) \quad (\text{B-22})$$

and the noise component is eliminated more efficiently.

B.2 Discrete and Finite Correlation Function.

In practical applications only correlation functions of finite length are obtained and most often in a discrete (tabulated) form. From the detailed analysis of the limitations imposed by the finite length of the correlation function (7, 8) two important conclusions shall be cited.

The finite length of the correlation function reduces the Fourier transform to the Fourier series analysis, with only discrete frequencies present. These frequencies are at a distance $\Delta f = \frac{1}{2T}$ if the total length of the function is $2T$. Two frequencies closer than Δf cannot

be distinguished.

The discrete nature of a correlation function renders it impossible to distinguish between a frequency component and another component of the related frequency from the series

$$f, 2kf_N - f, 2kf_N + f, \dots, k = 1, 2, \dots$$

where $f_N = 1/2\Delta\tau$ is the Nyquist frequency. To avoid the ambiguity introduced by this folding process it is preferable that the amplitudes of all components outside the principal frequency band, 0 to f_N , be negligible compared to those within.

APPENDIX C: Analysis of Correlator Response

C.1 Correlator Amplitude Response

For the analysis of the magnetic tape recordings of the thermocouple voltages a TMC Correlation Computer (Model 257, NE 1363) in conjunction with the TMC Computer of Average Transients (CAT 400 C, NE 1364) was used. In the preliminary investigations it was found that the amplitude ratios obtained for the thermocouple voltage records did not match the phase angle differences as expected from the theoretical model. Since the phase differences agreed with the expected values, the amplitude responses of the correlator, the tape recorder, the recording and the playback circuits were investigated. The correlator response was tested by three methods: autocorrelation of unbiased square wave input, autocorrelation of unbiased sinusoidal input and correlation of sinusoidal inputs with various bias voltages, periods and correlator settings.

With the square wave input 17 runs were performed with flat-to-flat amplitude ranging from .162 V to 5.57 V, the maximal permissible input voltage of the correlator being ± 3 V. The square wave was generated by an oscillator (Krohn-Hite Oscillator, Model 400 C, NE 1343) and the flat-to-flat voltage was determined by a precision voltmeter (Keithley Electrometer 600 A, NE 906). The frequency of the oscillator was .148 Hz and the correlator settings were: A*A (autocorrelation), 128 points, multiplier 16. Timing was manual and an integration time of 2 minutes was used.

The autocorrelation function obtained was fitted by the analytic form

$$y = a_0 + a_1 (-1)^{\text{int}(2x/a_2)} (1 - (2x)_{\text{mod } a_2}) \quad (\text{C-1})$$

where a_0 is the constant component, a_1 the amplitude and a_2 the period of the sawtooth function. The sum of error squares was minimized by a general multivariable function minimization code. Subsequently this code was found to be too slow to be used for the least squares analysis with several parameters and the code described in Appendix F was developed for the analysis of the experimental data.

The results of the square wave tests are plotted in Fig. 28. On a linear plot some nonlinearity was visible and indeed on the log-log plot the experimental points seem to define a line with exponent (slope) 1.085. The slope was determined graphically and no further analysis was performed as the square wave input is not representative of the records analyzed on the correlator.

A second set of correlator amplitude response tests was performed using a sine wave input generated by the oscillator (same as above). The input amplitude was again measured by the voltmeter. 15 tests were performed with identical inputs and 8 tests with different amplitudes to the two correlator inputs. The correlator settings were: A*B (cross-correlation), 128 points, multiplier 16. The period of the input oscillations was 10 seconds. The correlator output was analyzed by the program described in Appendix F and the results are plotted in Fig. 29.

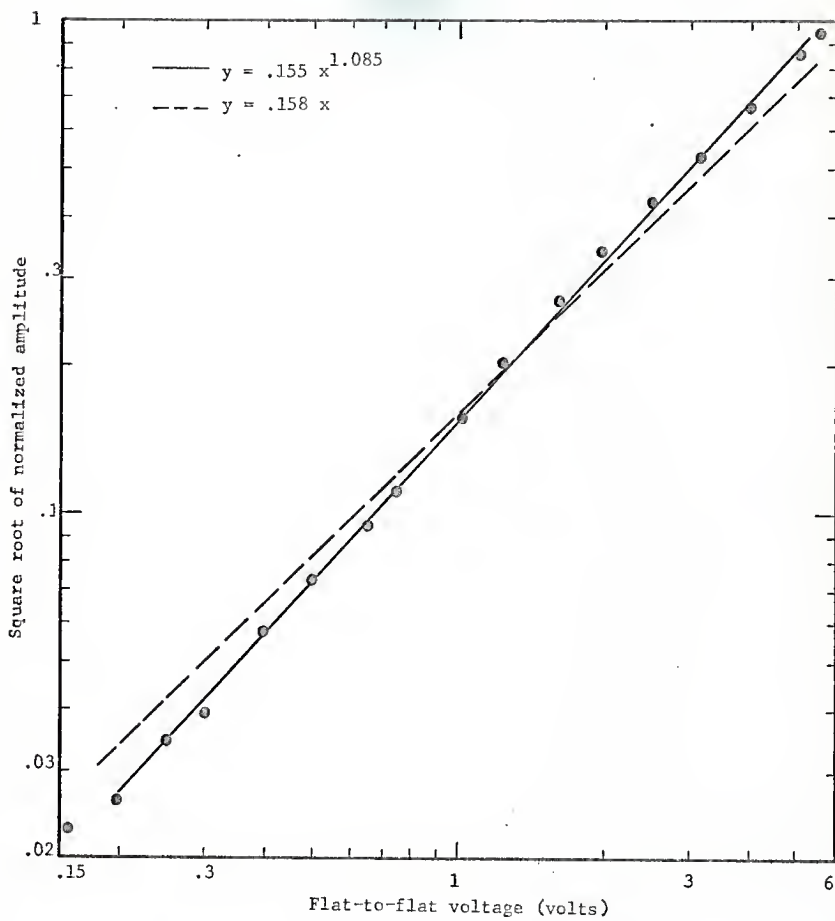


Figure 28. Correlator amplitude response. Square wave input

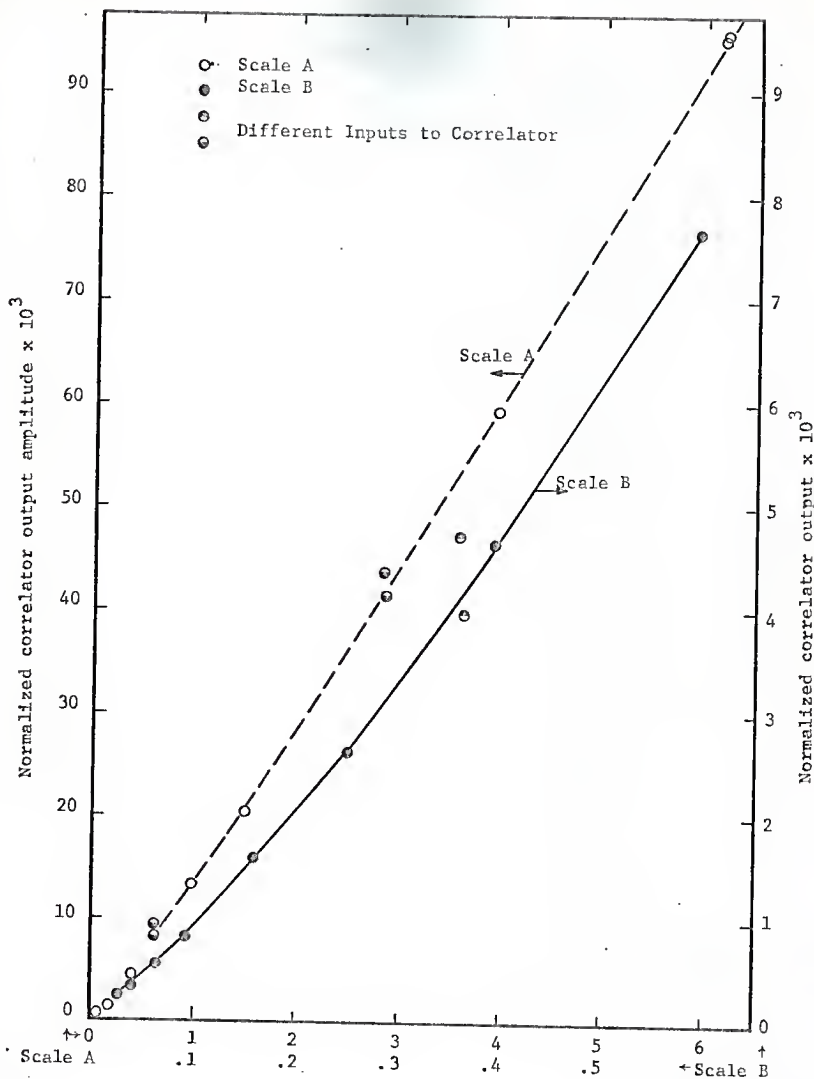


Figure 29. Correlator amplitude response test. Sine wave input.

Note that the product of the two input amplitudes is used as the abscissa and the correlator output amplitude as the ordinate, in Fig. 29. The square roots of these quantities are related for the first correlator test.

The nonlinearity is again evident. To determine whether it is significant a regression analysis for 13 runs with equal input (auto-correlation runs) was performed. Two models were fitted to the data points,

Model A

$$y = a_0 x^2 \quad (C-2)$$

Model B

$$y = a_0 x^{a1} \quad (C-3)$$

where y is the correlator output amplitude and x is the input voltage. A simple computer program was devised for the sum of squares minimization for the nonlinear model B. For model A the least sum of error squares was found to be 2.34×10^7 (arbitrary units) and for the model B with exponent 2.172 the sum of squares was 3.34×10^6 . The 99% confidence margin around the smaller sum of squares is 3.88×10^6 and thus the difference in exponent can be considered highly significant. At the same time the spread of the points around this curve is small enough that the amplitude information could be used for the measurements. Yet the eight test runs with different inputs were considerably off the line fitted to the autocorrelation points. Invariably the points for runs where correlator input B had higher amplitude than A are above the

line and vice versa. Note the very good agreement between the exponent obtained in this test and the one obtained graphically for the square wave input tests (2.172 versus 2×1.085).

To establish a relationship which would take into account the effects of inputs A and B separately, a third series of tests was performed. To each input various bias voltages were applied and two periods of oscillations, two correlator settings and two integration times were used. The input amplitudes as the main variables of investigation and the background variables were randomized for the 30 test runs performed. The oscillator was used to generate the sinusoidal input voltage and the exact ratios were obtained on the analog computer, the components of which are within .1% tolerance. The results of the tests are plotted in Fig. 30. The abscissa is the product of the two input voltage amplitudes and the ordinate is the correlator output amplitude. The correlator output was analyzed with the computer program described in Appendix F.

A very wide spread of the test results is evident. Although some spread was expected from the results of the previous test for different amplitudes of the two correlator inputs, a detailed inspection reveals that it is due here not only to the different response of the two inputs but also to a considerable extent to the other variable conditions in the tests. In Fig. 31 the 10 test results are plotted for which the product of the two input voltage amplitudes was 1. The spread within the group of four tests where B input was 2 volts is more than 10%, which is much in excess of the tolerable error. The bias voltage seems

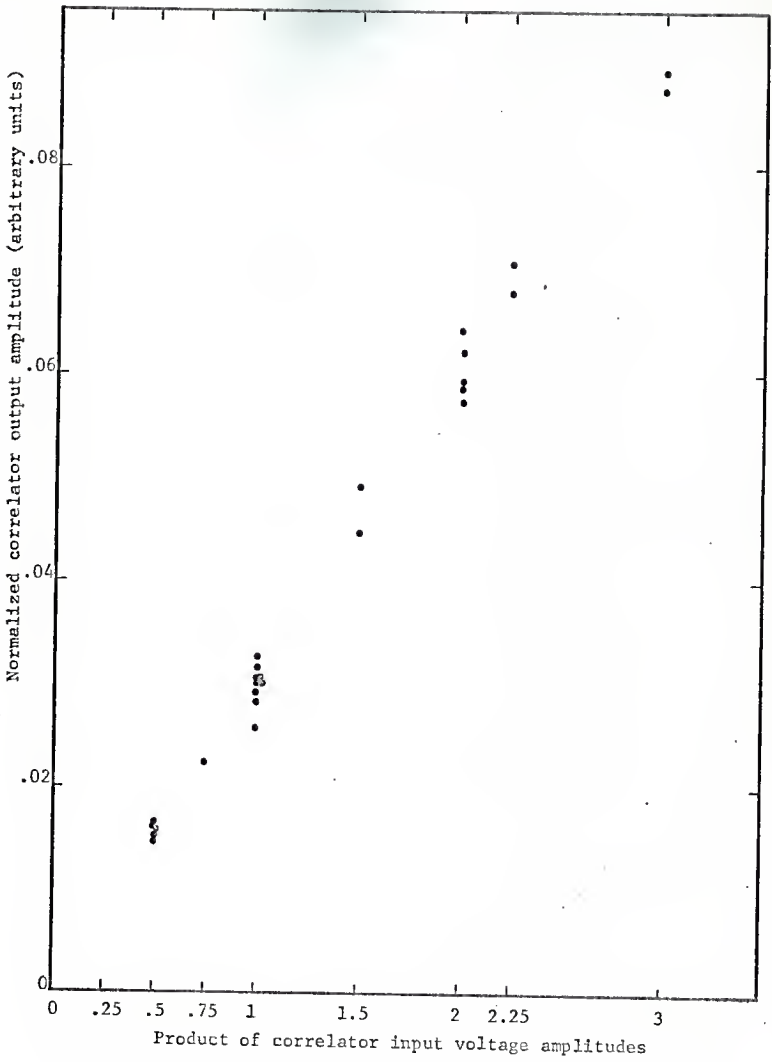


Figure 30. Correlator amplitude response. Randomized sine inputs.

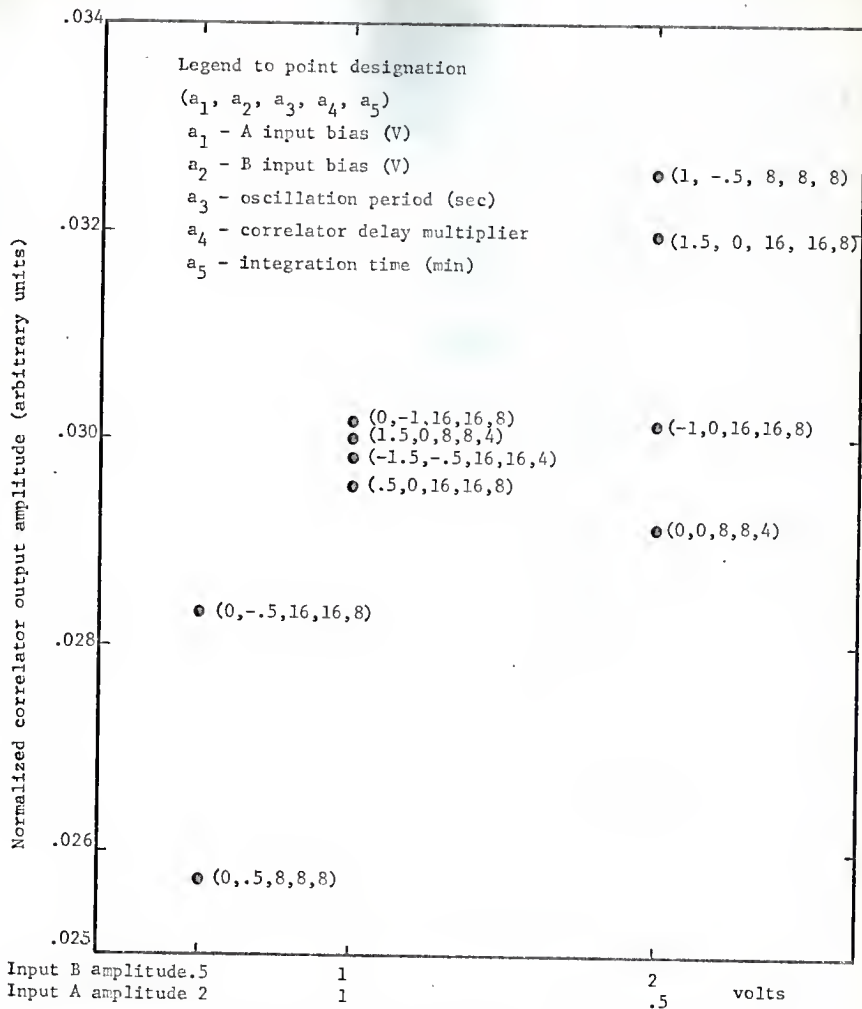


Figure 31. Correlator amplitude response. Sinusoidal inputs, product of voltage amplitudes = 1.

to be quite important though not the only influence involved. No simple correlation between the parameters is evident and even if a satisfactory model would be developed it would be very difficult to apply it as in the experimental temperature records the bias is variable for both inputs.

At this point it was concluded that the amplitude information obtained from the correlations of the experimental records cannot be relied upon and only the phase information was used in the experimental data analysis.

C.2 Response of Individual Correlator Channels.

A number of correlator outputs from the experimental records were analyzed and it was observed that the randomness criterion for the residues (cf. App. F 2.7) was rarely met. The residues were plotted and a recurring pattern was observed, similar to the correlator bias response, Fig. 24, obtained later. Since the prominent features of the residuals pattern are easily identified with certain correlator channel numbers the effect was attributed to the correlator. Several tests were performed with a constant voltage as the input of the correlator. The correlation function had the shape as presented in Fig. 24, and not only was the general trend repeated in different runs but also the fine detail of the function, i.e. the fluctuations of the output for individual channels is not random but due to some characteristics of the equipment. Further it was found that the amplitude and the sign is correlated with the input A. It is guessed that the cause of this unevenness is in the temporary storage for the input A, as this

is the input that is delayed by the correlator. The amplitude of the largest deviation from the mean horizontal line is approximately $.7 \times 10^{-3}$ of the norm count for a 1 V bias voltage input.

For further analyses of the correlator outputs this correlator background function was incorporated as one of the component functions in the least square fit in the code described in Appendix F. The correlator background function is found to be a statistically significant component of the correlator output in a great majority of cases. A correlation also exists, as expected, between the mean deviation from the norm count and the correlator background function coefficient.

In approximately 25% of the cases the randomness criterion for the residues after the least squares analysis (cf. App. F 2.7) is still not satisfied. A possible reason for this may be that the background function is also nonlinearly dependent on the bias of the input.

C.3 Accuracy of Phase and Period Determination.

The accuracy of the phase angle determination from the correlator output can be estimated from the phase angle found in the correlator tests, where the inputs were of the same or opposite phase with no lag. Of the 30 tests in the last group of correlator tests (see preceding section) 18 were with opposite phase and 12 with phase 0. The mean deviation from the expected value was .00291 and .00107, respectively for the two subgroups, and the standard deviation estimates were .00410 and .00506. It can thus be concluded that the phase angle error shall exceed .01 radians or approximately $.5^\circ$ in less than 90% of the cases.

The least squares analysis of the correlator output sometimes gives narrower confidence limits, down to .001 rad, but this only indicates that the data define the angle with that precision and not that these are the limits within which the real angle is located with the specified probability.

To determine the accuracy of the delay increment timing of the correlator a test was made with square wave input. The period of oscillation of the square wave was measured with an electronic timer (Eckman Time Interval Meter, Model 7250R, NE 763). The measured period of the input was compared to the period of the autocorrelation function. It was found that the correlator delay timing is 1.5 to 2% slow, i.e. the delay increments are that much longer than specified. In present measurements the period of the temperature oscillations was determined by the synchronous motor speed and the gear ratio and not from the correlator output.

APPENDIX D: Analysis of the Recording Circuit, Playback Circuit and
Tape Recorder Response.

D.1 Recording and Playback Circuits.

To eliminate high frequency electronic noise, filtering circuits were used during recording of the thermocouple voltages and during the record analysis. The signals were also amplified both during recording and during analysis. For the filtering and amplifying circuits the components of an analog computer were used (Electronics Associates Co. PACE TR-10, NE 816). The resistors and the capacitors, which determine the amplification and the time constants are guaranteed to be within .1% of the nominal value. Measurements of the resistance of the resistors showed even less deviation between individual parts. The schematics of the circuits are shown in Fig. 32.

The filtering function is performed by an integrator with resistance in the feedback loop. The transfer function of such a circuit is

$$\frac{\bar{U}_o}{\bar{U}_i} = \frac{R_f/R_i}{R_f C_f s + 1} \quad (D-1)$$

where index f denotes feedback and i input components. The direct current gain of such filter is R_f/R_i and the break frequency (angular) is $\omega_b = R_f C_f$.

In the recording circuit two filtering units were used, with the following elements:

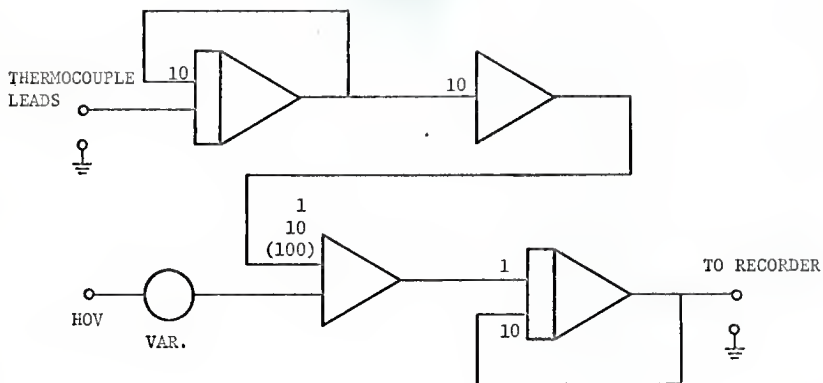


Figure 32.a. Recording filtering and amplifying circuit.

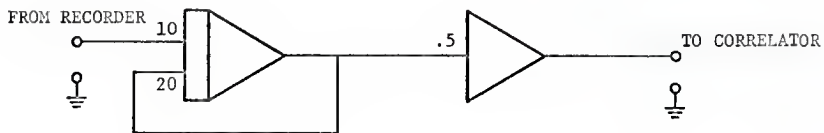


Figure 32.b. Playback filtering and amplifying circuit.

Figure 32. Filtering and amplifying circuits.

$$C_f = 10^{-5} f$$

$$R_f = 10^5 \Omega$$

$$R_i = 10^4 \Omega$$

Thus the filter had a 10 fold amplification and the time constant was 1 sec, the corresponding break frequency is $\omega_b = 1 \text{ sec}^{-1}$, $f_b = .159 \text{ Hz}$. The record was played back at 16 times the recording speed and the tape output was passed through another filter with time constant .05 sec (break frequency $\omega_b^1 = 20 \text{ sec}^{-1}$, $f_2^1 = 3.18 \text{ Hz}$). At the recording speed this would correspond to a break frequency $\omega_b = 1.25 \text{ sec}^{-1}$, $f_b = .198 \text{ Hz}$. The shortest period of the temperature oscillations used was 1.92 minutes, which corresponds to a frequency of .0087 Hz and is more than a decade below the break frequencies, in the region where the response can be considered the same for all practical reasons as for direct current.

More important than the absolute lag caused by the filtering circuits is the difference between the circuits. A test was performed to determine this. A sinusoidal voltage was passed through the four parallel recording circuits, recorded and the record analyzed on the correlator. To simulate the actual conditions, different amplifications were used in the four circuits, ranging from 10^3 to 10^5 , the input signal being previously appropriately reduced for each circuit. The correlator outputs were analyzed by the computer program described in Appendix F. The phase angle determined was in all cases within .008 radians (approx. $.45^\circ$) from 0 or π , depending on the sign of the record. This is within the limits of the accuracy of the phase angle determination from the correlator output (cf. section C 3.). The recording and playback circuits and the tape recorder

thus do not seem to add any error to the phase between the inputs. The limits of accuracy for the electronic equipment presently used can be considered .01 rad or .5°.

D.2 Tape Recorder Amplitude Response.

In the examination of the results of the circuitry and the tape recorder phase angle accuracy it was noticed that the amplitudes of the correlation functions were not identical as they should have been. As a possible source of the incongruence the tape recorder amplitude response was investigated. A sinusoidal voltage was introduced to the inputs of the four recording channels. The autocorrelation function of each record was obtained and subsequently analyzed with the computer program. The results are presented below.

Tape recorder channel	Normalized autocorrelation function amplitude	Square root of normalized amplitude
1	.03550	.188
2	.04600	.214
3	.04640	.215
4	.0496	.222

The differences are due to the imperfect condition of the recorder data converter circuits. The weaker gain of channel 1 was observed early in the course of investigations, but the repair was not possible as the malfunctioning component substitute was not available. The imperfection of the tape recorder further justifies the decision not to attempt to use the amplitude information of the temperature oscillations.

APPENDIX E: Regression Analysis

E.1 Least Squares Principle

Of several possible criteria for obtaining a "best" fit of an analytic curve to a set of data points the least squares principle is most often applied. In the case of normally distributed errors the curve fitted in this sense is the curve of maximal likelihood, as can be seen from the following (14).

Assume that the errors of a sample y_1, y_2, \dots, y_n , corresponding to the independent variable vectors x_1, x_2, \dots, x_n from the time values are random with expectation zero, with no correlation (covariance matrix is diagonal $V(e = I\sigma^2)$ and normally distributed, $e \sim N(0, I\sigma^2)$.

The likelihood function for the sample is in that case

$$\begin{aligned}
 P(y_1, y_2, \dots, y_n) &= \prod_{i=1}^n \frac{1}{\sigma(2\pi)^{1/2}} \exp(-e_i^2/2\sigma^2) = \\
 &= \frac{1}{\sigma^n (2\pi)^{n/2}} \exp(-e^T e / 2\sigma^2) \quad (E-1)
 \end{aligned}$$

The maximum likelihood estimate of an analytical model is thus the one that minimizes the sum of squares of the differences between the observed values and the predicted values. If there is reason to believe that the errors have a different distribution than normal other criteria for the maximal likelihood estimate can be obtained.

E.2 Least Square Determination of Linear Parameters

A set of observations is given, y_1, y_2, \dots, y_n and the assumed analytical model is a linear combination of k functions of the independent variables

$$\hat{y}(x) = b_1 Z_1(x) + b_2 Z_2(x) + \dots + b_k Z_k(x) \quad (\text{E-3})$$

The problem of finding the values of the linear constants b_i is one of solving the system of equations, in matrix notation

$$\begin{bmatrix} Z_1(x_1) & Z_2(x_1) & \dots & Z_k(x_1) \\ Z_1(x_2) & Z_2(x_2) & \dots & Z_k(x_2) \\ \dots & \dots & \dots & \dots \\ Z_1(x_n) & Z_2(x_n) & \dots & Z_k(x_n) \end{bmatrix} \begin{bmatrix} b_1 \\ b_2 \\ \dots \\ b_k \end{bmatrix} = \begin{bmatrix} y_1 \\ y_2 \\ \dots \\ y_n \end{bmatrix} \quad (\text{E-4})$$

or

$$Zb = y \quad (\text{E-4a})$$

In the practical cases when the observations y_i are subject to errors the number of the observations should largely exceed the number of the parameters to be determined and we have an overdetermined inconsistent system. A consistent system is obtained by adding an error vector,

$$Zb = y + e \quad (\text{E-5})$$

and the solution of this overdetermined system shall be sought in the least sum of square errors sense.

The sum of squares of the errors is

$$e^T e = (Zb - y)^T (Zb - y) = b^T Z^T Z b - y^T Z b - b^T Z^T y + y^T y \quad (E-6)$$

The necessary condition for a minimum is that all the derivatives according to individual parameters are equal to zero

$$\begin{aligned} \frac{\partial (e^T e)}{\partial b_i} = & (0, 0, \dots, 0, 1, 0, \dots, 0, Z^T Z b + b^T Z^T Z (0, \dots, 0, 1, 0, \\ & \dots, 0, Z^T y - 2(0, \dots, 0, 1, 0, \dots, 0, Z^T y) = 0 \quad (E-7) \end{aligned}$$

The k such equations for the parameter vector b at the point of minimal sum of squares can be assembled into a new matrix equation

$$Z^T Z b = Z^T y \quad (E-8)$$

If the square matrix $Z^T Z$ is not singular we have the solution

$$b_0 = (Z^T Z)^{-1} Z^T y \quad (E-9)$$

which satisfies the system Eq. (E-4) in the sense of minimizing the sum of squares of the errors. At this point the standard deviation of the errors can be estimated, the unbiased estimate being

$$s_e^2 = e^T e / (n-k) \quad (E-10)$$

To check the validity of the assumed analytical model the errors (residues) should be tested. If the errors are not random the analytical model Eq. (E-3) is not appropriate.

E.3 Confidence Limits of the Parameters

If the errors are distributed normally the F-test is applicable to the sum of squares of the errors. The minimal sum of squares of the differences between the observations and the analytical model points is compared to the sum of squares of the differences between the least square analytical model (parameter vector b_0) and the analytical model with a different parameter vector, b .

Here the error sum of squares of the observations around the least square solution has $n-k$ degrees of freedom and the additional sum of squares of a compared fit has k degrees of freedom (n being the number of data points and k the number of parameters in the model equation).

The two sums of squares are defined as

$$SS(b|b_0) = (\hat{y}[b] - \hat{y}[b_0])^T (\hat{y}[b] - \hat{y}[b_0]) = (b-b_0)^T Z^T Z (b-b_0) \quad (E-11)$$

$$SS(b_0) = (y - \hat{y}[b_0])^T (y - \hat{y}[b_0]) = (y - Zb_0)^T (y - Zb_0) \quad (E-12)$$

where y_i are the observed values and $y_i(b_0)$ and $y_i(b)$ are the values predicted by the model with different parameter vectors. The criterion

for the nonsignificance of the additional error sum of squares at the $(1-\alpha)$ confidence level is

$$SS(b|b_0)/SS(b_0) \leq k F_{(1-\alpha)}(k, n-k)/(n-k) \quad (E-13)$$

This relation can be expressed as

$$(b-b_0)^T Z^T Z (b-b_0) \leq (Zb_0 - y)^T (Zb_0 - y) k F_{(1-\alpha)}(k, n-k)/(n-k) = \Delta SS \quad (E-14)$$

In the k -dimensional space of the parameters b_i the relation defines a region inside which the actual parameter vector is situated with the specified probability, on the basis of the information contained in the data. The equality sign defines the confidence region limit. As we have a quadratic form on the left side the form of the confidence region is a hyperellipsoid. For visual presentation the case of two linear parameters shall be used (Fig. 33).

The confidence region is fully determined by the vector b , the matrix $Z^T Z$ and the confidence margin of the sum of squares, ΔSS . For each individual parameter a confidence interval can be obtained. The confidence interval for each parameter can be defined either as the width of the ellipsoid on the line parallel to the axis of the parameter (points C and D in Fig. 33), or by the "support plane" distance, i.e. by tangential planes on the ellipsoid (points A and B). The latter definition is more suitable as such interval contains the whole range that the parameter can assume within the confidence region. The two intervals

coincide when the principal axes of the ellipsoid are parallel to the axes of the parameters, i.e. when the matrix $Z^T Z$ is diagonal (the functions $Z_i(X)$ are orthogonal). Note that the support plane confidence limits should not be applied simultaneously to several parameters, e.g. point E in Fig. 33 lies outside the confidence region though both parameters are within the confidence intervals.

The extreme value of a parameter on the confidence region boundary is reached in the point that satisfies Eqs. (E-15) and (E-16). The equation of the confidence region boundary is

$$(b-b_o)^T Z^T Z (b-b_o) = \Delta SS \quad (E-15)$$

and the partials according to other parameters are

$$\partial / \partial b_i [(b-b_o)^T Z^T Z (b-b_o)] = 0 \quad i = 1, 2, \dots, k \quad i \neq j \quad (E-16)$$

After differentiation $k-1$ equations are obtained

$$(0, 0, \dots, 0, 1, 0, \dots, 0) Z^T Z (b_{mj} - b_o) = 0 \quad (E-17)$$

where the only element different from zero in the first vector is at position j .

Substituting these equations into Eq. (E-15) we have

$$(0, \dots, 0, b_{j,mj} - b_j, 0, \dots, 0) Z^T Z (b_{mj} - b_o) = \Delta SS \quad (E-18)$$

We can treat the equations for the support plane points of all parameters together by forming a matrix equation

$$\begin{bmatrix} b_{1,m1} - b_{1,0} & 0 & \dots & 0 \\ 0 & b_{2,m2} - b_{2,0} & \dots & 0 \\ \dots & \dots & \dots & \dots \\ 0 & 0 & \dots & b_{k,mk} - b_{k,0} \end{bmatrix} Z^T Z \begin{bmatrix} b_{m1} - b_o \\ \dots \\ b_{mk} - b_o \end{bmatrix} =$$

$$= \Delta S S \cdot I \quad (E-19)$$

where b_{mi} indicates the parameter vector at the support plane point for parameter i and $b_{i,mi}$ indicates the value of parameter i at such point.

Multiplying by corresponding inverses and noting that the multiplication with diagonal matrices is commutative we obtain

$$\begin{bmatrix} b_{m1} - b_o & | & b_{m2} - b_o & | & \dots & | & b_{mk} - b_o \end{bmatrix} \begin{bmatrix} b_{1,m1} - b_{1,0} & 0 & \dots & 0 \\ 0 & b_{2,m2} - b_{2,0} & \dots & 0 \\ \dots & \dots & \dots & \dots \\ 0 & 0 & \dots & b_{k,mk} - b_{k,0} \end{bmatrix} =$$

$$= (Z^T Z)^{-1} \Delta S S \quad (E-20)$$

We are at this point interested only in the confidence limits of the individual parameters and not in the parameter vectors in the support plane contact points. For the confidence limits of the individual

parameters we have

$$(b_{i,mi} - b_{i,0})^2 = c_{i,i} \Delta SS \quad (E-21)$$

where $c_{i,i}$ is the diagonal element of the matrix $(Z^T Z)^{-1}$. The half width of the support plane confidence interval is

$$b_{i,mi} - b_{i,0} = [c_{i,i} e^T e_k F_{(1-\alpha)}(k, n-k)/(n-k)]^{1/2} \quad (E-22)$$

E.4 Linearized Confidence Limits for Nonlinear Parameters

The model which is fitted to the observed data may contain nonlinear parameters. The matrix method described above is not applicable for finding the least squares solution nor is the method for obtaining the confidence limits. However the model function can be expanded in a Taylor series and only the linear term retained if the confidence region is small enough that this approximation is sufficiently accurate. The additional error due to the deviation in the parameters is then given by

$$e - e_0 = \begin{bmatrix} \frac{\hat{y}}{\partial b_1}(x_1) & \frac{\hat{y}}{\partial b_2}(x_1) & \dots & \frac{\hat{y}}{\partial b_k}(x_1) \\ \frac{\hat{y}}{\partial b_1}(x_2) & \frac{\hat{y}}{\partial b_2}(x_2) & \dots & \frac{\hat{y}}{\partial b_k}(x_2) \\ \vdots & \vdots & \ddots & \vdots \\ \frac{\hat{y}}{\partial b_1}(x_n) & \frac{\hat{y}}{\partial b_2}(x_n) & \dots & \frac{\hat{y}}{\partial b_k}(x_n) \end{bmatrix} (b - b_0) = P(b - b_0)$$

(E-23)

and the additional sum of squares is $(b-b_0)^T P^T P (b-b_0)$. The approximate confidence region is limited by the surface

$$(b-b_0)^T P^T P (b-b_0) = \Delta SS \quad (E-24)$$

A similar procedure can be followed in determining the support plane confidence interval as in the linear case and the result

$$(b_{j,mj} - b_{j,0})^2 = \gamma_{j,j} \Delta SS \quad (E-25)$$

is obtained, where $\gamma_{j,j}$ is the diagonal element of the matrix $(P^T P)^{-1}$.

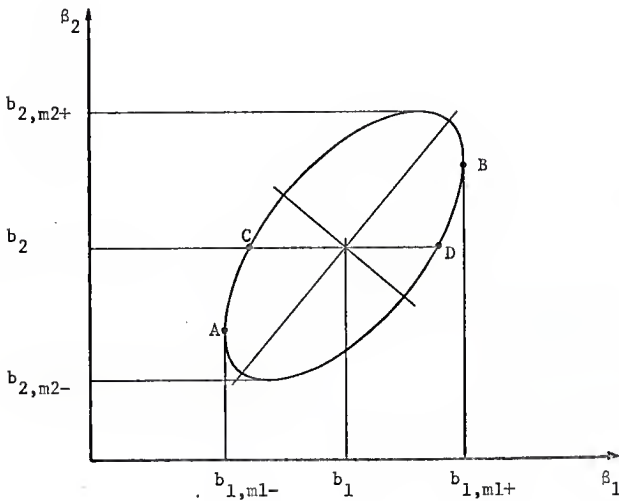


Figure 33. Parameter confidence region for two linear parameters.

APPENDIX F. Correlator Output Analysis Computer Program

F.1 General

From the correlator output the prominent harmonic component is to be obtained, as well as its amplitude, phase, period and possibly higher harmonic components with periods that are multiples of the fundamental harmonic period. Because the records also contain some drift, usually nonlinear, and furthermore since the response of individual channels of the correlator is not uniform (cf. Appendix C), the appropriate analytic form which has to be fitted to the correlator output is

$$\hat{y}_i = b_1 + \sum_{j=1}^{\text{npoly}-1} b_j P'_j(x_i) + b_{\text{npoly}} F_{\text{cb}}(x_i) + \sum_{j=1}^{\text{nharm}} [b_{\text{npoly}+j} \cos \frac{2\pi j x_i}{t_o} + b_{\text{npoly}+j+1} \sin \frac{2\pi j x_i}{t_o}] \quad (\text{F-1})$$

where $P'_j(x_i)$ is a polynomial of order j and $F_{\text{cb}}(x_i)$ is the correlator bias response function. The Legendre polynomials, approximately orthogonal on the sample points, are used, though this does not simplify the computation as the least squares fit is obtained by the matrix method.

One parameter in the expansion appears nonlinearly, the period of the fundamental harmonic, t_o . If several nonlinear parameters were involved a general sum of squares minimization algorithm would have to

be used (14, 23), but with only one nonlinear parameter, a simpler and faster method can be applied.

The input data is considered to be an equidistant table of functional values, and only the ordinate at each point is supplied. The abscissae are generated and associated internally with each data point. This is necessary because erroneous points are rejected by the code and the data set is no longer equidistant.

The code features the ability to determine the initial guess for the prominent frequency period. The initial guess has to be close enough to the true value as otherwise a local minimum of sum of squares may be obtained instead of the desired solution. The recognition of the prominent harmonic is possible even if several erratic points are present or if due to general slope the local extremes of the harmonic component are inconspicuous.

Erratic points in the correlator output are often observed, due to malfunction of the electronic components of the correlator or in the transfer of data. The residuals of the least squares fit are checked and each of them compared to the standard deviation estimate. If the sum of squares of the residuals above a present value (3.291σ for 99.9% confidence level) exceeds half of the confidence limit margin such points are rejected and the fitting of the analytical model repeated.

The residuals are subsequently checked for randomness and the result of the check is displayed.

Ultimately the confidence limits for the parameters are calculated.

For the nonlinear parameter only the linearized confidence limit estimate is obtained. For the harmonics the amplitude and the phase angle is calculated as well as the confidence limits for the phase angle. The parameters correlation matrix is also displayed.

Several additional output options are available, various matrices can be displayed during the least squares analysis and the residuals can be punched on cards for further analysis.

Details of the algorithms employed are given below. The program is written in FORTRAN IV and double precision has been used throughout.

F.2 Code Description

The program provides for the maximum of 15 parameters. If the number of linear parameters alone is 15 the confidence limits estimate for the nonlinear parameter is not available. The present coding provides for a maximum of 256 input data points.

The code is composed of the following programs

Name	No. of FORTRAN statements
MAIN	232
LINLSQ	46
ZXIIN (ZXI)	35
ANGLE	8
XIMIN	90
PFRE	77
RCHECK	32
REJECT	36

Name	No. of FORTRAN statements
WMAT	55
MATINV	<u>76</u>
Total	687

FORTRAN library subroutine TIME is called for timing of the execution of each case. The program was tested and operated on the KSU IBM 360/50 system.

F.2.1 Main Program

The arrays used in the program are dimensioned to allow up to 256 points and up to 15 parameters.

The batch and case data are read as specified in the section F.3. According to the specified value of the variable NPREL the REJECT and PFRE subroutines are executed or skipped. If NPREL is larger than one all portions of the main program are executed, as described in the following.

Segments of the input data table of length NPTR are submitted to the subroutine REJECT for inspection for erratic points. For the first quarter of the first segment the rejection normal deviate is set at 1.96 (95% confidence). In subsequent steps only the rejection of the middle two quarters of the segment is effective, at the 99% confidence level, and the segments overlap to cover the whole length of the data series. In the last quarter of the last segment the rejection is again effective at 95% confidence level.

Subsequently, if NPREL is specified greater than 1 a least square

polynomial of the order NPREL-1 is subtracted from the data series. Matrix method for the calculation of the least squares polynomial is used. This option is provided to enable the recognition of the prominent harmonic even if it is superimposed on a steep slope. In such case there may be no local maxima, on the basis of which the subroutine PFRE calculates the initial guess. After the subroutine PFRE is invoked the original data series is restored for further processing.

If NDUMP is specified larger than one only points with index divisible by NDUMP are retained. This truncation of data enables faster calculation and often the precision lost is not crucial.

The polynomial columns of the matrix Z , their number specified by NPOLY + 1, are initialized for the points that were not rejected. The independent variable (lag time) is transformed so that the data points are on the interval -1 to 1. Column 2 of the matrix Z contains the value $(i-n/2)/(n/2)$ where i is the index of the data point and n is the number of the data points. This column provides the argument for the calculation of the harmonic function in the subroutine ZXIIN (ZXI). The other polynomial columns of the matrix Z are initialized with Legendre polynomials, which are approximately orthogonal on the discrete set of points in the interval -1 to 1. If IDEBUG is divisible by 29 (cf. F-3.1) the column NPOLY+1 is initialized with a special function which has to be provided as input data for the batch of cases. This provision enables inclusion of the correlator bias response function as one of the components of the correlation function expansion.

The harmonic functions columns are initialized by the subroutine ZXIIN (entry ZXI).

The minimization of the sum of squares by adjusting the period of the fundamental harmonic is performed by the subroutine XIMIN and the parameter vector and the vector of the residuals is returned. The check for randomness of the residuals is performed by the subroutine RCHECK.

For the determination of the confidence limits of the parameters the matrix of the partial derivatives of the fitted function according to the parameters is formed (cf. section E.4). The partials according to the linear parameters are the values of the component functions and only the derivative according to the nonlinear parameter, the period of the fundamental harmonic, is to be calculated. If the number of linear parameters is equal to the maximal dimension of the array Z (presently 15) the confidence limits for the nonlinear parameter are not available. The confidence limits are determined according to Eq. (E-22). The $F_{95\%}(k, 120)$ values are supplied as the code data, where k is the number of parameters, 1 to 15.

The residuals are checked for erroneous points. The rejection level is set at 99.8% confidence (normal deviate 3.09) and the criterion for repeating the least square analysis is the sum of squares of the residuals above normal deviate 3.291. If this sum exceeds half of the sum of squares confidence margin at 95% confidence level (Eq. (E-14)) the calculations are repeated.

The amplitude of each harmonic is calculated from the cosine and

sine expansion parameters, as well as the phase lag in radians and independent variable increments (lag units), so that the harmonic can be represented as $A \cos\left(\frac{2\pi}{t_0} x - \phi\right)$, A being the amplitude and ϕ the phase lag. If the confidence interval of both components of the harmonic (cosine and sine) includes the origin the amplitude is considered insignificant and is not calculated. A pessimistic estimate of the phase angle confidence limits is obtained by taking the larger of the confidence intervals of the two parameters at the distance of the amplitude of the harmonic as the angular confidence interval.

The parameters correlation matrix is the matrix $(P^T P)^{-1}$, where P is the matrix of the partial derivatives, Eq. (E-23), normalized so that each row and column is divided by the square root of the diagonal element. If the component functions are mutually orthogonal on the given set of points the parameter correlation matrix is a unit matrix.

Subroutines needed by this program are listed above and their description is given in the following sections.

The output format is illustrated by two sample outputs presented in sections F.6 and F.7. The effect of the IDEBUG options on the output is described in section F.3.1.

F.2.2 Subroutine REJECT

Given a vector of equidistant functional values of the length M (maximum 50) the subroutine REJECT constructs by the matrix method an approximation polynomial of the specified order $N-1$ (N maximum is 10). The deviations of the input data points are compared to the

standard deviation estimate for the deviations around the approximation polynomial. If the ratio exceeds the specified value (FSS) the data point is set equal to zero, otherwise it is set equal to one.

If in the subsequent references of the subroutine the length of the functional value vector and the order of the polynomial are the same the matrix operations of the least squares fitting are not repeated.

Subroutine MATINV and subroutine package WMAT are referred by this subroutine.

F.2.3 Subroutine PPRE

Given a vector of equidistant functional values the amplitude, phase and period of the prominent frequency is estimated. Local maxima and minima of the function are determined, the criterion being that a given point is higher (lower) than any of the four neighbouring points on either side. The most frequent distance between adjacent maxima and minima is taken as the estimate of the period. Phase is determined from the location of the extremal points and the amplitude estimated as one-half of the difference between the average of the maxima and minima. In order that the subroutine be effective the maxima must be recognizable and any erroneous points, which may be mistaken for extremes must be identified. The functional value vector must be previously scanned by the REJECT subroutine and if overall slope is excessive a polynomial has to be subtracted.

F.2.4 Subroutine XIMIN

In this subroutine the minimization of the sum of squares for the

nonlinear parameter, the period, is performed. A good approximation for the period has to be given, sufficiently close to the minimizing value. Two points are chosen, one on each side of the guess at the distance δ_p , the convergence criterion for the period. Sums of squares are calculated for all three points by the subroutine LINLSQ, as well as the least squares parameters vector and the residuals. The dependence of the sum of squares on the period is approximated by a parabola through the three points. The point at the bottom of the parabola is taken as a new guess and the point with the maximal sum of squares is rejected. The first two criteria for convergence are:

1. $(x_i - x_j) < 1$, χ being the deviation of the period estimate from the initial guess in the units of δ_p , the convergence criterion specified on the case input or assigned by default (.05 delay increments) in the calling program.
2. $(SS(x_i) - SS(x_j))_{\max} < \delta_f \text{ASS kF}_{(1-\alpha)}(k, n-k)/(n-k)$ i.e., the maximal difference of the sums of squares must be a fraction of the confidence limit margin. δ_f is specified in the case input or assigned by default ($\delta_f = .05$) by the calling program.

When these convergence criteria have been reached it is further required that the middle point in x be the one with the lowest sum of squares. The three point set is moved till this is achieved. Thus satisfactory assurance is given that the minimum point has been enclosed. By specifying 19 as a factor in IDEBUG this last convergence criterion is omitted.

The optional printouts from this subroutine are listed in F.3.1.

Following subroutines are called by this subroutine: ZXIIN (entry ZXI), LINLSQ, MATINV and the subroutine package WMAT.

F.2.5 Subroutine ZXIIN, ZXI

The columns of the matrix Z containing the trigonometric functions are adjusted to the current period of the fundamental harmonic. To save computing time, sine and cosine values are computed directly for each 10th point on the equidistant scale and for the intermediate points the values are calculated by the addition theorem formulas. As the matrix Z does not contain all the equidistant points the value in the column 2 of Z is used as the argument of the harmonic function (see section F.2.1 on the values in polynomial columns of matrix Z).

The subroutine is dimensioned for the maximal size of the matrix, Z is 256*15.

F.2.6 Subroutine LINLSQ

Given a matrix of the values of the component functions and the observed values to be fitted by a linear combination of the component functions, the vector of linear parameters (coefficients of the component functions), the error vector (residuals) and the sum of squared errors are calculated. The matrix method is used, as described in Appendix E.

The subroutine arrays are presently dimensioned for up to 15 parameters and up to 256 observation points, i.e. the maximal dimensions of the Z matrix are 256*15. According to specified IDEBUG values at each execution of the subroutine the arrays $Z, Z^T Z, (Z^T Z)$ and the error vector can be displayed.

F.2.7 Subroutine RCHECK

The randomness of the residuals is tested by a "run" test; the number of uninterrupted sequences of residuals of equal sign is compared to the expected number of such sequences if either sign would be equally probable for each residual.

If r is the number of runs and n is the number of residuals we have (20):

Expected value

$$E(r) = (2n-1)/3 \quad (F-2)$$

Variance

$$V(r) = (16n-29)/30 \quad (F-3)$$

The distribution approaches the normal distribution for large n . Normal distribution is assumed and if the normal deviate is less than 1.645 the randomness is not rejected at the 95% confidence level.

F.2.8 Subroutine package WMAT

Matrix operations are performed at various entry points of the subroutine. Variable dimensions of the arrays can be used and the dimensioning is compatible with the WATFOR compiler.

F.2.9 Subroutine MATINV

Matrix inversion, solution of a system of linear equations and the calculation of the determinant value are performed by the subroutine. The variable dimension feature is incorporated. The subroutine was

written at Argonne National Laboratory.

F.2.10 Function ANGLE

The angle in radians in the range $-.436$ to $2\pi-.436$ is returned, given the non-normalized cosine and sine components as the arguments.

F.3. Input Preparation

The data deck consists of the initialization data, case data sets and end-of-batch data.

F.3.1 Initialization Data

Item 1.1 Format 2013; FORTRAN label IDBG(I), I = 1,20

- Product of IDBG(I) is formed (default for each IDBG(I) = 1) and tested in the code for the content of a particular prime factor. The prime factors have the following effect:
- 2 The polynomial part of matrix Z is printed in the main program (once).
 - 3 Matrix of derivatives, P, is printed by the main program (once).
 - 5 Matrix Z is printed at each entry in subroutine LINLSQ.
 - 7 Matrix $Z^T Z$ is printed at each entry in subroutine LINLSQ.
 - 11 Product $(Z^T Z)^{-1} (Z^T Y)$ is printed at each entry in subroutine LINLSQ (check for inversion accuracy).
 - 13 Error (residuals) vector is printed at each entry in subroutine LINLSQ.
 - 17 Values of XINEW and FINEW in subroutine XIMIN are printed

at each computation.

- 19 Third convergence criterion is omitted for exit from XIMIN subroutine (cf. section F.2.4).
- 29 A special function is introduced to the matrix Z in the column $NPOLY + 1$, the function thus becomes one of the component functions for expansion of the data set. If this option is specified the data cards containing the functional values of the special function must follow.

Items 1.2 to 1.30 Format 6X,9I8; FORTRAN label CORBG(I), I=1, 256

These data cards are to be supplied only if $IDEBUG_{\text{mod } 29} = 0$.

The values of the special function are to be supplied, preferably the range of the values should be -100,000 to 100,000, which is internally transformed to the range -1 to 1, to make the function comparable in norm to the Legendre polynomials and the circular functions.

F.3.2 Case Data

Item 2.1 Format 20A4; FORTRAN label A(I), I=1, 20

Title of the case. Columns 77-80 should be left blank as the text 'BIS' is introduced when a portion of the calculation is repeated after deviate points are removed.

Item 2.2 Format 7I3,2D10.0; FORTRAN label N,NPOLY, NHARM, NPTR, NORRE, NPREL, NDUMP, NDPER, DFI

- N Number of data points. If equal to zero computation is stopped.
- NPOLY Order of polynomial to be fitted. If $\text{IDEBUG}_{\text{mod}29} = 0$ the highest order of the polynomial is reduced by one and a special function is introduced instead. See above for necessary change in input data. Default NPOLY = 3.
- NHARM Number of harmonics. Number of associated linear parameters is $2 * \text{NHARM}$. Default NHARM = 3.
- NPTRE Number of points in a section on which rejection of erroneous points is enacted. Default NPTRE = 16.
- NORRE NORRE-1 is the order of the approximation polynomial used in rejection of the erroneous points by sections. Default NORRE = 4.
- NPREL NPREL-1 is the order of the polynomial to be subtracted from the input data prior to the estimate of the prominent harmonic. If NPREL is less than 1 no action is undertaken. If NPREL is less than zero the period of the previous case is used as the initial guess. Subroutines REJECT and PFRE are not called in this case.
- NDUMP If NDUMP is greater than 1 only points with index divisible by NDUMP are retained. Number of points is thus reduced to N/NDUMP .
- DPER Convergence criterion for the period, used in subroutine XIMIN (cf. section F 2.4). Default DPER = .05.

DFI Convergence criterion for the sum of squares, used
in subroutine XIMIN (cf. section F 2.4). Default DFI = .05.

Items 2.3 and subsequent. Format 6X, 918; FORTRAN label (1Y(I), I = 1,N),
NC.

N points of the functional values at equidistant points
and the norm count. Norm count (of the correlator) is
subtracted from functional values. It should not be
equal to zero as the amplitude of each harmonic is divided
by the norm count for normalized amplitude output.

F.3.3 Subsequent Cases

Items 2.1 through 2.3 are repeated for each case.

F.3.4 End of Batch

Items 4.1 and 4.2.

Two cards behind the last case data cause a normal stop
if the second card has a blank in the columns 1 to 3.
First card may contain a text to be printed before exit.

F.4. FORTRAN labels used in the program

F.4.1 Main Program

FORTRAN label	Mathematic symbol	Meaning
A(20)		case title (literal)
AA		local variable

FORTRAN label	Mathematic symbol	Meaning
AMP		amplitude of prominent harmonic, guess of PFRE subroutine
B(15)	b	parameters vector
BB(15)		work vector (parameters)
BIS		literal constant 'BIS'
DET		dummy for MATINV argument
DFI		convergence criterion for sum of squares
DPER		convergence criterion for period
F(15)		F-test values, $F_{95\%}(i,120)$
FIC		confidence margin for sum of squares
FIMIN		minimal sum of squares
FKN		confidence margin for sum of squares factor
I		index
IC		index
ICORBG(256)	$F_{cb}(x_i)$	special function values
IDBG(20)		IDEBUG options input
IDEBUG		execution and output options specifier
IHARM		index
IRESP		dummy, response of RCHECK subroutine
IS		index
ITIME1		case execution start time
ITIME2		case execution stop time
IY(256)		input data vector
J		index
K		number of linear parameters
KC		index
KK	k	number of parameters (including period)
KS		index
N		number of data points
NC		norm count of input data
NDUMP		data point dumping specification
NGOOD	n	number of data points not rejected
NHARM		number of harmonics
NORRE		order 1 of approximation polynomial for rejection
NPOLY		order of polynomial to be fitted
NPOLY1		number of polynomial columns in Z matrix, NPOLY+1
NPREL		order-1 of the polynomial to be subtracted before calling PFRE
NPTRE		number of points per segment to be examined by REJECT subroutine
NR		local variable
NREJ2		$NPTRE/2$
NREJ4		$NPTRE/4$
PER	t_o	period, independent variable increment units
PER1		local variable

FORTRAN label	Mathematic symbol	Meaning
PH		lag, indep. var. increment units
PHA		phase lag, independent variable increment units, guess by PFRE subroutine
PHI		phase lag, radians
PHIMAX		phase lag, radians, upper limit
PHIMIN		phase lag, radians, lower limit
PHXMA		lag, increment units, upper limit
PHMI		lag, increment units, lower limit
RE		approximate confidence region radius
SC		deviation level for sum of squares repeat criterion at residual examination
SCC		deviation level for point rejection at residual examination
SE	s_e	standard deviation estimate
SSR		sum of squares for repeat criterion
TYME		time of case execution
Y(256)	y	data vector, good points only
YY(3,256)		row 1: data points; row 2: 1 for good points, 0 for rejected points; row 3 used by subroutine PFRE
YW(256)		work vector, residuals
W(50)		work vector
z(256,15)	Z,P	values of component functions, matrix of partials
ZT	Z^T	
ZTZ	$Z^T Z$	
ZTZI	$(Z^T Z)^{-1}$	

F.4.2 Subroutine PFRE

FORTRAN label	Meaning
AL	average minimum
AH	average maximum
AMP	amplitude estimate
H(20)	indices of maximal points
HIST(100)	histogram of distances of the extremes
HMX	local variable
I	index
ID	row dimension of Y
IH	number of maxima near peak in histogram
II	index
IL	number of minima near peak in histogram
IM	index of peak in histogram

FORTRAN	
label	Meaning
IMH	local variable
IML	local variable
L(20)	indices of minimal points
M3	index of row in Y to be used in subroutine
N	column dimension of Y
NH	number of maxima detected
NL	number of minima detected
NM	N-1
NMA	local variable
NP	number of distances of extremes
PER	period, independent variable increments
PH	local variable
PHA	lag, independent variable increments
Y(ID,N)	row 1: functional values; row 2: 0 for rejected points, 1 for retained points; row M3: used by subroutine for calculations.

F.4.3 Subroutine ZXIIN (ZXI)

Local variables and indices not listed.

FORTRAN	
label	Meaning
C(256)	cosine values vector
CC	cosine of unit independent variable increment
1STEP	spacing of harmonic function evaluations by FORTLIB function reference
N	number of original data points
NC	index of cosine column
NS	index of sine column
NGOOD	number of good data points
NHARM	number of harmonics
NPOLY	number of polynomial columns -1
S(256)	sine values vector
SS	sine of unit independent variable increment
X1	period, independent variable increment units
XIP	period at previous subroutine execution
Z(256,15)	component function values matrix

F.4.4 Subroutine XIMIN

FORTRAN label	Mathematic symbol	Meaning
B(15)	b	parameter vector
BX(3,15)		parameter vector storage
DET		dummy for MATINV argument
DFI		sum of squares convergence criterion
DPER		period convergence criterion
ER(N)	e	errors (residuals) vector
FKN		sum of squares confidence margin factor
FIMAX		maximal sum of squares
FIMIN		minimal sum of squares
FINEW		new sum of squares
FIX(I)		sum of squares storage
I		index
IDEBUG		IDDEBUG options variable
II		index
IM		maximal sum of squares point index
LX		substituted point index
IW		counter of repetitions
J		index
K	(k)	number of parameters, excluding period
N	n	number of rows in matrix Z
PER	t	period
R	o	local variable
X		matrix of periods, column 1: unity elements; column 2: period deviations from PER in δ units; column 3: column 2 squared. p
XIM		maximal period deviation
XINew		new value of period deviation (new estimate)
XINV(3,3)		x^1
W(15)		work vector, parameters
WI(15)		work vector
WW(3)		work vector
Y(256)	y	data points, good points only
Z(256,15)	Z	matrix of component functions values

F.4.5 Subroutine LINLSQ

FORTRAN label	Mathematic symbol	Meaning
B(K)	b	parameter vector
DET	e	dummy for MATINV argument
ER(N)		error (residuals) vector

FORTRAN label	Mathematic symbol	Meaning
FI		sum of square errors
FII		dummy
I		index
IDEBUG		IDEBUG options variable
II		index
J		index
K	k	number of parameters (columns of matrix Z)
N	n	number of rows of matrix Z
Y(N)	y	data points vector
Z(256,15)	Z	component functions values matrix
ZPR(15,15)	$(Z^T Z)^I (Z^T Z)$	
ZT(15,256)	Z^T	
ZTI(15,15)	$(Z^T Z)^I$	
ZTZ(15,15)	$Z^T Z$	

F.5. Output

Output format is illustrated by two sample problem outputs. The output can be augmented by the IDEBUG options described in section F.3.1. These options should be used with discretion as a large amount of output can be generated.

F.6. Sample Problems

The facsimile of two sample problem outputs are presented on pages 163 to 170.

F.6.1 Sample Problem 1.

The input data is a table of 256 computer generated values of the function $y = 100,000 \cos(2\pi(i-1)/51.3) + 100,000$. The values were truncated to integers and this truncation produces a certain noise. The first parameter, the constant a_0 in Eq. (F-1), is -.53, due to the

truncation, the expected value being $-.5$. This value is in the confidence interval of the parameter. The true amplitude, 100,000 is also within the confidence interval of the calculated parameter. The slope (parameter 2) and the sine component are statistically insignificant.

F.6.2 Sample Problem 2.

The analysis of the correlator output of the test A15 11, 550 lb, correlator run 7 is presented. The graph of the correlator output (Fig. 34) displays two irregularities which can be obviously attributed to the malfunction of the correlator, as the correlation function is very smooth elsewhere.

Points 1, 2 and 182 were rejected by the subroutine REJECT prior to the least squares analysis. Further points are rejected after the first least squares search, the normal deviate being above 5. Finally the standard deviation estimate is at 24.12 and the residuals are found to be random.

IDDEBUG was specified 29 and the correlator response function was supplied. It is found to be a significant component of the correlator output (parameter 5, value 63.06, confidence interval ± 22.56).

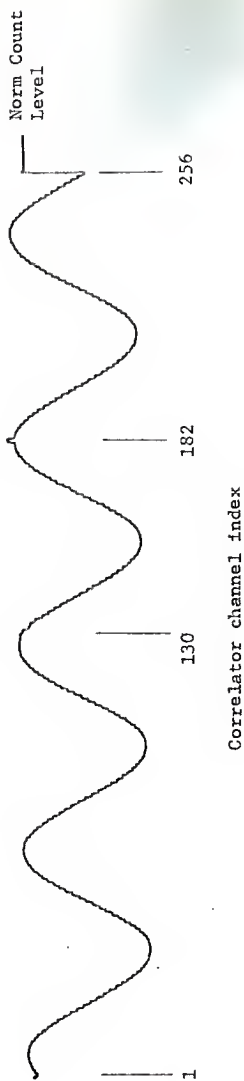


Figure 34. Correlation function, correlator run no. 7, Al 5 - I 1,550 lb.

F 7. Program Listing and Sample Outputs

MAIN

```

C   MAIN PROGRAM FOR ONE NONLINEAR PARAMETER LEAST SQUARES ESTIMATE
      IMPLICIT REAL*8(A-H,O-Z)
      DIMENSION YY(3,256), IY(256), YW(256), W(50), Z(256,15),
1     ZT(15,256), ZTZ(15,15), BB(15), ZTIZ(15,15)
      REAL*4 A(20)
      REAL*8 B(15)/15*1.00/
C   F VALUE F(1,120,95%) USED, I CAN BE 1 TO 15
      REAL F(15)/3.92,3.07,2.68,2.45,2.29,2.17,      2.09,2.02,1.96,
1     1.91,1.87,1.83,1.80,1.77,1.75/
      COMMON ZI,ZIZ,      ZTIZ
      COMMON/INT/IY
      DIMENSION IDBG(20)
      COMMON/OBG/ IOEBUG
901  READ 901,(IOBG(I),I=1,20)
      FORMAT(20I3)
      IOEBUG=1
      DO 5 I=1,20
        IF(ICBG(I).EQ.0) IDBG(I)=1
5     IOEBUG=IOEBUG*IDBG(I)
      PRINT 902,IOEBUG,(IOBG(I),I=1,20)
902  FORMAT(' IOEBUG=',110,20I4)
C   NOTE NECESSARY CHANGE IN INPUT IF MOO(IOEBUG,29)=0
      DIMENSION ICDRBG(256)
      IF(MOO(IOEBUG,29).EQ.0) READ 910,(ICDRBG(I),I=1,256)
1     CONTINUE
      CALL TIME(ITIME1)
      READ 905,(AI(I),I=1,20)
905  FORMAT(20A4)
      PRINT 906,(A(I),I=1,20)
906  FORMAT('1',20A4,T100,'PAGE 1')
      READ 900,N,NPOLY,NHARM,NPTRE,NCRRE,NPREL,NOUMP,DPER,DFI
C   IF NPREL IS NEGATIVE THE PERIOD OF THE PREVIOUS CASE IS USED
      IF(N.EQ.0) CALL EXIT
      IF(NPOLY.EQ.0) NPOLY=3
      IF(NHARM.EQ.0) NHARM=3
      IF(NPTRE.EQ.0) NPTRE=16
      IF(NCRRE.EQ.0) NCRRE=4
      IF(OPER.EQ.0.00) DPER=.0500
      IF(OFI.EQ.0.0) OFI=.0500
      PRINT 903,N,NPOLY,NHARM,NPTRE,NCRRE,NPREL,NOUMP,DPER,OFI
903  FORMAT(' OPTIGNS SPECIFIED OR ASSIGNED BY DEFAULT, N=',I4,' NPO
1     ILY=',I4,' NHARM=',I4,' NPTRE=',I4,' NORRE=',I4,' NPREL=',
2     I4,' NOUMP=',I4,' OPER=',F7.3,' OFI=',F7.3/';)
900  FORMAT(7I3,20I0.0)
      READ 910,(IY(I),I=1,N),NC
910  FORMAT(6X,9I8)
      PRINT 911,(IY(1),I=1,N)
      PRINT 912,NC
911  FORMAT(' INPUT: /' /(' ',10I10))
912  FORMAT(' NORM COUNT',I10)
      DO 10 I=1,N
        YY(2,I)=1.
10     YY(1,I)=DFLOAT(IY(I))-NC
      IF(NPREL.LT.0) GOTO 59
C   REJECTION FOR FIRST 1/4 SEGMENT AT 95% CONFIDENCE LEVEL
      DO 15 I=1,NPTRE
15     W(I)=YY(I,I)
      CALL REJECT(' W',NPTRE,NORRE,1.9600)

```

MAIN

```

DO 16 I=1,NPTRE
16 YY(2,1)=W(I)
NREJ4=NPTRE/4
NREJ2=NPTRE/2
DO 31 I=1,N,NREJ2
IF(I+NPTRE-1.GT.N) GOTO 31
DO 25 J=1,NPTRE
C 25 W(J)=YY(1,J+I-1)
REJECTION FOR INTERIOR POINTS AT 99% CONFIDENCE LEVEL
CALL REJECT(W,NPTRE,NORRE,2.576D0)
DO 30 J=NREJ4,NPTRE
30 YY(2,I+J-1)= W(J)
31 CONTINUE
DO 32 I=1,NPTRE
32 W(I)=YY(1,N-NPTRE+I)
CALL REJECT(W,NPTRE,NORRE,2.576D0)
DO 33 I=NREJ4,NPTRE
33 YY(2,N-NPTRE+I)=W(I)
DO 35 I=1,NPTRE
C 35 W(I)=YY(1,N-NPTRE+I)
REJECTION FOR LAST 1/4 SEGMENT AT 95% CONFIDENCE LEVEL
CALL REJECT(W,NPTRE,NORRE,1.96D0)
NR=NPTRE-NREJ4
DO 40 I=NR,NPTRE
40 YY(2,N-NPTRE+I)= W(I)
PRINT 920
920 FORMAT('0 REJECT SUBROUTINE CALLED'/'0')
K=0
DO 50 I=1,N
IF(YY(2,I).EQ.0.D0) K=K+1
50 IF(YY(2,I).EQ.0.D0) PRINT 930,I
930 FORMAT(' POINT',I4,' REJECTED')
IF(K.EQ.0) PRINT 940
940 FORMAT(' NO POINTS REJECTED')
C PERE CALLED NOW WITH OPTION OF FIRST SUBTRACTING A POLYNOMIAL
IF(NPREL.LI.0) GOTO 99
IF(NPREL.LI.2) GOTO 90
DO 60 I=1,N
60 Y(I)=YY(1,I)
C STORE FUNCTIONAL VALUES
DO 70 I=1,N
Z(I,1)=1.D0
DO 70 J=2,NPREL
70 Z(I,J)=Z(I,J-1)*I
DO 75 I=1,15
75 B(I)=1.D0
CALL WMPTRA(Z,ZT,N,NPREL,256,15)
CALL WMPRD(ZT,Z,ZTZ,NPREL,N,15,256)
CALL MATINV(ZTZ,NPREL,B,1,DET,15)
CALL WMPRDV(ZT,Y,W,NPREL,N,15)
CALL WMPRDV(ZTZ,K,8,NPREL,NPREL,15)
CALL WMPRDV(Z,B,YW,N,NPREL,256)
DO 80 I=1,N
80 YY(1,I)=Y(I)-YW(I)
90 CALL PERE(YY,3,N,3,AMP,PER,PHA)
PRINT 950,AMP,PER,PHA
950 FORMAT('0INITIAL GUESS'/'0AMPLITUDE',T18,F8.2/' PERIOD',T18,F10.4/
1 ' LAG', '(PHASE)',T18,F10.4)

```

MAIN

```

IF(NPREL.LT.2) GOTO 100
DO 95 I=1,N
95 YY(1,I)=Y(I)
GOTO 100
99 PRINT 955,PER
955 FORMAT('PERIOD OF PREVIOUS CASE USED FOR INITIAL GUESS, PERIOD'
1,F10.4)
100 K=1
C DUMP POINTS ACCORDING TO SPECIFIED NOUNP
IF (NOUNP.LE.0) GOTO 106
DO 105 I=1,N
105 IF(MOD(I,NOUNP).NE.0) YY(2,I)=0.D0
PRINT 956,NOUNP
956 FORMAT('ONLY POINTS WITH INDEX DIVISIBLE BY' ,I3,' RETAINED')
106 CONTINUE
C INITIALIZE VECTOR Y AND ARRAY Z WITH GOOD POINTS ONLY
DO 110 I=1,N
Y(K)=YY(1,I)
Z(K,2)=DFLOAT(I-N/2)/(N/2)
C FOLLOWING STATEMENT INITIALIZES COLUMN NPOLY1 OF Z TO THE NORMAL
C VALUES OF THE CORRELATOR BACKGROUND, IF MOD(IDEBUG,29) = 0
C NOTE NECESSARY CHANGE IN INPUT
IF(MOD(IDEBUG,29).EQ.0) Z(K,NPOLY+1)= ICORBG(1)/1.06
110 IF(YY(2,I).NE.0.D0) K=K+1
NGOOD=K-1
IF(NGOOD.EQ.0) GOTO 172
NPOLY1=NPOLY+1
IF(MOD(IDEBUG,29).EQ.0) NPOLY1=NPOLY
DO 120 I=1,NGOOD
Z(I,1)=1.00
IF(NPOLY1.LT.3) GOTO 119
DO 118 J=3,NPOLY1
118 Z(I,J)=((2*J-1)*Z(I,J-1)*Z(I,2)-(J-1)*Z(I,J-2))/J
119 CONTINUE
120 CONTINUE
IF(MOD(IDEBUG,29).NE.0) GOTO 124
DO 123 I=1,NGOOD
123 PRINT 958,I,(Z(I,J),J=1,NPOLY1)
124 CONTINUE
958 FORMAT(' ',I3,(15,10F10.5))
C INITIALIZE SUBROUTINES ZXI
CALL ZXIIN(Z,NPOLY,NHARM,N)
K=NPOLY+2*NHARM+1
KK=K+1
FKN=K*F(KK)/(NGOOD-KK)
CALL XIMIN(Z,B,Y,YW,NGOOD,K,PER,DPER,FIMIN,OFI,FKN)
PRINT 959,(A(I),I=1,20)
PRINT 960,NPOLY,NHARM,(I,B(I),I=1,K),KK,PER
959 FORMAT('1',20A4,100,'PAGE 2')
960 FORMAT('OMINIMUM FOUND'/ORDER OF POLYNOMIAL',I3,' NUMBER OF H
LARMONICS',I3 '/PARAMETERS'/ ' '/(' ',I3,G15.6))
DO 121 I=1,N
121 Y(I)=0.D0
DO 122 I=1,NGOOD
122 Y(10INT(Z(I,2)*N/2+.1+N/2))=YW(I)
PRINT 961,(Y(I),I=1,N)
961 FORMAT('ORESIDUALS (EXACT ZERO DENCIES REJECTED POINTS)'/ ' '/
1(' ',10F10.2))

```

MAIN

```

IF(MOD(IDEBUG,23).NE.0) GOTO 117
PUNCH 975, IY(I), I=1, N)
975 FORMAT(6X, 9F8.2)
117 CONTINUE
SE=DSQRT(FIMIN/(NGDOD-K-1))
FIC=FKN*FIMIN
PRINT 966, SE, FIMIN, FIC
966 FORMAT('DSTANDARD DEVIATION ESTIMATE', F8.2, '      SUM OF SQUARES
I=', F16.0, '      95% CONFIDENCE MARGIN=', F16.0)
CALL RCHECK(YR, NGDOD, IRESP)
126 CONTINUE
DETERMINING THE LINEARIZED CONFIDENCE LIMITS
IF NUMBER OF PARAMETERS IS GREATER THAN FIFTEEN ONLY ESTIMATE OF
LINEAR PARAMETERS IS AVAILABLE
PRINT 964, (A(I), I=1, 20)
964 FORMAT('1', 20A4, T100, 'PAGE 3'/'LINEARIZED CONFIDENCE LIMITS'/' ')
IF(NPOLY+2*NHARM+2 .GT. 15) PRINT 965
IF(NPOLY+2*NHARM+2 .GT. 15) KK=K
IF(NPOLY+2*NHARM+2 .GT. 15) GOTO 135
965 FORMAT('TDD MANY PARAMETERS-PERIOD CAN NOT BE INCLUDED IN THE CON
FIDENCE LIMITS CALCULATION')
B(KK)=PER
PER1=-2.0D*3.1415926/PER**2
DO 13D I=1, NGDOD
Z(I, KK)=D.0D
CO 13D J=1, NHARM
KC=NPOLY+2*J
KS=NPOLY+2*J+1
130 Z(I, KK)=Z(I, KK)+PER1*(-B(KC)*Z(I, KS)+B(KS)*Z(I, KC))*(Z(I, 2)*N/2+
I N/2-1)
IF(MOD(IDEBUG, 3).NE.0) GDTD 134
CO 133 I=1, NGDOD
133 PRINT 95B, I, (Z(I, J), J=1, KK)
134 CONTINUE
CALL WMTRA(Z, ZT, NGDOD, KK, 256, 15)
CALL WMPRO(ZI, Z, ZTZ, KK, NGDOD, KK, 15, 256)
CALL MATINV(ZIZ, KK, W, I, DET, 15)
135 CONTINUE
CO 138 I=1, KK
138 W(I)=DSQRT(DABS(FKN*FIMIN*ZIZ(I, I)))
PRINT 97C, (I, B(I), W(I), I=1, KK)
970 FORMAT(' ', I3, F15.2, '      +/-', G15.5)
REAL*4 BIS/'BIS' '/'
SSR=0.0D
SC=3.291*SE
SCC=3.09*SE
CO 125 I=1, N
IF(DABS(Y(I)) .GT. SC) SSR=SSR+Y(I)**2
IF(DABS(Y(I)) .GT. SCC) YY(2, I)=C.0D
125 IF(DABS(Y(I)) .GT. SCC) PRINT 962, I
962 FORMAT(' POINT', I4, ' SHOULD BE REJECTED')
IF(SSR. LT. FIC/2) GOTO 139
PRINT 963
963 FORMAT(' CALCULATIONS SHALL BE REPEATED WITH MORE POINTS REJECTED'
1)
A(19)=BIS
K=1
GOTO 106

```

MAIN

```

139 CONTINUE
DO 149 IHARM=1,NHARM
IC=NPOLY+2*IHARM
IS=NPOLY+2*IHARM+1
AMPL=DSQRT(B(IC)**2+D(IS)**2)
RE=DMAX1(DABS(W(IC)),DABS(W(IS)))
IF(RE.GT.AMPL) PRINT 805,IHARM
IF(RE.GT.AMPL) GOTO 148
805 FORMAT('AMPLITUDE OF THE HARMONIC',I3,' NOT SIGNIFICANT')
PHI=ANGLE(B(IC),B(IS))
DPHI=ANGLE(AMPL,RE)
PHIMAX=PHI+DPHI
PHIMIN=PHI-DPHI
AMPN=AMPL/NC
AA=3.1415926*2/PER
PH=PHI/AA
PHMA=PHIMAX/AA
PHMI=PHIMIN/AA
PRINT 810,IHARM,AMPL,AMPN,PHI,PHIMAX,PHIMIN,PH,PHMA,PHMI
810 FORMAT('OPHASE ANGLE FOR THE HARMONIC',I4,' AMPLITUDE,NOMINAL',
F10.2,' AMPLITUDE,NORMALIZED',G15.5/
2,' RADIANS',I5,F9.5,' VALUES ON CONFIDENCE LIMITS UPPER',F9.5,
3,' LOWER',F9.5/' LAG UNITS',I5,F8.4,' VALUES ON CONFIDENCE
4LIMITS UPPER',F8.4,' LOWER',F8.4)
148 CONTINUE
149 CONTINUE
DO 150 I=1,KK
150 W(I)=DSQRT(DABS(ZTZ(I,I)))
DO 160 J=1,KK
DO 160 J=1,KK
160 ZTZ(I,J)=ZTZ(I,J)/(W(I)*W(J))
PRINT 820
820 FORMAT('OPARAMETERS CORRELATION MATRIX'/'O')
DO 170 I=1,KK
170 PRINT 830,I,(ZTZ(I,J),J=1,KK)
830 FORMAT(' ',I3,3X,15F8.4)
830 FORMAT(' ',I3,3X,10G12.5/' ',I60,5G12.5)
172 CALL TIME(ITIME2)
TYME=(ITIME1-ITIME2)*(-.1D-1)
PRINT 840,TYME
840 FORMAT('OCASE COMPUTATION TIME ',F10.2,' SECONDS')
GOTO 1
END

```

LINLSQ

```

SUBROUTINE LINLSQ(Z,B,Y,ER,N,K,FI)
IMPLICIT REAL*8(A-H,O-Z)
DIMENSION B(K),Y(N),ER(N),ZT(15,256),ZTZ(15,15),Z(256,15)
COMMON ZT,ZTZ
CALL WMTRA(Z,ZT,N,K,256,15)
COMMON/DBG/IDEBUG
IF(MOD(IDEBUG,5).NE.0) GOTO 11
DO 1 I=1,N
1 PRINT 120,I,(Z(I,J),J=1,K)
11 CONTINUE
120 FORMAT(' ',I3,(10G12.3))
DO 4 I=1,K
DO 4 J=1,K
ZTZ(I,J)=0.DO
DO 4 II=1,N
4 ZTZ(I,J)=ZTZ(I,J)+ZT(I,II)*Z(II,J)
DO 6 I=1,K
DO 6 J=1,I
6 ZTZ(I,J)=ZTZ(J,I)
DIMENSION ZTI(15,15),ZPR(15,15)
CALL WMASGN(ZTI,ZTZ,K,K,15)
IF(MOD(IDEBUG,7).NE.0) GOTO 12
DO 3 I=1,K
3 PRINT 120,I,(ZTI(I,J),J=1,K)
12 CONTINUE
CALL WMPROV(ZT,Y,B,K,N,15)
CALL MATINV(ZTZ,K,B,1,DET,15)
IF(MOD(IDEBUG,11).NE.0) GOTO 13
CALL WMPRO(ZTI,ZTZ,ZPR,K,K,K,15,15)
DO 5 I=1,K
5 PRINT 100,(ZPR(I,J),J=1,K)
13 CONTINUE
100 FORMAT(' ',I3,(10G12.4))
CALL WMPROV(Z,B,ER,N,K,256)
DO 10 I=1,N
10 ER(I)=Y(I)-ER(I)
IF(MOD(IDEBUG,13).NE.0) GOTO 19
PRINT 100,(ER(I),I=1,N)
19 CONTINUE
FI=0.DO
DO 20 I=1,N
20 FI=FI+ER(I)**2
FII=FI
21 CONTINUE
RETURN
END

```


ZXIIN

```

SUBROUTINE ZXIIN(Z,NPOLY,NHARM,N)
  IMPLICIT REAL*8(A-H,O-Z)
  DIMENSION Z(256,15),S(256),C(256)
  XIP=0.00
100 IF(NPOLY+2*NHARM+1.GT.15) PRINT 100
  FORMAT(' NUMBER OF PARAMETERS TOO LARGE, QUIT CASE')
  IF(NPOLY+2*NHARM+1.GT.15) N=0
  PI=3.141592653
  RETURN
  ENTRY ZXI(Z,XI,NGOOD)
  IF(XI.EQ.XIP) GOTO 15
  XIP=XI
  ISTEP=10
  DO 10 I=1,NHARM
    ARG=2*PI*I/XI
    CC=DCOS(ARG)
    SS=DSIN(ARG)
    ISYEP=10
    DO 5 II=1,N,ISTEP
      IE=II+ISTEP-1
      IF(IE.GT.N) IE=N
      C(II)=DCOS(ARG*(II-1))
      S(II)=DSIN(ARG*(II-1))
      II2=II+1
      DO 5 J=II2,IE
        S(J)=S(J-1)*CC+C(J-1)*SS
5      C(J)=C(J-1)*CC-S(J-1)*SS
      NS=NPOLY+1+2*I
      NC=NPOLY+I*2
      DO 10 J=1,NGOOD
        INDX=IDINT(Z(J,2)*N/2+N/2+.1D0)
10      Z(J,NC)=C(INDX)
15 RETURN
  END

```

XIMIN

```

SUBROUTINE XIMIN(Z,B,Y,ER,N,K,PER,CPER,FIMIN,CFI,FKN)
IMPLICIT REAL*8(A-H,O-Z)
DIMENSION Z(256,15),B(K),Y(N),ER(N),XINV(3,3),X(3,3),FIX(3),BX(3,
1 15),W(15),WI(15),WK(3)
COMMON/INT/ XINV,X,FIX,BX,W,WI,WK
COMMON/OBG/ IDEBUG
DO 10 I=1,3
X(I,1)=1.00
X(I,2)=- 2.00+I*1.00
X(I,3)=X(I,2)**2
CALL ZXI(Z,PER+X(I,2)*CPER,N)
CALL LINLSQ(Z,W,Y,ER,N,K,FIX(I))
DO 10 J=1,K
10 BX(I,J)=W(J)
FIMIN=OMINI(FIX(1),FIX(2),FIX(3))
12 R=(FIX(3)-FIX(2))/(FIX(2)-FIX(1))
IF(R.LT..9500 .OR. R.GT.1.0500) GOTO 50
DO 15 I=1,K
15 W(I)=BX(2,I)
IX=1
IF(FIX(3).LT.FIX(1)) IX=3
FIX(2)=FIX(IX)
X(2,2)=X(IX,2)
X(2,3)=X(IX,3)
DO 17 I=1,15
17 BX(2,I)=BX(IX,I)
IF(IX.EQ.3) X(3,2)= 2*X(2,2)-X(1,2)
IF(IX.EQ.1) X(1,2)=2*X(2,2)-X(3,2)
X(IX,3)=X(IX,2)**2
CALL ZXI(Z,PER+X(IX,2)*OPER,N)
CALL LINLSQ(Z,W,Y,ER,N,K,FIX(IX))
DO 18 J=1,K
18 BX(IX,J)=W(J)
GOTO 12
50 CALL WPMASGN(XINV,X,3,3,3)
DO 51 I=1,3
51 WK(I)=FIX(I)
CALL MATINV(XINV,3,WK,1,0ET,3)
XINEW=-.5*WK(2)/WK(3)
IW=0
55 CALL ZXI(Z,PER+XINEW*OPER,N)
CALL LINLSQ(Z,W,Y,ER,N,K,FINEW)
IF(MOD(IDEBUG,17).EQ.0) PRINT 101,XINEW,FINEW
101 FORMAT(' XINEW=',F8.4,' FINEW=',G15.6)
FIMIN=OMINI(FIMIN,FINEW)
FIMAX=FIMIN
IM=0
DO 60 I=1,3
FIMAX=OMAXI(FIMAX,FLX(I))
60 IF(FIX(I).EQ.FIMAX) IM=I
IF(IM.EQ.0) PRINT 100
100 FORMAT(' ERROR IN XIMIN, AT 60')
IF(IM.EQ.0) IM=1
DO 65 I=1,K
65 WI(I)=BX(IM,I)
FIX(IM)=FIMIN
X(IM,2)=XINEW
X(IM,3)=XINEW**2

```

X1MIN

```

XIM =X(1,2)
DO 66 I=1,3
66 IF(FIX(I).EQ.FIMIN) XIM =X(1,2)
DO 70 I=1,K
70 BX(IM,I)=X(I)
IF(MOD(IDEBUG,19).EQ.0) GOTO 74
IF(DMAX1(X(1,2),X(2,2),X(3,2))-DMIN1(X(1,2),X(2,2),X(3,2)).GT.
I 1.DO) GOTO 50
IF(FIMAX/FIMIN .GT.OFI*FKN+1.CO) GOTO 50
IW=IW+1
IF(IW.GT.3) PRINT 135
IF(IW.GT.3) GOTO 74
135 FORMAT(' X1MIN FORCED EXIT, X1MIN IS NOT BETWEEN TWO POINTS WITH
HIGHER SUM OF SQUARES')
IF(XIM.EQ. DMIN1(X(1,2),X(2,2),X(3,2)))GOTO 72
IF(XIM.EQ. OMAX1(X(1,2),X(2,2),X(3,2)))GOTO 73
74 CONTINUE
DO 76 I=1,3
76 X(I,2)=PER+X(I,2)*OPER
PRINT 110,(X(I,2),FIX(I),I=1,3)
110 FORMAT('O SUBROUTINE X1MIN EXIT LAST THREE POINTS ..'/
I(' PERIOD=',F8.4,' SUM OF SQUARES=',G15.5))
GOTO 71
72 XINEW=XIM*1.2-OMAX1(X(1,2),X(2,2),X(3,2)) *.2
GOTO 55
73 XINEW=XIM*1.2-DMIN1(X(1,2),X(2,2),X(3,2)) *.2
GOTO 55
71 CONTINUE
IL=1
DO 80 I=1,3
80 IF(FIX(I).EQ.FIMIN) IL=I
PER=X(IL,2)
DO 85 I=1,K
85 B(I)=BX(IL,I)
RETURN
END

```

PERE

```

SUBROUTINE PERE(Y, ID, N, M3, AMP, PER, PHA)
INITIAL ESTIMATE OF THE PROMINENT FREQUENCY

C
C
IMPLICIT REAL*8(A-G, O-Z), INTEGER (I)
DIMENSION Y(ID, N), L(20), H(20), HIST(100), IDUMY(116)
COMMON/TNT/ HIST, L, H, IDUMY
PER=0.
PHA=0.
AMP=0.
NM=N-1
DO 1 I=1, 20
  L(I)=0
  H(I)=0
1
C
C
SHIFT FUNCTION FROM ROW 1 TO ROW M+3 AND CONSTRUCT SUBSTITUTION FOR
ERRATIC POINTS
DO 10 I=2, NM
  Y(M3, I)=Y(1, I)
10 IF(Y(2, I).EQ.0.)Y(M3, I)=(Y(1, I-1)+Y(1, I+1))/2
  NMA=NM-4
  NL=0
  NH=0
C
FIND THE LOCAL MAXIMAL AND MINIMAL POINTS
DO 15 I=6, NMA
  IF(Y(M3, I).GT.DMAX1(Y(M3, I-4), Y(M3, I-3), Y(M3, I-2), Y(M3, I-1),
  Y(M3, I+1), Y(M3, I+2), Y(M3, I+3), Y(M3, I+4))) GOTO 11
  IF(Y(M3, I).LT.DMIN1(Y(M3, I-4), Y(M3, I-3), Y(M3, I-2), Y(M3, I-1),
  Y(M3, I+1), Y(M3, I+2), Y(M3, I+3), Y(M3, I+4))) GOTO 13
  GOTO 15
11 NH=NH+1
  H(NH)=I
  GOTO 15
13 NL=NL+1
  L(NL)=I
15 CONTINUE
C
CONSTRUCT HISTOGRAM OF THE DISTANCES BETWEEN ADJACENT MAXIMA
DO 18 I=1, 100
  HIST(I)=0.
  DO 20 I=2, NH
    II=H(I)-H(I-1)
    20 HIST(II)=HIST(II)+1
    DO 25 I=2, NL
      II=L(I)-L(I-1)
      25 HIST(II)=HIST(II)+1
    HMX=HIST(1)
    IM=1
C
DO 30 I=1, 100
  IF(HMX.LE.HIST(I)) IM=I
30 HMX=MAX0(HMX, HIST(I))
  PER=0.
  NP=0
  INL=IM-2
  IMH=IM+2
  DO 35 I=INL, IMH
    PER=PER+I*HIST(I)
35 NP=NP+HIST(I)
  IF(NP.LT.1) GOTO 60
  IF(NP.LT.1) PER=0.

```

PFRE

```

PER=PER/NP
CO 40 I=2,NH
IF(DABS(H(I))-H(I-1)-PER).GT.2.DO) H(I-1)=0
DO 45 I=2,NL
45 IF(DABS(L(I))-L(I-1)-PER).GT.2.DO) L(I-1)=0
IF(DABS(H(NH))-H(NH-1)-PER).GT.2.DO) H(NH)=0
IF(DABS(L(NL))-L(NL-1)-PER).GT.2.DO) L(NL)=0
IH=0
IL=0
PH=0.
AH=0.
AL=0.
CO 50 I=1,NH
IF(H(I).EQ.0) GOTO 50
PH=PH+DMOD(DFLOAT(H(I)),PER)
IH=IH+1
AH=AH+Y(M3,H(I))
50 CONTINUE
DO 55 I=1,NL
IF(L(I).EQ.0) GOTO 55
PH=PH+DMOD(DFLOAT(L(I))+PER/2,PER)
IL=IL+1
AL=AL+Y(M3,L(I))
55 CONTINUE
PHA =PH/(IH+IL) -1.
C FOLLOWING STATEMENT EXPRESSES PHASE LAG IN RADIANS WHEN C IS REMOVED
C PHA=6.283185*PHA /PER
AMP=(AH/IH-AL/IL)/2.
60 RETURN
END

```

RCHECK

```

SUBROUTINE RCHECK(Y,N,IRESP)
  CHECK PERFORMED ON THE NUMBER OF RUNS OF THE SAME SIGN
  IMPLICIT REAL *8(A-H,C-Z)
  DIMENSION Y(N),K(256)
  COMMON /INT/ K
  NRUN=N-1
  NMM=N-1
  DO 10 I=2,N
10 IF(Y(I)*Y(I-1).LT.0.) NRUN=NRUN+1
  NP=0
  NM=0
  DO 20 I=1,N
  IF(Y(I).LE.0.) NM=NM+1
20 IF(Y(I).GT.0.) NP=NP+1
  M1=2*NP*NM/(NP+NM)+1
  SIG=DSQRT(2.00*
  I NP*NM*(2.*NP*NM-NP-NM)/((NP+NM)**2*(NP+NM-1.)))
  Z=(NRUN-M1+.5DC)/SIG
  IF(DABS(Z).LT.1.645DC) IRESP=0
  IF(DABS(Z).LT.1.645DC) GOTO 30
  IF(Z.GT.0.) IRESP=1
  IF(Z.LT.0.) IRESP=-1
  PRINT 100,M1,NRUN,Z
  DO 25 I=1,N
  K(I)=0
25 IF(Y(I).GT.0.)K(I)=1
  PRINT 110,(K(I),I=1,N)
100 FORMAT('SEQUENCE OF SIGNS IS NOT RANDOM AT THE 90% SIGNIFICANCE L
  IVEL, EXPECTED NO. OF RUNS IS',I4,' ACTUAL NO. IS',I4,' NORMAL
  2 DEVIATE IS',F8.3 /'SEQUENCE OF SIGNS'/ '0')
110 FORMAT(' ',I28I1)
  GOTO 40
30 PRINT 120,M1,NRUN,Z
120 FORMAT('RANDOMNESS NOT REJECTED AT 90% CONFIDENCE LEVEL, EXPECTED
  1 NO. OF RUNS IS',I4,' ACTUAL NO. OF RUNS IS',I4,' NORMAL DEVIAT
  2 E IS',F8.3)
40 RETURN
  END

```

REJECT

```

SUBROUTINE REJECT(Y,M,N,FSS)
IMPLICIT REAL*8(A-H,O-Z)
DIMENSION Y(M),YY(50),X(50,10),XT(10,50),XTX(10,10),XTXI(10,10),
1 W(10,50),WW(50,50),ICUMY(56)
REAL*8 B(10)/10*1.00/
COMMON YY,X,XTX,WW
COMMON/INT/XTXI,ICUMY
COMMON /A/ W,XT
DATA MP/O/,NP/O/
IF(M.EQ.MP.AND.N.EQ.NP) GOTO 40
DO 10 I=1,M
X(I,1)=1.00
DO 10 J=2,N
10 X(I,J)=X(I,J-1)*I
CALL WMTRA(X,XT,M,N,50,10)
CALL WMPRD(XI,X,XTX,N,M,N,10,50)
CALL WMASGN(XIXI,XTX,N,N,10)
CALL MATINV(XIXI,N,8,1,DET,10)
CALL WMPRO(XIXI,XT,W,N,N,M,10,10)
CALL WMPRD(X,W,WW,M,N,M,50,10)
DO 20 I=1,M
20 WW(I,I)=WW(I,I)-1.
CALL WMPRD(XIXI,XTX,W,N,N,N,10,10)
NP=N
MP=M
40 SS=0.
DO 45 I=1,M
YY(I)=0.
DO 44 K=1,M
44 YY(I)=YY(I)+WW(I,K)*Y(K)
45 SS=SS+YY(I)**2
S=OSQRT(SS/(M-N))
DO 50 I=1,M
Y(I)=1.00
50 IF(DABS(YY(I)).GT.FSS *S) Y(I)=0.00
RETURN
END

```

WMAT

```

SUBROUTINE WMAT(A,B,C,AA,AT,N,M,L,NFUL,MFUL,V,W)
REAL*8 A(NFUL,M),B(MFUL,L),C(NFUL,L),AA(NFUL,M),AT(MFUL,N),V(M),
1 W(N)
ENTRY WMPRO(A,B,C,N,M,L,NFUL,MFUL)
DO 10 I=1,N
DO 10 J=1,L
C(I,J)=0.
DO 10 KK=1,M
10 C(I,J)=C(I,J)+A(I,KK)*B(KK,J)
RETURN
ENTRY WMTRA(A,AT,N,M,NFUL,MFUL)
DO 20 I=1,N
DO 20 J=1,M
20 AT(J,I)=A(I,J)
RETURN
ENTRY WMASGN(A,AA,N,M,NFUL)
DO 30 I=1,N
DO 30 J=1,M
30 A(I,J)=AA(I,J)
RETURN
ENTRY WMADD(A,AA,N,M,NFUL)
DO 40 I=1,N
DO 40 J=1,M
40 A(I,J)=A(I,J)+AA(I,J)
RETURN
ENTRY WMSUB(A,AA,N,M,NFUL)
DO 50 I=1,N
DO 50 J=1,M
50 A(I,J)=AA(I,J)-A(I,J)
RETURN
ENTRY WMNUL(A,N,M,NFUL)
DO 60 I=1,N
DO 60 J=1,M
60 A(I,J)=0.
RETURN
ENTRY WMUNIT(A,N,M,NFUL)
K=MINO(NFUL,M)
DO 69 I=1,N
DO 69 J=1,M
69 A(I,J)=0.
DO 70 I=1,K
70 A(I,I)=1.00
RETURN
ENTRY WMPROV(A,V,W,N,M,NFUL)
DO 80 I=1,N
W(I)=0.
DO 80 K=1,M
80 W(I)=W(I)+A(I,K)*V(K)
RETURN
ENTRY WVPDM(W,A,V,N,M,NFUL)
DO 90 I=1,M
V(I)=0.
DO 90 K=1,N
90 V(I)=V(I)+W(K)*A(K,I)
RETURN
END

```


MATINV

```

      B(J,K)=B(ICOLUM,K)
      B(ICOLUM,K)=SWAP
250  CONTINUE
C
C
      DIVIDE PIVOT ROW BY PIVOT ELEMENT
260  K=ICOLUM
      A(ICOLUM,K)=1.0
      DO 350 K=1,N
      A(ICOLUM,K)=A(ICOLUM,K)/AMAX
350  CONTINUE
      IF (M.LE.0) GO TO 380
      DO 370 K=1,M
      B(ICOLUM,K)=B(ICOLUM,K)/AMAX
370  CONTINUE
C
C
      REDUCE NON-PIVOT ROWS
380  DO 550 J=1,N
      IF (J.EQ.ICOLUM) GO TO 550
      T=A(J,ICOLUM)
      A(J,ICOLUM)=0.0
      DO 450 K=1,N
      A(J,K)=A(J,K)-A(ICOLUM,K)*T
450  CONTINUE
      IF (M.LE.0) GO TO 550
      DO 500 K=1,M
      B(J,K)=B(J,K)-B(ICOLUM,K)*T
500  CONTINUE
550  CONTINUE
C
C
      INTERCHANGE COLUMNS AFTER ALL PIVOT OPERATIONS HAVE BEEN PERFORMED
600  DO 710 I=1,N
      I1=N+1-I
      K=INDEX(I1)/4096
      ICOLUM=INDEX(I1)-4096*K
      IF (K.EQ.ICOLUM) GO TO 710
      DO 705 J=1,N
      SWAP=A(J,K)
      A(J,K)=A(J,ICOLUM)
      A(J,ICOLUM)=SWAP
705  CONTINUE
710  CONTINUE
C
711  CONTINUE
      RETURN
      ENO

```

ANGLE

```

FUNCTION ANGLE(RC,RS)
IMPLICIT REAL*8(A-H,O-Z)
R=DSQRT(RC**2+RS**2)
ANGLE=0ARCOS(RC/R)
IF(RC/R.GT..900) ANGLE= DSIGN(ANGLE,RS)
IF(RC/R.LT..900 .AND. RS.LT. 0.00) ANGLE=6.2831853-ANGLE
RETURN
ENO

```

COSINE TEST DATA Y(I)=100000*COS(12*PI*(I-1)/51.3)+100000 NPOLY= 1 NHARM= 1 NPTR= 16 MORRE= PAGE 1.
 OPTICS SPECIFIED OR ASSIGNED BY DEFAULT, N= 256 NPREL= 0 NDUMP= 4
 DPER= 0.050 DF= 0.050

INPUT

200000 199250 197014 193325 182337 191827
 1233914 122166 110087 97856 82658 173674
 138003 207184 9827 5221 2035 316
 118509 130715 141845 37856 47893 58711
 199932 199932 197840 197840 162621 171618
 148460 137347 125734 13735 101530 89303
 34094 25399 11476 11476 6566 4473
 6836 12052 26220 35020 35020 4773
 194947 138480 193880 193880 149493 195716
 198085 140729 129266 129266 1983364 191455
 151582 140729 19970 19970 113544 92963
 36901 10363 16450 16450 32790 3773
 99081 111304 123359 123359 32211 41768
 193758 197304 193393 193393 135083 156729
 164512 154695 144057 144057 199959 196710
 49999 30490 30490 30490 32227 108867
 1572 4468 19795 19795 22458 84796
 83238 95407 95407 95407 19771 29642
 187058 124416 124416 124416 13159 4942
 175911 153733 153733 153733 199908 192254
 64363 45768 45768 45768 372520 197520
 16 3447 3447 3447 37258 17730
 67820 9441 9441 9441 10379 19262
 178156 190951 190951 190951 10379 19262
 100000 185192 185192 185192 195348 128093

REFLECT SUBROUTINE CALLED

NO POINTS REJECTED

INITIAL GUESS

AMPLITUDE 9991.25
 PERIOD 51.2857
 LAG(PHASE) 0.1190

SUBROUTINE XMIN EMIN
 PERIOD= 51.3000 SUM OF SQUARES= 33.652
 PERIOD= 51.3000 SUM OF SQUARES= 33.652
 PERIOD= 51.3000 SUM OF SQUARES= 33.652

174191 165463 153776 145153
 62085 51064 407776 31375
 70148 1363 4113 82300
 179860 82032 94185 106028
 183883 196448 193177 158073
 77236 65510 54300 43776
 676 9035 35226
 55393 7830 30522
 169068 17385 190426
 191455 185829 170488
 92963 80828 157231
 3773 17831 74947
 41768 17385 74957
 156729 52132 62216
 196710 182834 192296
 108867 9663 184277
 84796 192254 84796
 29642 3815 4942
 4942 2815 4942
 192254 193993 172339
 197520 193993 188073
 17730 19013 19030
 19262 27058 18030
 128093 150608 30955
 150608 150608 150608

COSINE TEST DATA Y(I)=100000* $\cos(2*\pi*(I-1)/51.3)$ +100000

MINIMUM FOUND

ORDER OF POLYNOMIAL I NUMBER OF HARMONICS I

PARAMETERS

- 1 -0.527385
- 2 -0.568655D-02
- 3 100000.
- 4 0.710610D-02
- 5 51.3000

RESIDUALS (EXACT ZERO POINTS REJECTED POINTS)

0.49	-0.39	-0.25	0.47	0.30	0.19	0.06	0.50
-0.37	-0.29	0.15	-0.47	0.20	-0.21	-0.03	-0.45
0.16	0.07	0.21	0.34	0.46	-0.38	-0.01	0.02
-0.12	0.28	0.46	-0.16	-0.24	-0.30	-0.05	-0.12
-0.13	0.16	0.43	0.36	-0.66	0.28	0.13	0.04
-0.13	-0.40	-0.21	-0.33	-0.46	-0.69	-0.16	0.03
-0.07	0.15	0.30	0.23	-0.14	0.24	0.39	-0.21
0.16	-0.04	0.33	0.02	0.32	-0.06	-0.32	0.23
-0.21	0.48	0.01	0.48	-0.14	0.71	-0.44	-0.36
0.11	-0.49	0.40	-0.11	-0.08	-0.21	0.24	0.60
-0.11	-0.06	-0.59	-0.41	-0.38	-0.58	0.13	-0.32
0.14	0.21	-0.48	-0.20	-0.26	-0.22	0.84	0.39
-0.34	0.49	0.04	0.44	-0.14	-0.42	0.69	-0.48
-0.35	-0.60	0.60	-0.26	0.00	0.32	0.03	0.33
-0.28	0.56	0.40	0.34	-0.15	-0.44	-0.67	-0.13
-0.01	-0.07	0.06	0.09	-0.34	0.07	-0.19	-0.41
-0.20	0.40	-0.97	-0.81	-0.08	-0.10	0.29	-0.76
-0.18	-0.03	0.94	0.12	0.34	0.25	0.17	-0.25
0.17	-0.31	-0.73	0.59	0.16	0.21	-0.47	0.50
0.27	-0.89	0.27	-0.45	0.43	0.50	-0.03	-0.23
-0.19	0.75	-0.66	-0.36	0.18	0.34	0.57	0.42
			-0.05	-0.09	0.42	0.00	-0.74

STANDARD DEVIATION ESTIMATE 0.37 SUM OF SQUARES 34. 95% CONFIDENCE MARGIN= 1.

RANDOMNESS NOT REJECTED AT 90% CONFIDENCE LEVEL, EXPECTED NO. OF RUNS IS 128

ACTUAL NO. OF RUNS IS 121 NORMAL DEVIATE IS -0.815

COSINE TEST DATA $Y(I)=100000*\text{COS}(2*\text{PI}*(I-1)/51.3)+100000$

LINEARIZED CONFIDENCE LIMITS

1	-0.53	+/	0.70126D-01
2	-0.01	+/	0.12146
3	100000.03	+/	0.98508D-01
4	0.01	+/	0.19880
5	51.30	+/	0.56300D-05

PHASE ANGLE FOR THE HARMONIC VALUES I AMPLITUDE NOMINAL 100000.03 AMPLITUDE NORMALIZED 1.0000
 RADIANS 0.00000 VALUES ON CONFIDENCE LIMITS UPPER 0.00000 LOWER -0.00000
 LAG UNITS 0.00000 VALUES ON CONFIDENCE LIMITS UPPER 0.00000 LOWER -0.00000

PARAMETERS CORRELATION MATRIX

1	1.0000	-0.65066D-02	0.11316D-01	-0.13617	0.15631
2	-0.65066D-02	1.00000	0.14568D-01	0.76186D-01	0.16582D-02
3	0.11316D-01	0.14568D-01	1.00000	-0.47296D-01	0.55644D-01
4	-0.13617	0.76186D-01	-0.47296D-01	1.00000	-0.86700
5	0.15631	0.16582D-02	0.55644D-01	-0.86700	1.00000

CASE COMPUTATION TIME 18.60 SECONDS

AL 5 I I CROSS LAY 550 LB RECOED I/5 RUN 7

LINEARIZED CONFIDENCE LIMITS

1	-6974.76	+/	13.409
2	-593.28	+/	26.234
3	-48.82	+/	28.246
4	-1.69	+/	29.282
5	70.31	+/	28.622
6	8027.41	+/	28.883
7	6383.93	+/	30.132
8	52.03	+/	0.15410D-01

POINT 127 SHOULD BE REJECTED
 POINT 128 SHOULD BE REJECTED
 POINT 130 SHOULD BE REJECTED
 POINT 131 SHOULD BE REJECTED
 CALCULATIONS SHALL BE REPEATED WITH MORE POINTS REJECTED

SUBROUTINE XMIN EXIT LAST THREE POINTS
 PERIOD= 58.0327 SCW OF SQUARES= 0.139590 06
 PERIOD= 58.0327 SCW OF SQUARES= 0.139590 06
 PERIOD= 58.0327 SCW OF SQUARES= 0.139590 06

LINEARIZED CONFIDENCE LIMITS

1 -6977.95 +/- 6.0057
 2 -594.76 +/- 10.834
 3 -32.13 +/- 12.803
 4 -2.48 +/- 13.984
 5 62.06 +/- 22.259
 6 8023.48 +/- 12.916
 7 6371.42 +/- 16.230
 8 58.03 +/- 0.68983D-02

PHASE ANGLE FOR THE HARMONIC 1 AMPLITUDE NOMINAL 10245.55 AMPLITUDE, NORMALIZED 0.76261D-02
 RADIAN 0.6713 VALUES ON CONFIDENCE LIMITS UPPER 0.67316 LOWER 0.666911
 DEG UNITS 6.1987 VALUES ON CONFIDENCE LIMITS UPPER 6.2174 LOWER 6.1860

PARAMETERS CORRELATION MATRIX

1	1.0000	-0.39422D-01	0.26768	-0.55204D-01	0.88256D-01	0.60465D-01	0.15674
2	-0.39722D-01	1.0000	-0.26406D-01	0.32089	0.13785	-0.19492	-0.17342
3	0.269768	-0.26406D-01	1.0000	-0.36600	0.28800	-0.12101D-01	0.12044
4	-0.35204D-01	0.32089	-0.36600	1.0000	0.10000	0.13746	0.14973
5	0.88256D-01	0.13785	0.28800	0.10000	1.0000	0.18000	-0.33890
6	0.60465D-01	-0.12101D-01	0.12044	-0.12101D-01	0.18000	1.0000	0.75658
7	-0.17342	0.12044	0.14973	-0.18000	-0.33890	0.75658	1.0000
8	0.10957	-0.17342	0.18210	-0.21737	0.44019	-0.75458	-0.85008

CASE COMPUTATION TIME 48.21 SECONDS

THE TEMPERATURE WAVE METHOD
OF MEASURING THERMAL DIFFUSIVITY AND
THERMAL CONTACT CONDUCTANCE

by

MIHAEL TOMSIC

Dipl. Ing., University of Ljubljana, 1964

AN ABSTRACT OF A MASTER'S THESIS

submitted in partial fulfillment of the

requirements for the degree

MASTER OF SCIENCE

Department of Nuclear Engineering

KANSAS STATE UNIVERSITY
Manhattan, Kansas

1969

ABSTRACT

The temperature wave method of determining the thermal diffusivity and the thermal contact conductance was investigated. The theoretical development of the plane temperature wave behavior at the contact of two solids is given for an interface perpendicular to the direction of wave travel. The relative amplitude and the phase angle of the reflected and the transmitted wave in relation to the approaching wave were calculated in relation to the dependence of the thermal properties of the two contacting solids and the thermal conductance of the contact.

The experimental apparatus is described. The temperature waves were generated by alternately heating and cooling one end of the specimen (specimen pair) while the other end was kept at a constant temperature. The temperatures, represented by the thermocouple voltages, were recorded on a magnetic tape recorder. The records were analyzed using a hybrid analog-digital correlation computer. The theory of the correlation function is outlined and a computer program is described which performs a least squares fitting of a set of data with an analytical model containing one nonlinear parameter. The program is particularly adapted for the analysis of the correlation function containing a prominent harmonic and compensation for some imperfections of the electronic equipment used are included.

Results are given of the measurements of the thermal diffusivity of the aluminum alloy 2024-T4 and Armco iron and of the thermal contact conductance of the aluminum-aluminum and aluminum-iron contact in air

at different applied pressures. The agreement with the results from literature is very good for the thermal diffusivity measurements and good for the thermal contact conductance measurements.

The temperature wave method was found adequate for measuring the thermal contact conductance and suggestions are made for some further interesting investigations using this technique.